

6-2020

Preparation And Characterization Of γ -Al₂O₃ Doped With Selected Elements and Correlating Surface Properties with the Catalytic Activity in Methanol Dehydration to Dimethyl Ether

Mo'ath Ahmad Hasan Ahmad

Follow this and additional works at: https://scholarworks.uaeu.ac.ae/chem_theses

 Part of the [Chemistry Commons](#)

Recommended Citation

Hasan Ahmad, Mo'ath Ahmad, "Preparation And Characterization Of γ -Al₂O₃ Doped With Selected Elements and Correlating Surface Properties with the Catalytic Activity in Methanol Dehydration to Dimethyl Ether" (2020). *Chemistry Theses*. 9.
https://scholarworks.uaeu.ac.ae/chem_theses/9

This Thesis is brought to you for free and open access by the Chemistry at Scholarworks@UAEU. It has been accepted for inclusion in Chemistry Theses by an authorized administrator of Scholarworks@UAEU. For more information, please contact fadl.musa@uaeu.ac.ae.

United Arab Emirates University

College of Science

Department of Chemistry

PREPARATION AND CHARACTERIZATION OF γ -Al₂O₃ DOPED
WITH SELECTED ELEMENTS AND CORRELATING SURFACE
PROPERTIES WITH THE CATALYTIC ACTIVITY IN METHANOL
DEHYDRATION TO DIMETHYL ETHER

Mo'ath Ahmad Hasan Ahmad

This thesis is submitted in partial fulfilment of the requirements for the degree of
Master of Science in Chemistry

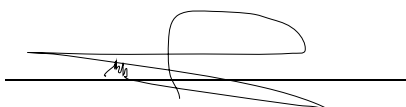
Under the Supervision of Professor Abbas Ahmed Khaleel

June 2020

Declaration of Original Work

I, Mo'ath Ahmad Hasan Ahmad, the undersigned, a graduate student at the United Arab Emirates University (UAEU), and the author of this thesis entitled "*Preparation and Characterization Of γ -Al₂O₃ Doped with Selected Elements and Correlating Surface Properties with the Catalytic Activity in Methanol Dehydration to Dimethyl Ether*", hereby, solemnly declare that this thesis is my own original research work that has been done and prepared by me under the supervision of Professor Abbas Ahmed Khaleel, in the College of Science at UAEU. This work has not previously been presented or published, or formed the basis for the award of any academic degree, diploma or a similar title at this or any other university. Any materials borrowed from other sources (whether published or unpublished) and relied upon or included in my thesis have been properly cited and acknowledged in accordance with appropriate academic conventions. I further declare that there is no potential conflict of interest with respect to the research, data collection, authorship, presentation and/or publication of this thesis.

Student's Signature: _____



Date: 14-June-2020

Copyright © 2020 Mo'ath Ahmad Hasan Ahmad
All Rights Reserved

Approval of the Master Thesis

This Master Thesis is approved by the following Examining Committee Members:

- 1) Advisor (Committee Chair): Dr. Abbas Ahmed Khaleel

Title: Professor

Department of Chemistry

College of Science

Signature  _____

Date 14/June/ 2020

- 2) Member: Dr. Mohammad Almeetani

Title: Professor

Department of Chemistry

College of Science

Signature  _____

Date 14/June/2020

- 3) Member (External Examiner): Dr. Nathir Al-Rawashdeh

Title: Professor

Department of Chemistry

Higher Colleges of Technology, United Arab Emirates

Signature  _____

Date 14 June 2020

This Master Thesis is accepted by:

Acting Dean of the College of Science: Professor Maamar Ben Kraouda

Signature Maamar Benkraouda Date June 29, 2020

Dean of the College of Graduate Studies: Professor Ali Al-Marzouqi

Signature Ali Hassan Date June 30, 2020

Copy ____ of ____

Abstract

The increasing demand for energy is associated with challenges that include environmental concerns and limited reserves. Dimethyl ether, DME, which can be obtained from different feedstocks, including natural gas and biomass, has recently been recognized as an ultraclean environmentally friendly fuel due to the fact that it possesses unique characteristics that make it an efficient alternative fuel for diesel fuel engines. In addition, DME is an industrially important intermediate for a variety of chemicals. A promising potential route for dimethyl ether production is catalytic dehydration of methanol over solid acid catalysts. Therefore, exploring new solid acid catalytic materials and understanding the mechanistic steps of methanol adsorption on their surfaces is of great importance for developing modified efficient catalysts for this process. In the present work, solid acid catalysts based on modified γ -Al₂O₃ were prepared by sol-gel method and were studied as catalysts for methanol to dimethyl ether conversion.

The main focus of the present thesis is to investigate the effect of selected metal dopants on the surface chemical properties of γ -Al₂O₃, especially acid-base characteristics, and to correlate these effects with their catalytic activity in dehydration of methanol to DME. The selected dopants include transition metal ions with different *d*-configurations and different oxidation states, such as Ti(IV), V(III) and Ni(II) to elucidate any possible electronic effect on the alumina surface chemical behavior.

The prepared catalysts were characterized by various physical and chemical techniques including adsorption of probe molecules, namely ammonia and methanol. The study showed very promising results where doping γ -Al₂O₃ resulted in significant textural and chemical modifications including an enhanced overall surface acidity. The catalytic activity study showed that the incorporation of certain concentrations of Ti(IV) and Ni(II) ions in the γ -Al₂O₃ matrix resulted in an enhanced catalytic activity. The catalytic activity of the catalysts was correlated with their textural, chemical, and structural modifications resulting from the presence of the dopant ions.

In addition, comparison between the studied alumina-based solids and selected ZSM5 zeolites showed that the acidic character of the OH groups on their surfaces vary and therefore, different routes of methanol adsorption and dehydration were proposed for the two types of materials. Methanol adsorption and dehydration was proposed to be associative on the surface of ZSM5 zeolites, where Brønsted acid sites played a key role in adsorption and dehydration reaction. On the other hand, dissociative adsorption on Lewis acid-base pairs dominates the interactions with γ -Al₂O₃-based solids.

Keywords: Methanol dehydration, Methanol adsorption, Dimethyl ether, Alternative fuel, Acid catalyst.

Title and Abstract (in Arabic)

تحضير وتوصيف سطحي لـ $\gamma\text{-Al}_2\text{O}_3$ المحتوية على عناصر أخرى مختارة عن طريق دراسة ارتباط صفات السطح بالنشاط التحفيزي في تحويل الميثانول إلى ثنائي ميثيل إيثر

الملخص

إن الطلب المتزايد على مصادر الطاقة يتزامن مع تحديات عديدة منها الاضرار البيئية والمصادر المحدودة، ثنائي ميثيل إيثر الذي يمكن إنتاجه من مصادر أولية عديدة مثل الغاز الطبيعي و الكتلة الحيوية تم اعتباره في الآونة الأخيرة بأنه وقود نظيف صديق للبيئة حيث أن ثنائي ميثيل إيثر يتميز بخصائص عديدة تجعله بديل فعال لوقود الديزل في محركات الديزل. إضافة إلى ذلك، يعد ثنائي ميثيل الإيثر مركب وسطياً مهماً في إنتاج العديد من الكيماويات المهمة. يتم إنتاج ثنائي ميثيل إيثر عن طريق تفاعل نزع الماء (البلهمة) من الميثانول بالاستعانة بمحفزات حمضية صلبة. لذلك، استكشاف محفزات حمضية جديدة وفهم الخطوات الميكانيكية لادمصاص الميثانول على سطح الحفاز يعتبر بالغ الأهمية من أجل تطوير مواد حفازة فعالة لهذا التفاعل. تم في هذا البحث تحضير محفزات حمضية تعتمد على أكسيد الألمنيوم (الألومينا) بطريقة ال "سول-جل" وتم دراسة فعاليتها وقدرتها على تحفيز تفاعل تحويل الميثانول إلى ثنائي ميثيل إيثر.

الهدف الرئيسي في هذه الأطروحة هو فحص تأثير التطعيم ببعض المعادن على الخصائص السطحية والكميائية لأكسيد الألمنيوم وخاصة الخصائص الحمضية-القاعدية وربط هذه التأثيرات بنشاطه التحفيزي في تحويل الميثانول إلى ثنائي ميثيل إيثر. تشمل المطعومات المختارة أيونات فلز انتقالية ذات تكوينات مختلفة وحالات أكسدة مختلفة، مثل Ti (IV) و V (III) و Ni (II) لتوضيح أي تأثير إلكتروني محتمل على السلوك الكيماوي لسطح الألومينا. لقد تم أيضا فحص تأثير إضافة معادن أخرى مثل السيليكون والمغنيسيوم.

لقد تم توصيف الخصائص الفيزيائية والكميائية للحفازات المحضرة باستخدام تقنيات مختلفة منها ادمصاص الأمونيا والميثانول. لقد أظهرت هذه الدراسة نتائج واعدة حيث إن تطعيم الألومينا أدى إلى تحسينات ملحوظة في الخصائص الكيماوية بما في ذلك زيادة حموضة السطح الكلية. أظهرت دراسة نشاط الحفاز أن إضافة تركيزات معينة من أيونات Ti (IV) و Ni (II) الكلية.

في الألومينا أدى إلى تحسين نشاط الحفاز. لقد ارتبط النشاط الحفازي للمحفزات بتعديلاتها التركيبية والكيميائية والهيكلية الناتجة عن وجود أيونات التطعيم. بالإضافة إلى ذلك، أظهرت المقارنة بين المواد الصلبة القائمة على الألومينا وزبولاييت ZSM5 أن الطابع الحمضي لمجموعات هيدروكسيل OH على أسطحها يختلف، وبالتالي، تم اقتراح طرق مختلفة لادمصاص وبلمة الميثانول لهذين النوعين المختلفين من المواد.

تم اقتراح ادمصاص الميثانول وبلمته ليكون مرتبطاً على سطح الزيولاييت ZSM5، حيث لعبت مواقع حمض برونستيد دوراً رئيسياً في تفاعل ادمصاص ونزع الماء. من ناحية أخرى، يهيمن ادمصاص الإنفصالي على أزواج لويس الحمضي/ القاعدي على التفاعلات مع المواد الصلبة القائمة على الألومينا $\gamma\text{-Al}_2\text{O}_3$.

مفاهيم البحث الرئيسية: ثنائي ميثيل إيثر، ادمصاص الميثانول، نزع جزيء الماء من الميثانول، وقود بديل، حفاز حمضي.

Acknowledgements

First and foremost, my thanks go to Prof. Abbas Khalil for his great gaudiness and supervision. I am grateful to him for his support throughout my thesis with patience and knowledge. It was an honor for me to work with him.

Special thanks go to my family, especially my parents, for their continues love, encouragement, and support along the way. Thanks, are also extended to my friends for their support and assistance.

Dedication

To my beloved parents and family

Table of Contents

Title	i
Declaration of Original Work	ii
Copyright	iii
Approval of the Master Thesis	iv
Abstract	vi
Title and Abstract (in Arabic)	viii
Acknowledgements	x
Dedication	xi
Table of Contents	xii
List of Tables	xiv
List of Figures	xv
List of Abbreviations.....	xvii
Chapter 1: Introduction	1
1.1 Overview	1
1.2 Statement of the problem and objectives of the present study	2
1.3 DME properties	3
1.4 DME production business	5
1.5 DME production methods	5
1.5.1 Indirect synthesis	6
1.5.2 Direct synthesis	6
1.6 Catalysis	7
1.6.1 Solid acid catalysts	8
1.6.2 Catalytic methanol dehydrations	9
Chapter 2: Catalysts Preparation and Characterization.....	17
2.1 Introduction and overview	17
2.1.1 Brief review of common preparation methods.....	17
2.1.2 Sol-gel process	18
2.1.3 Characterization techniques	24
2.2 Experimental methods.....	30
2.2.1 Catalyst preparation.....	30
2.2.2 XRD characterization	32
2.2.3 Temperature programmed desorption (TPD).....	33
2.2.4 Surface area and porosity measurements	33
2.2.5 TEM analysis.....	34
2.3 Results and discussion	34

2.3.1 Structural characterization.....	34
2.3.2 Textural and morphological characterization.....	37
Chapter 3: Catalytic Activity Study	44
3.1 Overview	44
3.2 Background	44
3.2.1 Types of reactors for DME synthesis.....	45
3.2.2 Dehydration reaction variables.....	45
3.3 Experimental methods.....	46
3.4 Data collection and product analysis	48
3.5 Results and discussion	50
3.5.1 Catalytic activity	50
3.5.2 Products' selectivity	58
Chapter 4: Mechanistic Study by Methanol Chemisorption	63
4.1 Introduction and overview	63
4.2 Experimental method: Methanol adsorption and intermediates study.....	64
4.3 Results and discussion	65
Chapter 5: Conclusion and Future Work	78
References	80
List of Publications	94

List of Tables

Table 1.1: Properties of DME in comparison with some other fuels.....	4
Table 1.2: A literature survey of the most studied catalysts for methanol to DME conversion during the last decade.....	15
Table 2.1: Surface area and pore characteristics of the investigated solids calcined at 500°C.....	38

List of Figures

Figure 1.1: Dimethyl ether production diagram.....	5
Figure 2.1: Graphical illustration of the 2-theta angle between the incident and reflected beam	26
Figure 2.2: Scheme of the steps of preparation of AlTiX% as an example	32
Figure 2.3: XRD patterns of γ -Al ₂ O ₃ doped with Ti ions and undoped γ -Al ₂ O ₃ after calcination at 500°C	35
Figure 2.5: XRD pattern of NiAl ₂ O ₄ after calcination at 500°C	36
Figure 2.4: XRD patterns of γ -Al ₂ O ₃ doped with Ni ions after calcination at 500°C.....	36
Figure 2.6: XRD patterns for ZSM5 samples	37
Figure 2.7: N ₂ adsorption-desorption isotherms of doped and undoped γ -Al ₂ O ₃ calcined at 500°C.....	39
Figure 2.8: Pore size distribution of doped and undoped γ -Al ₂ O ₃ calcined at 500°C.....	40
Figure 2.9: TEM images of γ -Al ₂ O ₃ , AlTi03 and AlTi10.....	41
Figure 2.10: NH ₃ -TPD profiles of selected zeolites compared with alumina-based catalysts and TiO ₂	43
Figure 2.11: DRIFT spectra of adsorbed species over AlTi03 compared to γ -Al ₂ O ₃ after adsorption at 50°C	43
Figure 3.1: Continuous flow fixed-bed reaction setup.....	48
Figure 3.2: 6-way valve scheme loading position injection position	49
Figure 3.3: Methanol conversion at 200°C over prepared γ -Al ₂ O ₃ compared with its commercial counterpart and TiO ₂	51
Figure 3.4: Methanol conversion at 200°C of AlTi with different concentrations compared with pure γ -Al ₂ O ₃	52
Figure 3.5: Methanol conversion at 200°C of AlNi with different concentrations compared with pure γ -Al ₂ O ₃	53
Figure 3.6: Methanol conversion at 200°C over TiO ₂ /Al ₂ O ₃ compared to AlTi03% and γ -Al ₂ O ₃	54
Figure 3.7: Methanol conversion at 200°C of AlM03% compared to Alumina.....	55
Figure 3.8: Methanol conversion at 200°C over AlM10 catalysts compared with pure γ -Al ₂ O ₃	56
Figure 3.9: Methanol conversion at 200°C over different ZSM5 zeolites.....	56
Figure 3.10: Methanol conversion at 200°C over AlM03% vs. selected Zeolites	57
Figure 3.11: DME selectivity in reactions at 200°C over AlM03% (Ni,Ti) vs Alumina and Zeolites	59

Figure 3.12: CO ₂ selectivity from reactions at 200°C over AlM03% vs Alumina catalysts	59
Figure 3.13: DME and CO ₂ selectivity in the reaction at 200°C over TiO ₂ /Al ₂ O ₃ vs AlTi03	60
Figure 3.14: Methanol conversion, DME selectivity, and CO ₂ selectivity over AlM03% compared to alumina in the temperature range from 150°C to 400°C	62
Figure 4.1: Methanol adsorption study setup	65
Figure 4.2: DRIFT spectra of adsorbed species over AlTi03, AlNi03, γ -Al ₂ O ₃ , and TiO ₂ after adsorption of methanol at 50°C	67
Figure 4.3: DRIFT spectra of adsorbed species over AlTi03, AlNi03, γ -Al ₂ O ₃ , and TiO ₂ after desorption of methanol at 150°C	69
Figure 4.4: DRIFT spectra of adsorbed species after adsorption at 50°C and subsequent desorption at different temperatures over AlTi03	71
Figure 4.5: DRIFT spectra of adsorbed species over AlTi03 and γ -Al ₂ O ₃ after purging at 400°C	71
Figure 4.6: DRIFT spectra of surface species over zeolites compared with γ -Al ₂ O ₃ and AlTi03 after adsorption of methanol at 50°C and desorption at 150°C	74
Figure 4.7: Suggested mechanistic steps for the adsorption of methanol on γ -Al ₂ O ₃ -based solids compared with ZSM5 zeolites	77

List of Abbreviations

AZO	Al-Doped Zinc Oxide
BID	Barrier Ionization Detector
CFCs	Chlorofluorocarbons
DME	Dimethyl Ether
DRIFTS	Diffuse Reflectance Infrared Fourier Transform
FCC	Face-Centered Cubic
GC	Gas Chromatograph
ITO	Indium Oxide
LPG	Liquefied Petroleum Gases
MeOH	Methanol
MO _x	Metal-Oxide
SAPO	Silicoaluminophosphate
STD	Syngas to Dimethyl Ether
Syngas	Synthetic Gas
TPD	Temperature Programmed Desorption
XRD	X-Ray Diffraction
ZSM5	Zeolite Socony Mobil-5

Chapter 1: Introduction

1.1 Overview

Dimethyl ether (DME) is a promising ultra-low emission and non-toxic environmentally friendly fuel that can work as a replacement to diesel in diesel engines. Besides its use as an alternative clean fuel, DME has a wide range of other applications such as its use as a green refrigerant gas, which will eliminate the hazardous effects of chlorofluorocarbons (CFCs) that are significant contributors to the problem of ozone layer depletion. In addition, DME is a potential building block for a wide variety of chemicals.

One of the main challenges of DME production is finding the best process conditions with high yield and low costs. Catalytic dehydration of methanol, which can be obtained from different feedstocks, is one of the promising processes for DME production. Thus, the purpose of this thesis is to develop and investigate more efficient cost-effective catalytic materials for this process at reasonable temperatures and to compare their efficiency with available typical catalysts. Catalytic methanol dehydration to DME reaction was studied at 200°C and atmospheric pressure using a fixed bed continuous flow reaction system. Catalysts based on γ -alumina doped with other metal ions including Ti(IV), Ni(II), and V(III) were developed and their catalytic activity was investigated and compared with other commercial solid-acid catalysts including γ -alumina and selected zeolites.

1.2 Statement of the problem and objectives of the present study

The energy and environment problems are intertwined due to the fast depletion of natural resources and a large build-up of greenhouse gases in the atmosphere. Crude oil is depleting very fast, and the transportation industry is one of the primary causes of oil depletion; it consumes approximately 57% of total petroleum production. In addition, the lifetime of natural resources has been reduced dramatically because of the rapid increase in population growth and globalization along with the misuse and extravagance of these resources. This overuse will lead to lack of energy supplies for future generations. These problems have raised concerns to search and innovate in the development of new clean alternative sources of energy, which have to be renewable and can be utilized in different ways in the industry without major modifications of the existing infrastructure [1]. Besides the investment in renewable energy research, great attention has been given to better utilization of natural gas as a source of clean fuel. One of the promising clean fuels that can be derived directly or indirectly from natural gas is DME.

DME can be produced from natural gas through catalytic processes where the catalytic materials play a key role in the efficiency of these processes. The main aim of the research of this thesis is to develop more efficient catalysts for the conversion of methanol, which is produced from natural gas, to DME. The developed catalysts are based on γ -Al₂O₃ doped with Ti(IV), Ni(II), and V(III) ions which were selected to study the effect of different *d*-configurations of the metal dopants as well as their oxidation state. The prepared alumina-based catalysts were also compared with two selected widely studied zeolites in the methanol to DME conversion reaction.

1.3 DME properties

Dimethyl ether (methoxymethane, IUPAC name) is the simplest ether compound. It is photochemically degradable to CO₂ and H₂O within a few hours. Some of the properties of DME are given in Table 1.1. It is known to be the cleanest high-efficiency compression ignition fuel with a high level of safety due to the fact that it has no toxic emissions and no carcinogenic or teratogenic effects.

DME has recently attracted significant attention as an environmentally friendly alternative fuel and as an efficient intermediate for a variety of industrially important chemicals such as acetic acid, methyl acetate, aromatics, gasoline, light olefins, higher ethers, oxygenates and many other chemicals. Also, its low vapor pressure and its ability to be biodegradable makes it a promising alternative as an aerosol propellant that can replace chlorofluorocarbon (CFC), Freon and R-134, which are the main contributors to ozone layer depletion.

DME has similar physical properties as that of liquefied petroleum gas (LPG), as it burns with a visible blue flame over a wide range of air/fuel ratios. Hence it can be used as an alternative fuel for cooking and heating or for LPG blending. Storing and handling of DME is not an issue since it has a similar vapor pressure as that of LPG so it could be transported and stored using the existing infrastructure of LPG. Furthermore, DME has excellent thermal and chemical properties to be a highly efficient diesel replacement due to its relatively low auto-ignition temperature and high cetane number (55-60) as shown in Table 1.1. The cetane number is related to how fast the fuel combustion is, and higher cetane numbers are associated with shorter ignition delays compared to lower numbers. Besides, compared to other fuels, DME has higher oxygen content and no direct

carbon-carbon bond, which leads to soot-free combustion thus eliminating the need for filters. This feature also makes the engine run much more quietly on DME compared to diesel. Also, DME is a very attractive choice as a clean fuel for transportation and domestic utilization because it has much fewer emissions of sulfur oxides and nitrogen oxides. Another attractive aspect of using DME as a fuel is that it can be produced from a variety of feedstocks including natural gas, crude oil, residual oil, coal and waste products [2, 3].

Although DME has many significant advantages over diesel, it has some drawbacks as it has a lower energy density than diesel fuel; therefore, it requires enlarging the volume of the storage tank to give the same amount of energy. Also, DME has a low viscosity which can lead to leakage in storage and delivery systems [4]. However, these are still minor problems that can be dealt with.

Table 1.1: Properties of DME in comparison with some other fuels

<i>Properties</i>	<i>DME</i>	<i>MeOH</i>	<i>LPG</i>	<i>Diesel</i>
<i>Chemical formula</i>	CH ₃ OCH ₃	CH ₃ OH	C2-C5	C3-C25
<i>Boiling point (°C)</i>	-25	64.6	-42	180-360
<i>Cetane number</i>	55-66	5	5	40-55
<i>Density at 20°C g/cm³</i>	0.67	0.79	0.49	0.832
<i>calorific value LHV, kcal/kg</i>	6925	4800	12000	10800

1.4 DME production business

The market size of DME was estimated to reach \$9.7 billion by the end of 2020, and this is distributed into four main sectors: (1) LPG blending, (2) diesel replacement as a transportation fuel, (3) gas turbine fuel in power generation sector, and (4) chemical precursor for different chemicals (for instance, olefins and petrochemicals) [1]. Moreover, DME had registered a compound annual growth rate of 15.67% from 2015 to 2020. China is considered to be the world's largest DME producer utilizing 90% of the total produced DME for LPG blending [5].

1.5 DME production methods

Currently, there are two ways for DME production as shown schematically in Figure 1.1. The first process involves an indirect route, where DME is produced by bimolecular dehydration of methanol over solid acid catalysts. The second method, which is arguably more efficient, is known as the direct synthesis of DME where the synthetic gas (a mixture of H_2 and CO , also known as syngas) is converted directly to DME using heterogeneous hybrid/bifunctional catalysts.

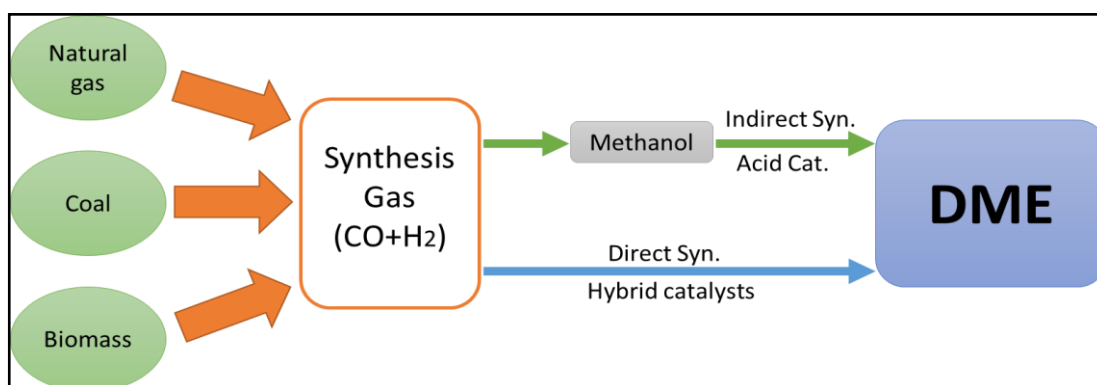


Figure 1.1: Dimethyl ether production diagram

1.5.1 Indirect synthesis

Indirect synthesis refers to DME production from methanol in a dual-step catalytic process in which methanol is firstly produced from the syngas or CO₂ using an appropriate catalyst, namely copper oxide or zinc oxide, then the methanol is purified followed by a dehydration reaction to produce DME according to Equation 1.1. This reaction takes place over solid acid catalysts such as γ -Al₂O₃, ZSM5, HY zeolites and silica-alumina, which are widely used for this process [6].

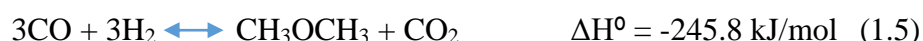
From an industrial perspective, one of the drawbacks for this method is the need of two distillation columns for the separation procedure which makes it an energy-consuming process and hence, more costly. However, in this process, the final product purification is much easier than in the direct single step [7], which is further discussed in the next section.



1.5.2 Direct synthesis

The direct (single step) method is based on combining the two steps described in the indirect synthesis in a single process, where the methanol is synthesized and converted to DME simultaneously in the same reactor using an integrated hybrid catalyst [8]. In this route, the catalyst should be bi-functional and composed of a metal catalyst and a solid acid to promote the two reactions in one pot. Cu/ZnO/Al₂O₃ is a well-established catalyst for this process that exhibits very good activity and selectivity. This method is also known as syngas to dimethyl ether (STD) process since methanol is produced from syngas, which can be manufactured from different sources including natural gas, through steam reforming, coal and petroleum coke, and from biomass [3]. STD was established by Topsoe as vapor

phase process containing three main reactions: water-gas shift reaction (Equation 1.2), methanol synthesis (Equation 1.3) and methanol dehydration (Equation 1.4) [9-11]. The overall reaction is expressed in Equation 1.5.



The STD process gives higher CO conversion in the methanol synthesis step and produces DME at lower costs. However, the final product separation process for high purity DME is relatively more complicated due to the existence of unconverted syngas and methanol, in addition to CO₂. Because of their similar fugacity, CO₂ and DME are difficult and costly to separate. Also, the total reaction of the STD process is highly exothermic therefore, the temperature of the process should be tightly controlled.

Overall, the direct synthesis of DME from syngas is thermodynamically more favorable compared to the indirect method. Furthermore, considering the cost of using a single reactor without the need for methanol purification, storing, and transporting this route could be economically preferred for large scale production [7, 12, 13].

1.6 Catalysis

Catalyzed chemical reactions are the core of many industrial and chemical processes. The catalyst production is also an accelerating industrial process. Therefore, developing an active, efficient and selective catalyst is one of the hottest research areas in the field of energy. Most of the industrial catalysts solid materials

are based on metals or metal oxides. Some catalysts are also based on sulfides or halides of metallic elements or semi-metallic elements, such as boron, aluminium, and silicon. Catalysts are classified into two main groups based on their phases compared to the reactants. Homogeneous catalysts are catalysts that have the same phase of the reactants. The second type of catalysts is heterogeneous catalysts which exist in a different phase compared to the reactants. Heterogeneous solid catalysts have several advantages over homogeneous catalysts including the ease of product separation, better selectivity, and avoiding the need for a large amount of solvents, which makes them more environmentally friendly [14, 15]. Most of the industrial processes, especially energy-related process, involve heterogeneous catalysts which are also the type of catalysts investigated in this project.

1.6.1 Solid acid catalysts

Solid acid catalysts are known to have an essential role in chemical industries. They are widely used in a variety of different energy-related industries, especially in petroleum refining [14]. The surface of solid acid catalysts is rich in acid sites; therefore, they promote surface acid-base reactions. The behavior of these catalysts is determined based on the dominant type of the acid sites, whether they are Brønsted or Lewis acid sites, as well as the strength and number of these sites.

It has been established that the presence of both Brønsted and Lewis acid sites is beneficial to catalyze the methanol to DME reaction. However, the strength and the acidic site density should be within an optimum range, because high acidity may result in the formation of unwanted hydrocarbons and coke, which will eventually lead to catalyst deactivation [16, 17]. One major drawback of solid acid catalysts is deactivation, where they can be easily deactivated by H₂O, H₂S, CO and Pb.

Meanwhile, solid acid catalysts can be modified to inhibit their deactivation and enhance their performance [4].

1.6.2 Catalytic methanol dehydrations

The dehydration reaction of alcohols is known to be promoted by acid catalysts. An ideal solid acid catalyst for methanol dehydration to DME should possess high activity and selectivity for the desired product, good thermal stability, and hydrophobic character. Hence, an important research objective is to develop a stable, robust and water-resistant catalyst that results in minimal carbon and coke formation. Among the different solid acid catalysts that have shown promising activity for this reaction are zeolites and alumina-based catalysts. Besides their appropriate surface chemical properties, these catalysts exhibit high thermal stability, high surface areas, and high porosity. In addition, they are cost-effective materials and therefore, they are the most widely studied materials for this reaction [1, 4, 18].

Among the studied catalysts; γ -Al₂O₃ [19], sulphated zirconia [20], and SAPO zeotypes [21] were found to exhibit good selectivity, but their activities are still low for attractive commercial implementation. While particular types of zeolites are more active and more stable in the presence of water, their product selectivity is relatively poor due to the formation of hydrocarbons and coke [19-22]. Therefore, developing more robust and stable catalytic materials is of great importance.

1.6.2.1 γ -Alumina

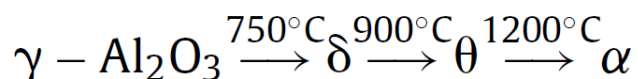
Commercial γ -Al₂O₃ is widely used as a powerful support for different metal catalysts due to its high surface area. Furthermore, γ -Al₂O₃ is an attractive catalyst in many industrially important processes, especially in the petroleum and energy

industries. One of the reactions where $\gamma\text{-Al}_2\text{O}_3$ is considered as a promising catalyst is the methanol dehydration reaction where it shows high activity and selectivity to DME.

These promising catalytic applications of alumina arise from a set of characteristics including its low cost, good thermal stability, high specific surface area, surface acid/base characteristics, and its interaction with metals active phase in the case of its use as a support for metal catalysts [16, 23, 24]. In addition to $\gamma\text{-Al}_2\text{O}_3$, alumina can exist in different phases, up to 7 different structures, that possess different textural and structural properties allowing for its use in a wide range of applications [23].

The most stable form is α -alumina, it possesses superb mechanical, electrical, thermal and optical properties as a result of its stable structure that based on hexagonal close packing of oxygen ions [16, 23]. The other seven metastable phases γ , κ , ρ , η , θ and χ also known as transition alumina, are nano-crystalline by nature. These forms of alumina are widely used as catalysts and as catalyst supports in many industrial processes, particularly in the petroleum refining. The γ -phase is one of the distinct polymorphic phases of alumina with numerous applications. The crystal phase of $\gamma\text{-Al}_2\text{O}_3$ is face-centered cubic (FCC) spinel structure. In this arrangement, oxygen atoms occupy the main positions of FCC structure, and Al^{3+} ions occupy both tetrahedral and octahedral sites. γ -phase alumina shows good catalytic activity and selectivity in methanol to DME reaction compared to other phases. Sung *et al.* [25] had tested the dehydration reaction of methanol with different crystalline phases of alumina and found that $\gamma\text{-Al}_2\text{O}_3$ exhibited the highest activity for methanol to DME conversion compared to its counterparts $\alpha\text{-Al}_2\text{O}_3$ and $\kappa\text{-Al}_2\text{O}_3$.

The formation of γ - Al_2O_3 can be achieved by proper thermal dehydration of hydroxides ($\text{Al}(\text{OH})_3$) or oxyhydroxide like Boehmite (AlOOH) within a temperature range between 400°C to 450°C . Treating it at higher temperatures will lead to the formation of other stable phases [26, 27], according to the sequence as shown below [16].



The heat treatment and calcination temperature are important factors that should be considered during the preparation, as the catalytic activity of γ -alumina for DME production is linked to the acid sites that form during the calcination step. γ - Al_2O_3 has both Brønsted and Lewis acid sites on its surface with moderate to strong acidity. These active sites play an important role in methanol adsorption and dehydration for the DME formation as will be described in Chapter 4. However, the Lewis acid sites and the hydrophilicity of alumina surface results in adsorbing of water molecules which can compete with other reactants at the active site that leads in catalyst poisoning and blocking the active sites [28]. In methanol dehydration, water is bi-product and can affect the catalytic activity as it can compete with methanol on the adsorption sites on alumina surface resulting in some deactivation [29, 30]. Therefore, developing a practically efficient catalyst necessitate more studies in two directions: First, understanding and reducing the effect of factors that limit its performance. Second, modifying its textural and chemical properties by doping with other elements in efforts to enhance its performance.

1.6.2.2 Zeolites

Zeolites are another type of solid acid catalysts that have shown promising catalytic activity and are widely studied and implemented in the dehydration reaction of methanol to DME. Zeolites are porous crystalline aluminosilicate, synthetic or naturally occurring, which usually have high surface areas due to the well-ordered pores network in their structures. They are made of silicates SiO_4 and aluminates AlO_4 that are tetrahedrally linked via oxygen atoms. Zeolites have extensive industrial uses as catalysts or as adsorbents, particularly in the petrochemical industry. Their different applications arise from their unique structure, thermal stability and large surface areas. In addition, zeolites have molecular-sized pores i.e. micropores (0.4-1.3 nm) [31], thus, zeolites could be used as molecular sieves in which the molecules will be separated based on their size and shape. However, the narrow micropores hinder diffusion and reactants flow which may affect their catalytic activity [7, 32].

Zeolites surfaces have both Lewis and Brønsted acid sites. Zeolite acidity arises from the presence of aluminum ions where the four-valent silicon atom is replaced by three-valent aluminum atom resulting in a charge difference for which a counter ion is needed to compensate for the charge difference. If the counter ion is a proton, a Brønsted acid site is formed. On the other hand, if a tetravalent transition metal is substituted into the framework, that metal site can act as a Lewis acid. Generally, the distribution, strength, and the number of these acid sites are the main factors that affect zeolites catalytic activity [1, 32, 33].

Having strong acid sites enhances the methanol dehydration reaction and conversion at low temperature, also they increase the preference for MeOH

adsorption over water which will minimize the water poisoning effect that would lead to deactivation. However, these sites are the main contributors in zeolites deactivation as they promote unwanted side reactions that form olefins, coke and hydrocarbons that result in blocking the pore structure [7].

There are different existing types of zeolites and many of them were used as solid acid catalysts, namely ZSM5, HZSM5, Y, FER and mordenite, which have shown good methanol to DME conversion and selectivity. Among all studied zeolites, Zeolite Socony Mobil-5 (ZSM5) is one of the most studied and the best catalyst reported for this reaction [34].

Literature reports show that three main factors affect zeolites catalytic activity; zeolites structure (size and shape of pores), the identity of cation for charge balance and framework of heteroatom substituent. The used cation could be monovalent or divalent and each one of them has its unique industrial application. Copper exchanged zeolites, as an example, are used for selective catalytic reduction of NO_x for exhaust gas cleanup. Nickel exchanged zeolites can be used to promote oligomerization. Sodium exchanged zeolites can be used as Lewis acids, such as their use in catalyzing dehydration of methyl lactate [35].

Another important characteristic of zeolites that plays a crucial role in their catalytic activity is the Si/Al ratio. Different Si/Al ratios result in different acidic properties. It has been reported that the activity of zeolite for methanol to DME conversion could be enhanced by decreasing the Si/Al ratio, which means increasing the overall surface acidity [36, 37].

1.6.2.3 Other catalysts

There are some other catalysts that have been studied for the dehydration process of methanol to DME, other than alumina and zeolite. Said *et al.* [38] investigated sulfated zirconia for this reaction and they found that under certain conditions sulfated zirconia is an efficient catalyst for the synthesis of dimethyl ether with high yield (83%) and excellent selectivity (100%). In another study, Vishwanthan *et al.* [39] tested a series of TiO₂-ZrO₂ mixed oxides with different molar ratios at temperatures in the range of 280-340°C, where the studied catalysts achieved good selectivity and high stability for temperatures below 300°C. Different silica-titania mixed oxide have also been tested for the methanol dehydration reaction, and they were found to have low catalytic activity [40].

Recently, polymeric heterogeneous catalysts, namely nafion resin, have attracted a great attention in DME synthesis. The nafion catalysts provide 40% methanol conversion with no catalyst deactivation and without coke formation. Aluminum phosphate (AlPO₄) has also been studied as a promising catalyst for the conversion of methanol to DME and it showed a relatively small amount of coke deposit and good water adsorption resistance [7]. These catalysts are composed of γ -Al₂O₃ modified with phosphorous, where their catalytic activity was found to depend on the preparation method, activation temperature and chemical composition, Al/P molar ratio [7]. Table 1.2 shows the most studied catalysts for the DME synthesis in the last decade.

Table 1.2: A literature survey of the most studied catalysts for methanol to DME conversion during the last decade

Catalyst	Pressure (atm)	Temperature °C	wt. Catalyst g	Conversion %	Selectivity %	Ref.
FER zeolite	1	240	0.07	85	100	[33]
RHO zeolite	-	200	-	93	100	[34]
FER zeolite	1	180	-	38	100	[36]
Sulfated zirconia	1	230	0.5	83	100	[38]
CuO—PdO/ γ -Al ₂ O ₃	1	250	0.2	80	100	[41]
CuO—PdO/ γ -Al ₂ O ₃	1	300	0.2	88	100	[41]
γ -Al ₂ O ₃	1	300	0.2	100	90	[41]
ZSM5	29.5	250	3	95	54	[41]
H-ZSM5	4	240	0.5	80	100	[41]
FER-10	-	200	-	80	100	[41]
Bmim ₃ PMo ₁₂ O ₄₀	-	250	0.05	80	100	[41]
Nb/TiO ₂	-	300	0.5	11.3	93	[41]
Hierarchical zeolite CaA	1	400	0.2	58	100	[42]
Zr loaded activated carbon	1	400	0.2	69	95	[43]
ZrO ₂ supported activated carbons	1	400	-	70	96	[44]
γ -Al ₂ O ₃	1	300	0.15	83	100	[45]
Cu/sulfated zirconia	1	275	0.5	87	100	[46]
P/Al ₂ O ₃	1	300	0.15	94	100	[47]
ZSM5	1	300	-	84	100	[48]
MgO/HZSM5	9.9	210	-	87	100	[49]
Al ₄ B ₆ O ₁₅	9.9	300	0.3	12.6	99.9	[50]
AlPO ₄ /ZSM5	1	300	1	84	89	[51]
ZrO ₂ - γ -Al ₂ O ₃	1	230	0.5	87	100	[52]
CuO—Fe ₂ O ₃ / γ -Al ₂ O ₃	1	290	0.15	70	100	[53]
C-PO ₃	1	300	0.2	20	95	[54]
γ -Al ₂ O ₃	2	330	-	82.6	99.9	[55]
CuO/ γ -Al ₂ O ₃	49	250	1	65	60	[56]

Table 1.2: A literature survey of the most studied catalysts for methanol to DME conversion during the last decade (continued)

Catalyst	Pressure (atm)	Temperature °C	wt. Catalyst g	Conversion %	Selectivity %	Ref.
ZnO-CuO/Al ₂ O ₃	1	300	0.1	80	75	[57]
SAPO-11	-	300	0.3	80	90	[58]
SAPO-11	1	250	0.4	84	100	[59]
FER-8	1	240	0.7	90	92	[60]
SBA-15	1	300	0.1	80	100	[61]
FER-zeolite	1	200	0.7	80	95	[62]
γ-Al ₂ O ₃	1	300	-	83	99.9	[63]
Al ₂ O ₃ /SBA-15	1	350	0.2	80	99	[64]
γ-Al ₂ O ₃ /Nb ₂ O ₅	1	240	-	77	99.9	[65]
polymer/ceramic membrane	1	180	-	37	100	[66]
HSiW/TiO ₂	1	180	0.2	80	100	[67]
γ-Al ₂ O ₃	1	250	0.4	90	100	[68]
WO _x /TiO ₂	-	300	0.5	15	87	[69]

Chapter 2: Catalysts Preparation and Characterization

This chapter describes the experimental procedures employed in the catalyst's preparation and characterization. It also describes the characterization results including the catalyst's morphological, textural, and surface chemical properties.

2.1 Introduction and overview

Choosing a suitable preparation method for a catalyst synthesis is critical as it usually shows a significant impact on the textural properties and the catalytic activity of the catalyst [16, 70]. Very often, different parameters within the same method could also affect the product properties [71]. Therefore, several factors should be considered including the preparation route, the reaction temperature, the pH of the starting solutions, and the calcination temperature of the prepared materials [17].

2.1.1 Brief review of common preparation methods

Different methods for preparing doped solid catalysts have been reported in the literature. The most common methods include sol-gel, co-precipitation, wet impregnation, gas-phase deposition and combined co-precipitation-ultrasound [7, 72].

Co-precipitation and sol-gel are currently the most widely used methods for preparing alumina-based catalysts [73]. Co-Precipitation method refers to the formation of a sparingly soluble solid phase from a liquid solution phase. On the other hand, the sol-gel method is usually defined as the construction of an oxide network through polycondensation reactions of a molecular precursor in a liquid. The term 'sol' refers to the stable dispersion of colloidal particles in a solvent which collides and agglomerate to form the gel that consists of a three-dimensional

continuous network. For the last decade, sol-gel became more adopted compared to other preparation methods. One study showed that nanoparticle of γ -Al₂O₃ prepared by a sol-gel method had a noticeable enhancement in the catalytic activity compared to its counterpart prepared by a precipitation method [7].

2.1.2 Sol-gel process

Sol-gel processing was initially developed as a tool for controlling the texture of metal-oxide (MO_x) phases. Recently this technique has become a universal method for the preparation of catalytic materials. The typical sol-gel process starts with dissolving a precursor of the desired compounds (e.g. metal salts or alkoxides) in an alcoholic solvent. For instance, alumina could be prepared by dissolving commercially available aluminium alkoxide (e.g. Aluminum-tri-sec-butoxide) in 2-propanol followed by the addition of water for hydrolysis. Deprotonation of the metal cation intermediate takes place resulting in the formation of metal hydroxides (M–OH–M), which condenses further (gelation) leading to form M–O–M polymeric framework. Generally, the morphology of the final product ranges from discrete particles (sol) to continuous polymer networks (gel), and nanoparticles. The desired morphology of the final product could be obtained by controlling the reaction temperature, duration, pH, and aging time. Therefore, these factors should be taken into account based on the type of application for the prepared material [17, 74]. The aging step of the gel is needed as an extension of the gelation process in which the gel network is fortified by an additional polymerization that can be controlled by changing the temperature and the type of the solvent [75].

After the gelation is complete, the gel is dried at an appropriate temperature to remove the solvent, water and any other by-products. Finally, the dried product is

thermally treated (calcined) at elevated temperatures (usually above 400°C) for 3-6 hours to obtain the final metal oxide product such as aluminium oxide that is obtained from its hydroxide gel. The conditions of this step play a key role in controlling the textural property of the final product. Mostly, conventional drying to form xerogel is used, although this method gives lower surface area and smaller pore volumes compared to the supercritical drying which results in an aerogel with significantly higher surface area and porosity. However, owing to the lower cost and easier processing of conventional drying, it becomes very often more convenient to use [75, 76].

2.1.2.1 Advantages of sol-gel method

There are several inherent advantages of the sol-gel method. For instance, its usually carried out at room temperature which provides the ability to use a wide range of starting materials. It also gives better homogeneity of materials, especially the synthesis of multi-components since its initiated with a solution of all needed precursors, which very often allows the synthesis of innovative and functional materials with advanced applications in different areas.

The textural properties (surface area, porosity, particle size and shape) of the prepared material could be effectively controlled by manipulating some of the process parameters like precursor, calcination temperature and pH [74]. Also, as previously stated, catalysts prepared by sol-gel method very often show better activity, which could be a consequence of unique textural properties such as higher porosity and better pore size distribution, as well as larger surface area compared to catalysts prepared by other methods [7]. Another significant advantage of sol-gel is the low production cost that makes it even more attractive. Moreover, in the

preparation of doped metal oxides, this technique perfectly controls the dopant content within the final product composition, where the dopant is introduced into the starting solution and ends up finely dispersed in the final product. Even a small amount of the dopant, such as organic dyes and rare earth elements, could be introduced and ends up nicely dispersed in the final product [74, 77].

Historically, the use of sol-gel technology has been introduced in the mid-1800s. In the last decade, the sol-gel method started to attract more attention as it could be applied under extraordinarily mild conditions. Therefore, it got involved in an enormous number of applications in different areas to produce materials of different sizes, shapes and formats (e.g., fibres, films, monoliths, and nano-sized particles). The obtained products from this technique are utilized in different fields such as energy, biotechnology, optics, electronics, health, pollution, and medicine. It can also be employed to produce products of different types of materials like inorganic pigments, drugs, magnetic nanoparticles and catalysts [74].

2.1.2.2 Literature overview of the sol-gel method

Sol-gel method was investigated as a route to prepare metal oxide dielectric films for high-performance electronic devices as was reported by Park *et al.* [78]. One of the aims of the researchers in this field is to develop a cost-effective method, taking into consideration time and complexity. While solution-based deposition was one of the most common procedures for this purpose, sol-gel method was not widely used in this field until the last decade where significant improvements in sol-gel technology were made toward a wide range of applications, particularly for metal oxide materials. Since then, the sol-gel method has played a central role in fabricating a new generation of high-performance printed electronic systems [78].

Silicon doped alumina thin films with a glass-like structure derived via the sol-gel process is an example in electronic applications. In these materials, the sol-gel processing helped in enhancing the homogeneity of the composite structure and in promoting ionic transportation to fix the defects of the alumina films [79]. In another study, the effect of doping was investigated for the electrical stability of Al-doped zinc oxide (AZO) as they are one of the promising alternatives to tin-doped indium oxide (ITO), which is used in different optoelectronic applications such as in spectro-electrochemistry [80]. The investigators in this study investigated the resistivity and stability of AZO thin films prepared by sol-gel method. The results showed an improvement in the stability of AZO films that were prepared at high annealing temperatures compared to ITO.

In the field of catalysis, the sol-gel method is widely employed for the preparation of mixed metal oxide and doped metal catalysts. The term doping here refers to the insertion of foreign element (usually metal) atoms in the inorganic network of the metal oxides for different purposes. For instance, alumina could be doped with different metals for the formation of active sites with distinct functionality or to promote the formation of a desirable phase structure. Desired modification by doping may include shifting phase transformation temperature or stabilizing the phase and suppress transformation to achieve optimized physical and chemical properties [79, 80]. As an example, in one study Ln doping in alumina stabilized the phase of alumina lattice by delaying the transformation of the phase ($\theta \rightarrow \alpha$) through increasing the phase transformation temperature by a notable magnitude [81].

In another study, sol-gel-prepared magnetic iron oxide, γ -Fe₂O₃, doped with titanium showed unique structural as well as textural properties including small particle size, around 5 nm, and high surface areas as well as large porosity. This phase of iron oxide is an essential material for different advanced applications including recording materials. It was also found that doping suppresses the transformation to alpha iron oxide, α -Fe₂O₃, which also has different applications, especially when fabricated in nanoscale particles, including their use in pigments and catalysis. Sol-gel-prepared magnetic nanoparticles have other advanced applications in the medical field such as bio-sensing, drug-delivery and as a therapeutic agent [81, 82].

In sol-gel preparation, there are several variables that affect the final product's activity and other properties. One of the most important variable is the precursor, which plays a vital role in the properties of the final product, especially metal oxides and mixed oxides [81, 83, 84]. For example, γ -Al₂O₃ could be prepared from different precursors such as aluminum *tri-sec*-butoxide (C₁₂H₂₇AlO₃), aluminum nitrate (Al(NO₃)₃) or aluminum chloride (AlCl₃). Owing to that, several studies have investigated the effect of the precursor on the catalytic activity of the prepared catalysts [85, 86]. Osman *et al.* [16] reported a study where they compared two of the readily available precursors to prepare γ -Al₂O₃ and they found that γ -Al₂O₃ prepared from aluminum nitrate precursor showed higher catalytic activity compared to the one prepared from aluminum chloride precursor under the same reaction conditions [16]. Similarly, Khaleel *et al.* [76] examined the preparation of γ -Al₂O₃ doped with Cr³⁺ and Cu²⁺ ions from three different precursors and he found that the type of precursor affects structural, textural and morphological properties of the catalysts. The study examined doping γ -alumina with different concentration of

Cr^{3+} and Cu^{2+} using three different precursors (acetyl acetonate, nitrate, and chloride), where the acetyl acetonate gave better results in terms of surface area, particle sizes and enhanced resistance to sintering. It was also found that for preparing bulk doped alumina with large metal loading, the acetyl acetonate precursor would be preferred over the nitrate and chloride [76].

Calcination conditions, especially temperature, is another preparation parameter that usually has a significant effect on the product's morphology and textural properties. Calcination is defined as a process of heating a substance under controlled temperature and in a controlled environment [88], which is usually described as heat treatment in air. This process is a crucial step for different aspects, as it controls the phase-type of the final product and has a noticeable effect on the crystal size, particle size distribution, surface area, porosity, magnetic properties, and the surface acid-base properties. There is a significant number of literature reports that has been published describing these effects on different catalytic applications [88-93]. The calcination conditions that have an impact on the product's properties include the temperature, time, heating rate and the steps involved, whether it is a single step or multi-steps heating. For example, it has been shown that for alumina, the surface area increased by increasing calcination temperature till it peaks around 500°C before it starts to drop again with increasing the temperature, which is due to the change of alumina structure and to the sintering process [88, 89, 94]. Concerning the calcination effect on porosity, it has been suggested that the average pore diameter would increase with increasing calcination temperatures and heating rate. On the other hand, the pore volume will decrease. However, the particle size usually increases until the pore structure collapses, and this mainly occurs when $\gamma\text{-Al}_2\text{O}_3$ is

calcined at temperatures above 1000°C. Moreover, increasing the calcination time usually enhances phase transformations [91].

The surface acidity of alumina was also found to be influenced by the calcination conditions. A study on the effects of the heating rate on the surface acidity suggested that the acid sites concentration increases with increasing heating rate as a result of the thermal shock that is caused by the high heating rate which fastens the dehydration process, creating structure and surface defects leading to the formation of more acid sites [92]. Another study also reported that the surface acidity increases with increasing the heating rate, which was referred to the increased number of Al^{+3} occupying the tetrahedral holes rather than octahedral [96]. However, the opposite is true when considering the effect of the temperature on the acidity as it has been reported that at higher calcination temperatures the amount of desorbed ammonia (which adsorbs on acid sites) dropped heavily indicating less acidity of the catalyst surface [94, 96].

2.1.3 Characterization techniques

The development and advancement in various materials characterization techniques helped in providing useful information and a better understanding of materials properties and performance in different applications. The following sections describe the main techniques that have been used in this study and their features.

2.1.3.1 Powder x-ray diffraction (XRD)

Characterization of the catalysts composition and their degree of crystallinity using powder X-ray diffraction (XRD) is an essential step before examining the

catalyst, in order to confirm having the desired structure of the employed catalyst. XRD is a nondestructive technique that provides detailed information about the crystallographic structure and the chemical composition of materials [98]. Even though the technique is usually termed as “powder diffraction” but it is not limited to powder samples only. Any single-crystalline or polycrystalline sample could be analyzed with this technique, together with monolithic solids, thin films, and powders. XRD is applied in different fields, including pharmaceuticals characterization, determining, and classifying minerals structures, and determining the structure of all crystalline solids. It is an essential research tool where its applications include [99]:

1. Phase identification: where the diffraction pattern act as a unique fingerprint of the phase
2. Quantitative phase analysis: where the size and shape of the unit cell, of any crystalline material, can be determined and then refined to very high accuracy.
3. In-situ analysis: where the analysis could be carried out under controlled conditions (i.e., atmosphere, temperature, pressure, and electrical field), which helps in monitoring the change in the material and allows for conducting kinetic studies.

The working principle of XRD is based on the diffraction of monochromatic X-ray beam which is high-energy electromagnetic radiation with a relatively short wavelength that is similar to the distance between atoms in a crystal. This radiation is usually emitted from Cu K α , which is the most commonly used source, which gives radiation with $\lambda= 0.15406$ nm.

In a typical X-ray diffraction experiment, the sample is placed on a holder that held in the way of the X-ray beam. The X-ray tube and the detector will move simultaneously in synchronized motion and the output signal will be recorded in the diffractogram which represents the intensity of the diffraction peaks as a function of the diffraction angle, 2-theta [99]. The radiation will hit the sample at a certain angle (theta) some of the radiation will be absorbed while the other will be reflected and diffracted in a different angle, 2-theta, this phenomenon is known as elastic scattering. The emitting angle (2-theta) represents the angle between the incident and diffracted beam, as shown in Figure 2.1.

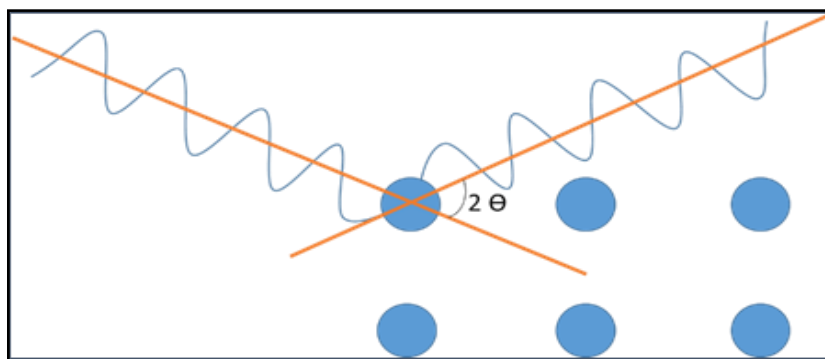


Figure 2.1: Graphical illustration of the 2-theta angle between the incident and reflected beam

The diffraction occurs when the scattered waves from an object constructively and destructively interfere with each other. The resultant peaks in the outcome diffractogram indicate that a constructive interference (in-phase) because of the highly ordered atoms. In contrast, when there are no peaks in the diffractogram, it simply means that the atoms or ions are not highly ordered over a long range, thus the waves are out of alignment resulting in destructive interference (out of phase).

2.1.3.2 Catalyst surface acidity assessment using TPD

A temperature programmed desorption (TPD) technique was developed particularly in the field of catalysis, where it was designed to provide information about acid sites density and strength of the solid surface. In addition, studying the interaction between the reaction gases and the solid surface could be applied to understand the mechanism of catalytic reactions [100]. One common application of TPD is temperature programmed desorption of ammonia (NH_3 -TPD). NH_3 -TPD is a well-established technique for characterizing catalyst acid sites concentration due to the basic nature of ammonia which allows it to bind with acidic sites on the surface. Also, the desorption of ammonia versus temperature is used to assess the strength of interaction, which indicates the strength of the acid sites. However, NH_3 -TPD can't distinguish between different types of acid sites. Therefore, the adsorption of other probes such as pyridine using FTIR spectroscopy is commonly used to distinguish between the different types of acid sites.

The working principle is simple where it is totally based on the chemisorption of a probe molecule (NH_3 in the NH_3 -TPD case) on the solid surface followed by desorption under heating in a temperature-programmed manner using a linear ramp. The area under the desorption curve can be used to calculate the number of acid sites using a calibration curve based on measuring pure ammonia in a blank experiment. The adsorption of ammonia occurs as one molecule per acid site; therefore, the ammonia concentration per catalyst mass can be used to determine the total acid sites concentration in the catalyst sample. The temperatures at which desorption occurs indicate the strength of the acid sites.

2.1.3.3 Gas physisorption for surface area and porosity characterization

Gas physical adsorption can be used to measure the surface area, pore volume, and pore size distribution of solid materials. These textural characteristics are essential parameters in heterogeneous catalysts where they usually have a significant impact on the catalytic activity, adsorption properties, and permeability of reactants and products of a reaction.

In this technique, the sample should be solid, and the analysis time varies depending on the surface area and the porosity of the sample as well as the rapidity with which the instrument achieves equilibrium. In a typical experiment, a mixture of nitrogen gas with a nonadsorbing ideal carrier gas (usually He) is allowed over the sample in a special glass cell at liquid nitrogen temperature, -196°C . The pressure of N_2 is gradually increased over the sample and the amount of gas needed to form a monomolecular layer on the solid surface can be determined from the volume of the gas adsorbed on the surface and the measured adsorbed volume is correlated with the solid surface area using BET (Brunauer, Emmett and Teller) theory, which predicts a linear relation when an appropriate function of the pressure P , saturation pressure P_0 and the adsorbed gas volume V is plotted against the relative pressure P/P_0 (Equation 2.1) as follows:

$$\frac{P}{V(P_0 - P)} = m \frac{P}{P_0} + b \quad (2.1)$$

The adsorbed gas in pores of smaller radii is bound more tenaciously to the surface and therefore condensation in micropores takes place at low relative pressures. Similarly, condensation in larger pores takes place at higher relative pressures. Plotting the volume of the gas adsorbed versus relative pressure gives

information about the nature of the pores and the pore size distribution in the material.

2.1.3.4 Transmission electron microscopy (TEM)

TEM is another essential powerful technique that is used in studying and analyzing the material's morphology by analyzing the transmitted electron intensities as well as the characteristic X-rays and the energies lost from the incident beam. Most solid materials could be studied using TEM with some restrictions that are related to technical constraints and large scattering of the electrons in solid samples. For that reason, the diameter of the sample shouldn't exceed 3 mm and its thickness should be less than 100 μm in order to have a transparent sample for successful analysis. Producing thin samples could be achieved with different techniques that are developed for this purpose such as ion milling, electropolishing, spraying or dusting.

In TEM, a high-energy beam of electrons is generated using tungsten film, a LaB₆ crystal or a field emission gun. The generated beam and the resultant diffraction pattern (transmitted beam and several diffracted beams) could be imaged on a fluorescent screen. From the diffraction pattern, the information about lattice spacing and symmetry are obtained for the desired sample. In addition, this technique is capable of providing a magnified image of the sample using the transmitted beam or one of the diffracted beams which will give information about the microstructure of the material including the size and shape of the particles. Therefore, TEM is an informative technique for studying topographical, morphological, compositional, and crystalline information of different materials. It can be utilized in a variety of different scientific, medical, educational, and industrial fields.

2.2 Experimental methods

2.2.1 Catalyst preparation

Pure and doped γ -Al₂O₃ catalysts were prepared using a template-free sol-gel method. Aluminium tri-sec-butoxide and titanium(IV) n-butoxide were used as precursors for the preparation of alumina doped with titanium, and 2-propanol was used as a solvent. Composites containing different dopant concentrations of 2%, 3%, 5%, 10%, and 15% were prepared and will be represented by the general formula AlTiX where X refers to the dopant molar percentage. In a typical preparation, 10 mL (0.0393 mol) of aluminum tri-sec-butoxide was dissolved in 80 mL 2-propanol and the required amount of Ti precursor was dissolved separately in 40 mL of the same solvent. The beakers were capped to prevent any possible hydrolysis and oxidation of aluminium tri-sec-butoxide. The two solutions were mixed by adding the Ti precursor solution to that of Al to minimize its exposure to air, as shown in Figure 2.2. The mixture was stirred for 15 min before the stepwise addition, under continuous stirring, of a stoichiometric amount of deionized water for hydrolysis. The amount of water was based on H₂O:Al ratio of 3:1 plus an excess amount of 20%. The mixture was stirred for 4 hours giving a colloidal gel, which was then aged for 24 hours at room temperature. The solvent was removed by evaporation in a water bath at 80°C and the obtained powder was dried in an oven at 120°C, 250°C, and 350°C for 1 hour at each temperature followed by calcination at 500°C for 4 hours. The same steps were followed for the preparation of other catalysts using different precursors for different dopants, where Ni(NO₃)₂·6H₂O and VCl₃ were used as precursors of Ni(II) and V(III), respectively.

For comparison, titanium(IV) oxide supported on alumina was prepared by the wetness impregnation method [101]. In a typical experiment, 12 mg of titanium(IV) n-butoxide were dissolved in 10 ml of 2-propanol and mixed with 4 g of commercial alumina giving a paste-like mixture. After mixing thoroughly, the mixture was dried overnight at room temperature then was dried in an oven at 120°C and 300°C for 1 hour at each temperature, followed by calcination at 400°C for 2 hours.

ZSM5 zeolites with different Si/Al ratio were purchased from Tianjin Hutong Global Trade Co., Ltd., China, and were used without any further treatment. Commercial alumina, CM- γ -Al₂O₃, was obtained from SASOL North America Inc.

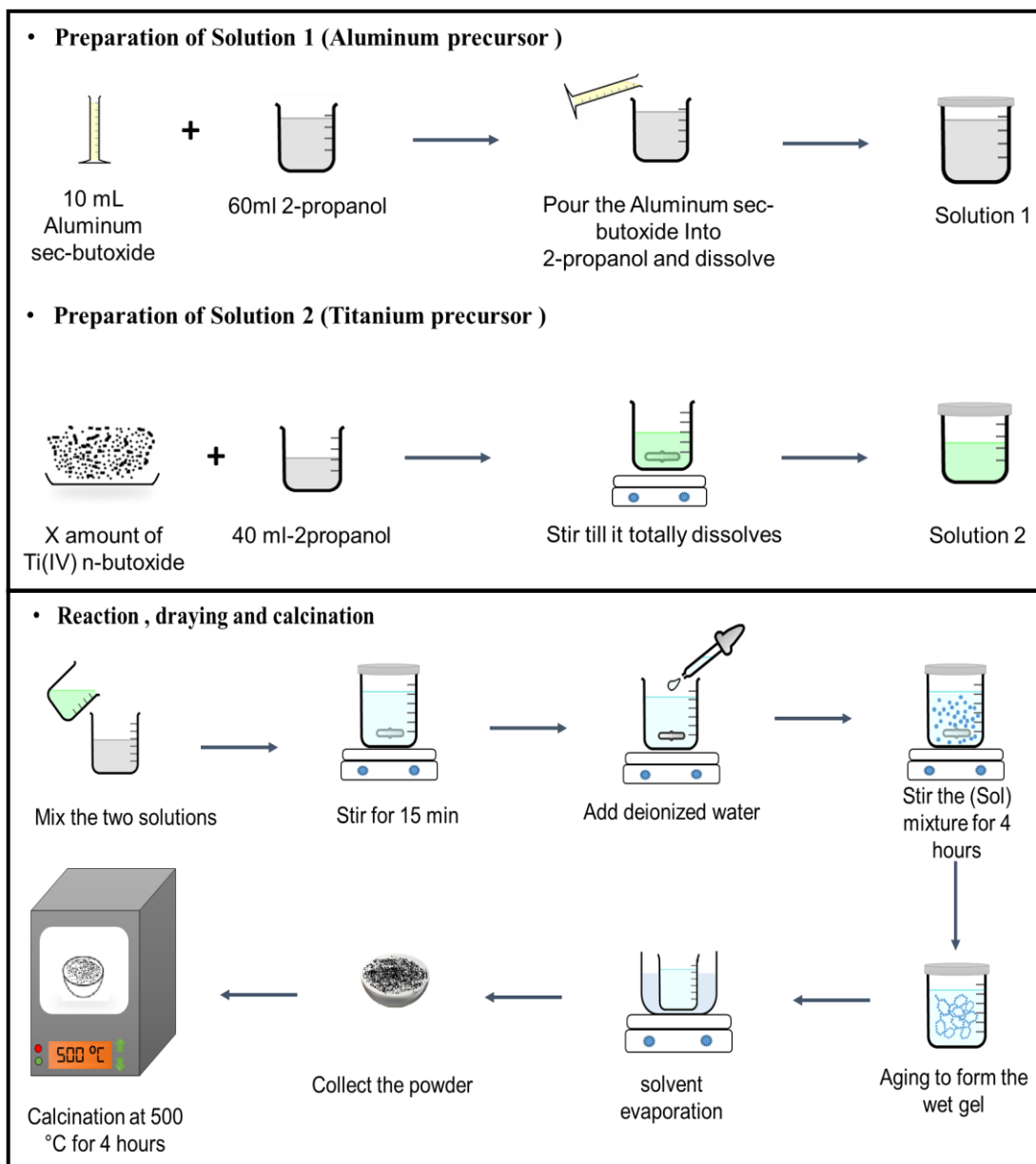


Figure 2.2: Scheme of the steps of preparation of AlTiX% as an example

2.2.2 XRD characterization

XRD patterns were obtained using a Shimadzu-6100 powder XRD diffractometer with Cu-K α radiation, $\lambda = 1.542 \text{ \AA}$, operating at a voltage of 40 kV and 30 mA current. The data were collected in the 2θ angle range of 20-80 deg., at a rate of 1 deg./min and 0.02° step size. Before the analysis, the sample was grinded well to a fine powder using a mortar and pestle. The sample was placed in an

aluminium holder with a diameter of 2.5 cm which was held firmly in its place in the XRD instrument.

2.2.3 Temperature programmed desorption (TPD)

NH₃-TPD was performed on a ChemBET TPR/TPD chemisorption instrument from Quantachrome equipped with a thermal conductivity detector. Each sample, 150 mg, was pretreated prior to adsorption in a fixed-bed quartz U-tube at 350°C for 80 min under helium flow of 30 mL/min. Then the sample was cooled down to 30°C under 75 mL/min of He to stabilize the signal. After cooling down, the sample was saturated with NH₃ using 30 mL/min flow of ammonia for 15 min. The sample was then purged under 30 mL/min of He for 30 min. The temperature was then ramped from 30°C to 800°C at a heating rate of 10°C/min under He flow at a rate of 30 mL/min. The amount of ammonia desorbed during the process was quantified with a TCD detector.

2.2.4 Surface area and porosity measurements

Surface areas measurements and pores characteristics were obtained using N₂ sorption at 77 K on a TriStar II volumetric gas sorption instrument from Micrometrics. Before measurements, samples were degassed at 200°C for 2 hours. Brunauer-Emmett-Teller (BET) theory was used for surface area calculation and pore size distributions were determined by Barrett-Joyner-Halenda (BJH) model based on the desorption branch of the N₂ isotherms.

2.2.5 TEM analysis

TEM images were obtained using a CM10 Philips electron microscope, where an ethanol suspension of the samples was deposited on a carbon film attached to a copper grid.

2.3 Results and discussion

2.3.1 Structural characterization

Figure 2.3 shows the XRD patterns of the prepared γ -Al₂O₃ and Ti-doped counterparts of different compositions after calcination at 500°C. The pure alumina samples always showed a well-defined γ -Al₂O₃ structure with characteristic broad Bragg reflections at 46° and 67° 2 θ [102].

Interestingly, the presence of Ti(IV) ions in concentrations up to 15% did not result in any detectable crystalline titanium oxide phase as indicated by the absence of any peak for TiO₂, which is usually very crystalline after calcination at the employed temperature, 500°C. The absence of segregated TiO₂ indicates the well dispersion of the dopant ions in the alumina network structure. In addition, the dispersion of the Ti ions in the alumina lattice is indicated by the enhanced amorphous nature of the composites where the dopant ions act as an impurity that hinders crystallization.

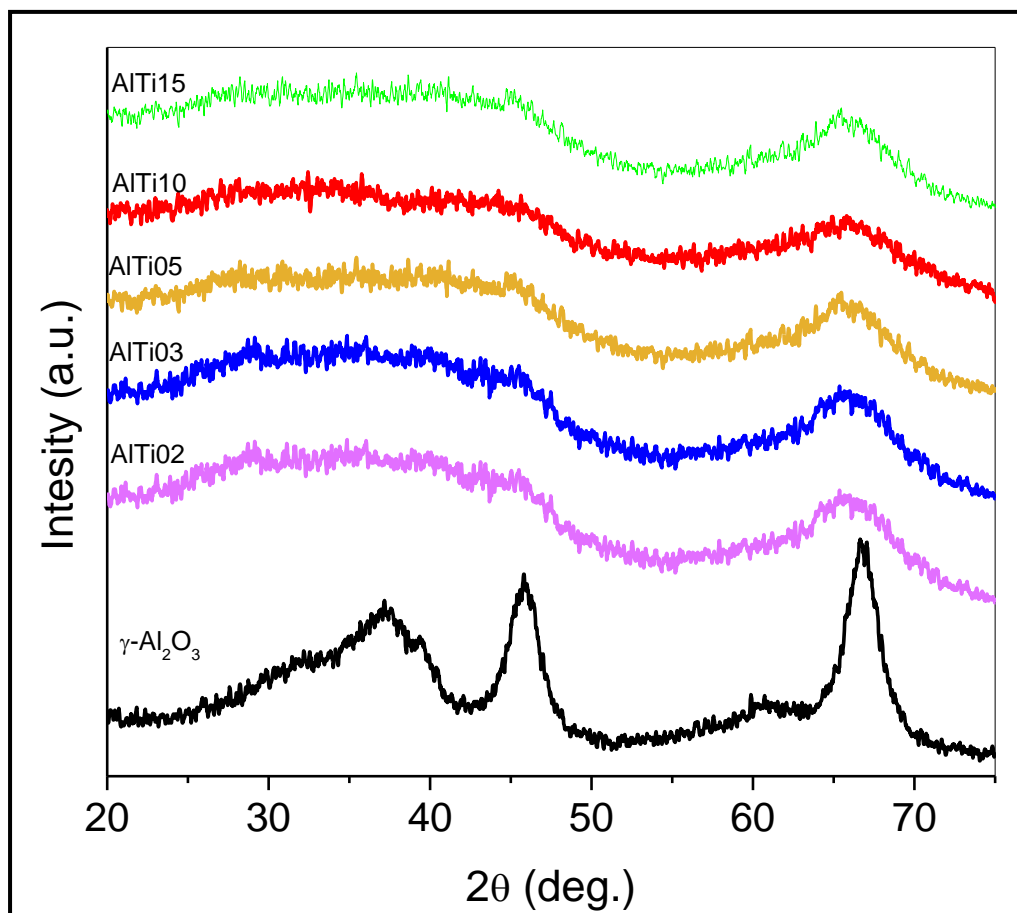


Figure 2.3: XRD patterns of $\gamma\text{-Al}_2\text{O}_3$ doped with Ti ions and undoped $\gamma\text{-Al}_2\text{O}_3$ after calcination at 500°C

Figure 2.4 represents XRD patterns of the prepared Ni-doped $\gamma\text{-Al}_2\text{O}_3$, where they showed very similar behavior to their counterparts of Ti-doped alumina. In the patterns of these composites, no peaks are observed for nickel oxide in the presence of Ni(II) ions in concentrations up to 10%. In addition, NiAl_2O_4 was prepared using a concentration of 33% Ni to compare its catalytic activity with the Ni-doped alumina samples, and its XRD pattern showed its formation as shown in Figure 2.5. Figure 2.6 shows the XRD pattern of the two studied zeolites samples, which match their reported reference patterns [103, 104]

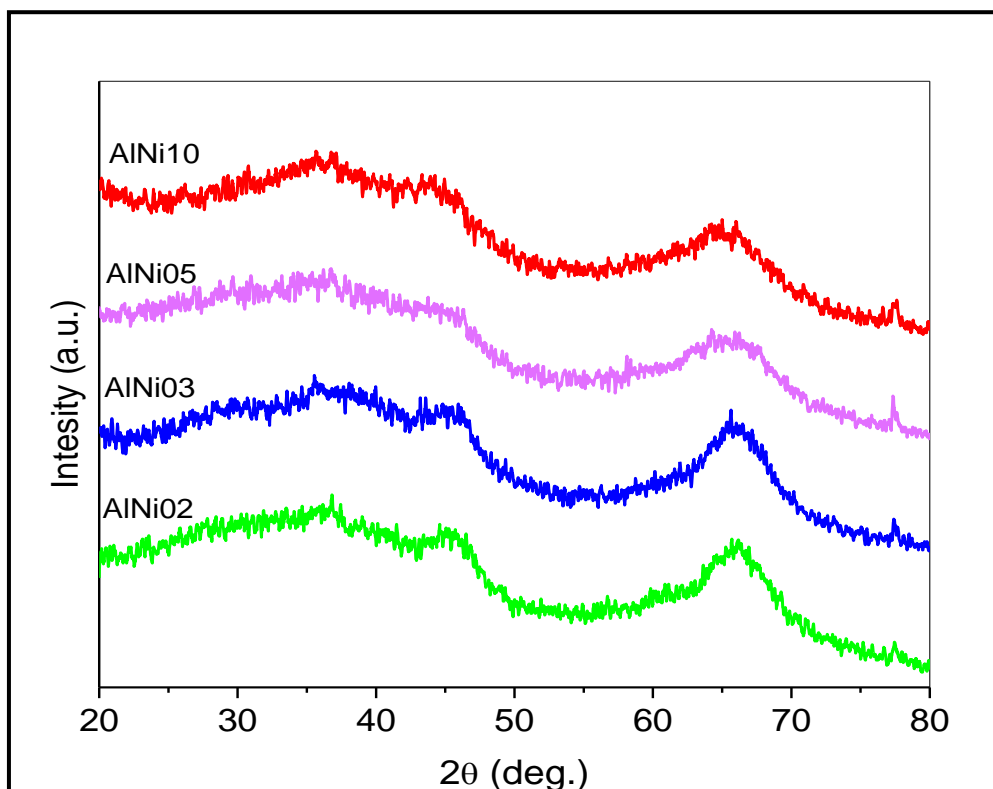


Figure 2.5: XRD patterns of γ -Al₂O₃ doped with Ni ions after calcination at 500°C

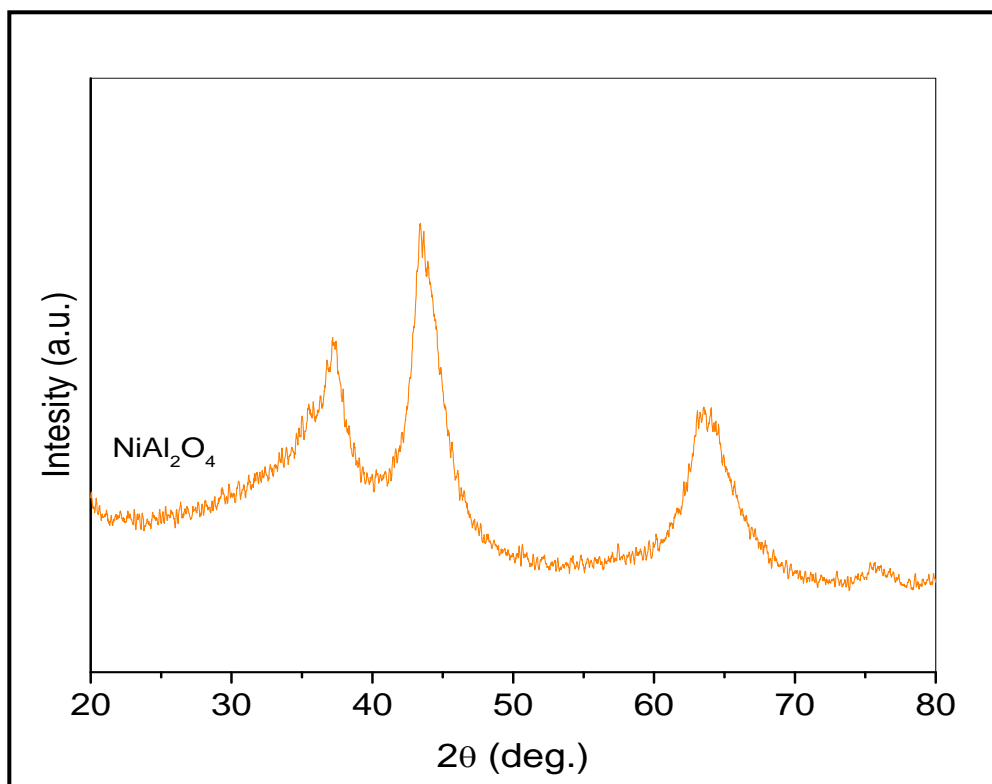


Figure 2.4: XRD pattern of NiAl₂O₄ after calcination at 500°C

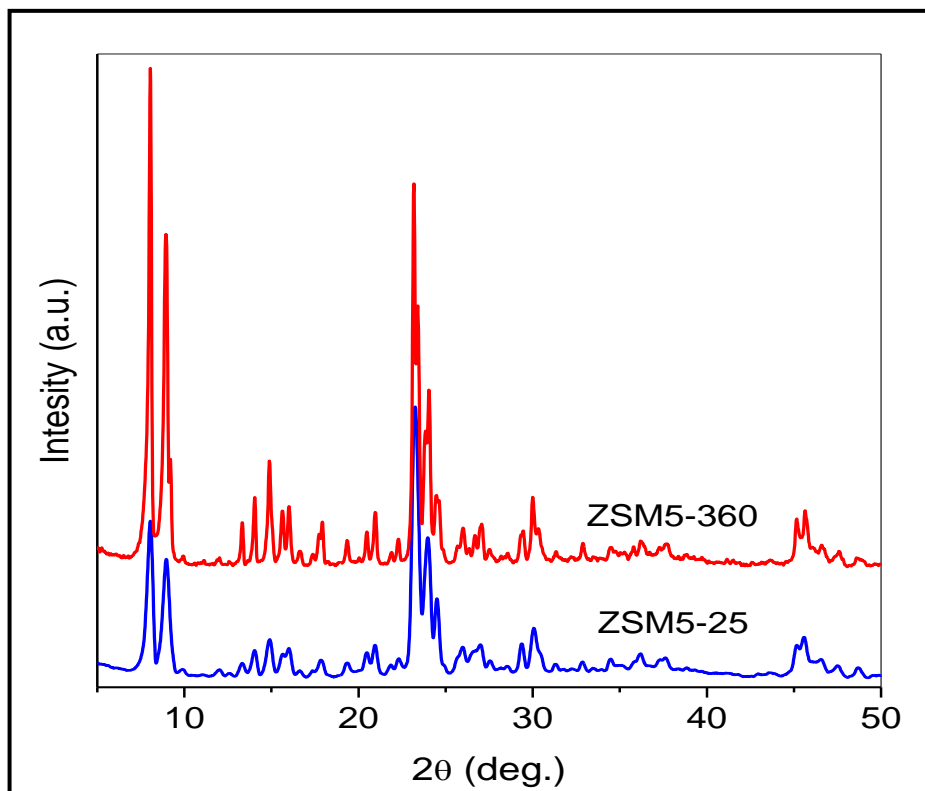


Figure 2.6: XRD patterns for ZSM5 samples

2.3.2 Textural and morphological characterization

The N₂ adsorption-desorption study showed modified textural properties for AlTiO₃ compared with the undoped γ -Al₂O₃. The textural modification includes higher surface area and smaller mesopores as shown in Table 2.1. However, the surface area decreased when the concentration of Ti was increased to 10%. On the other hand, the surface area and the total pore volume decreased more noticeably in the Ni-containing composites. While the reason behind the different effects from the different dopants is still not well understood, and was not investigated further, the surface areas and the total pore volumes are still relatively high compared with commercial nanoscale alumina powders, which usually have surface areas less than 200 m²/g and total pore volumes around 0.5 cc/g. The textural properties of the two zeolites shown in Table 2.1 are typical characteristics of zeolites where the total pore

volumes are considerably smaller than those of the other materials due to their crystalline structures that contain mainly micropores.

Table 2.1: Surface area and pore characteristics of the investigated solids calcined at 500°C

Composition	S _{BET} (m ² /g)	Pore volume (cc/g)	Average pore diameter (nm)
γ-Al ₂ O ₃	416	1.81	15.8
AlTi03	449	1.53	10.2
AlTi10	376	1.03	11.4
AlNi03	303	1.10	13.9
AlNi10	348	1.07	13.6
ZSM5-25	298	0.25	3.2
ZSM5-360	320	0.18	2.91

The textural characteristics of the composites in Table 2.1 are also shown in their adsorption-desorption isotherms and pore size distributions as presented in Figure 2.7 and Figure 2.8, respectively. Higher surface area and lower total pore volume of AlTi03, compared to undoped alumina is referred to the larger contribution of smaller mesopores. At higher concentration of Ti, 10%, the surface area decreased, the contribution of larger mesopores increased, and pore size distribution became less homogeneous as presented in Figure 2.8, which may indicate heterogeneity in the composite. The modified textural properties of AlTi03 can be referred to the effect of Ti ions as an impurity in the alumina matrix hindering particle growth and resulting in smaller primary particles that eventually aggregated creating more inter-particle pores in the mesoporous range. This is evident in Figure 2.7, where the hysteresis loop is shifted to a lower relative pressure range in the presence of 3% Ti. The pore size distribution of AlTi03 also showed a smaller

average pore diameter and narrower pore size distribution as presented in Figure 2.8. The observed higher surface area and textural homogeneity of AlTi03 compared with AlTi10 can be referred, in part, to its lower concentration of Ti ions that allowed better uniform dispersion within the alumina matrix. AlTi05 showed a catalytic activity similar to that of AlTi03, as will be discussed in Chapter 3, and was not fully characterized.

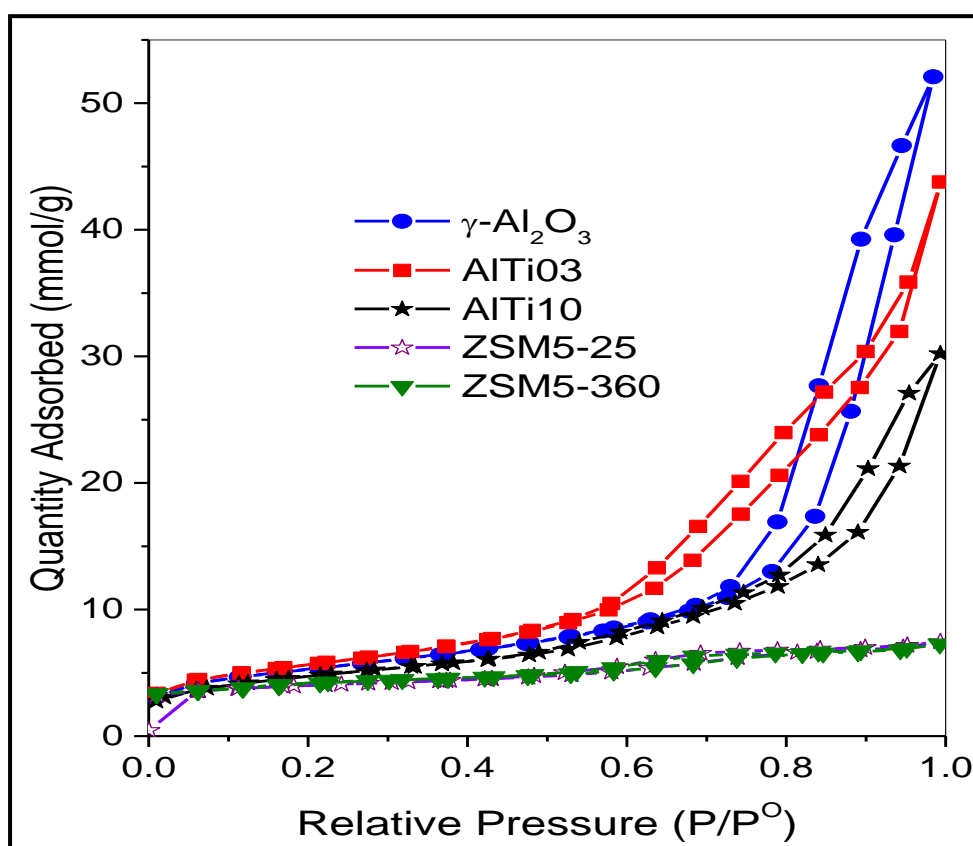


Figure 2.7: N₂ adsorption-desorption isotherms of doped and undoped γ -Al₂O₃ calcined at 500°C

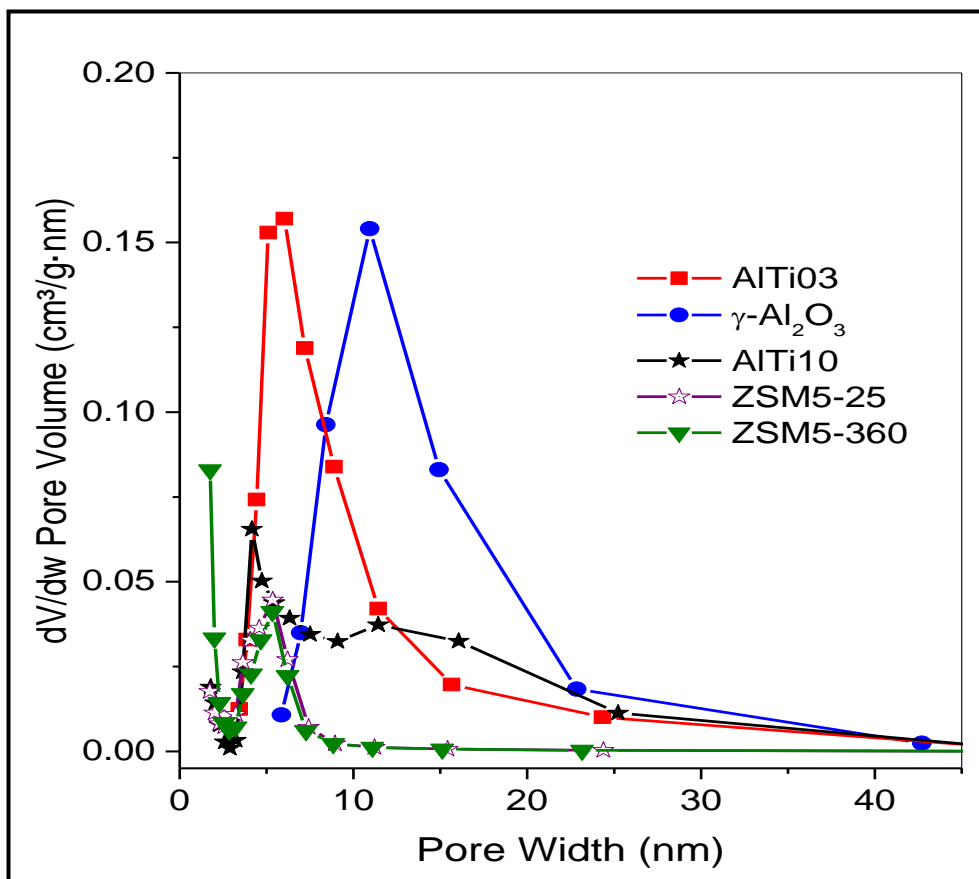


Figure 2.8: Pore size distribution of doped and undoped $\gamma\text{-Al}_2\text{O}_3$ calcined at 500°C

The effect of doping is also confirmed by the TEM images as shown in Figure 2.9, where the morphology of the particles has changed from needle-like to smaller nanoscale spherical particles of less than 10 nm in diameter that aggregate resulting in a significant amount of larger inter-particle pores in the mesoporic range, 2-50 nm. The less homogeneous aggregates of larger particles in the image of AlTi10 further supports its N_2 sorption results. These results also correlate with the enhanced amorphous nature of the doped samples as evident from their XRD patterns discussed above.

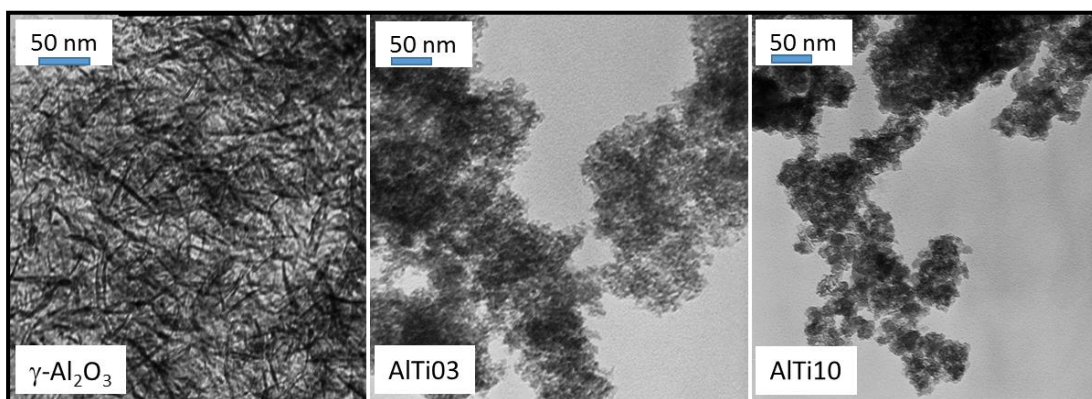


Figure 2.9: TEM images of γ -Al₂O₃, AlTi03 and AlTi10

The acidity of the surface of selected materials in this study was characterized by NH₃-TPD and their profiles are shown in Figure 2.10. The profile of AlTi03 shows a noticeable increase in the total acidity of its surface compared with pure alumina as indicated by the larger area under its peak. The maxima in their peaks are at about the same temperature indicating very similar strength of their acid sites. On the other hand, the profile of the Ni-containing composite shows a noticeable decrease in the total acidity as indicated by its smaller peak, which also shifts slightly to a lower temperature range indicating the presence of some weaker acid sites. For better understanding of the effect of the Ti ions, the profile of TiO₂ was also recorded and it showed considerably lower total acidity compared to the alumina-based catalysts. Its profile showed that significant amount of the ammonia desorbed at higher temperatures indicating the dominance of strong acid sites, which correlates with its catalytic performance and the methanol adsorption intermediates as will be discussed in Chapters 3 and 4. The profile of ZSM5-25 showed the highest overall acidity as indicated by its larger peaks that expand over a wide range of temperatures indicating the presence of sites of different acidity strength. Two overlapping peaks appear in the temperature range of 150°C-350°C that refers to weaker acid sites and another small broad peak in the range of 500°C-700°C, which refers to the stronger

acid sites. The high overall acidity of ZSM5-25 is referred to the high concentration of Al ion sites in its lattice. The high concentration of Al leads to a high concentration of bridging OH groups, Al-OH-Si, which are known to be more acidic than their terminal counterparts [105].

The profile of AlTiO₃ indicates total surface acid sites comparable to those of the studied zeolites. The role of Ti⁴⁺ ions in increasing the surface acidity can be referred, in part, to its high oxidation state where they act as Lewis acid sites when not fully coordinated on the surface. This characteristic is expected to enhance the concentration of surface OH groups to balance the charge difference compared with the Al³⁺ ions. The enhanced formation of OH groups is confirmed by DRIFT spectra of doped and undoped alumina as shown in Figure 2.11, which will be discussed further in Chapter 4, where more intense peaks for surface methoxy intermediates are observed. It could also be referred to the possible formation of bridging hydroxyl groups, Ti-OH-Al, similar to Si-OH-Al in zeolites. The profile of AlNiO₃ indicates lower overall acidity compared to pure alumina as indicated by the smaller area under its peak. This could be due to the lower charge on the Ni ions compared to aluminum ions that are smaller in size and higher in charge making them stronger Lewis acid sites.

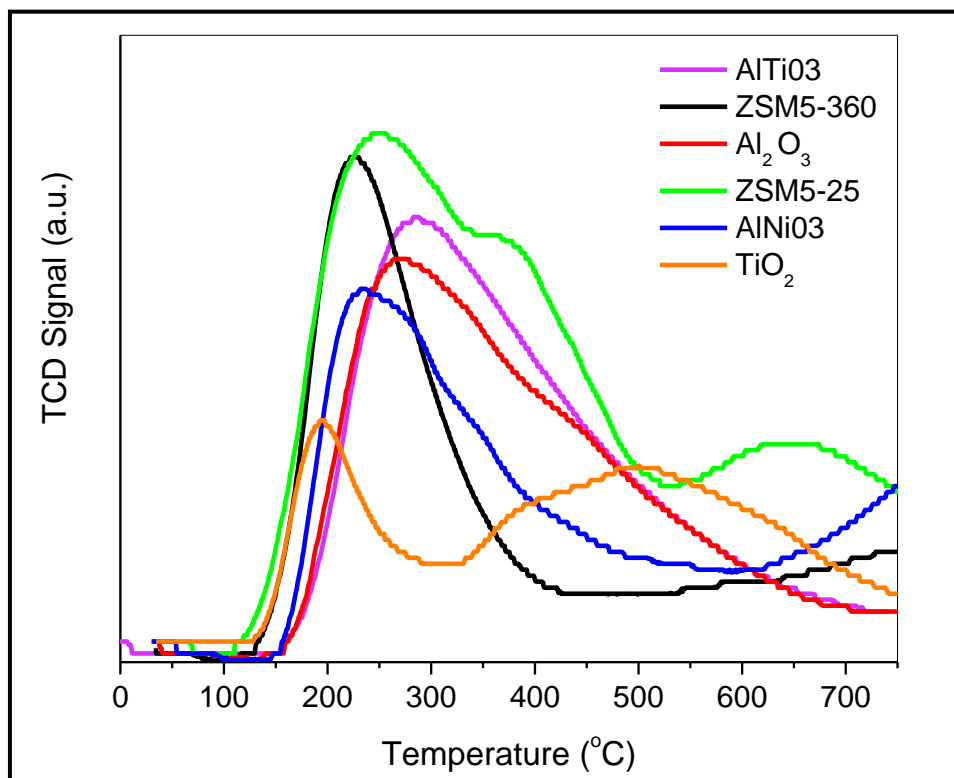


Figure 2.10: NH₃-TPD profiles of selected zeolites compared with alumina-based catalysts and TiO₂

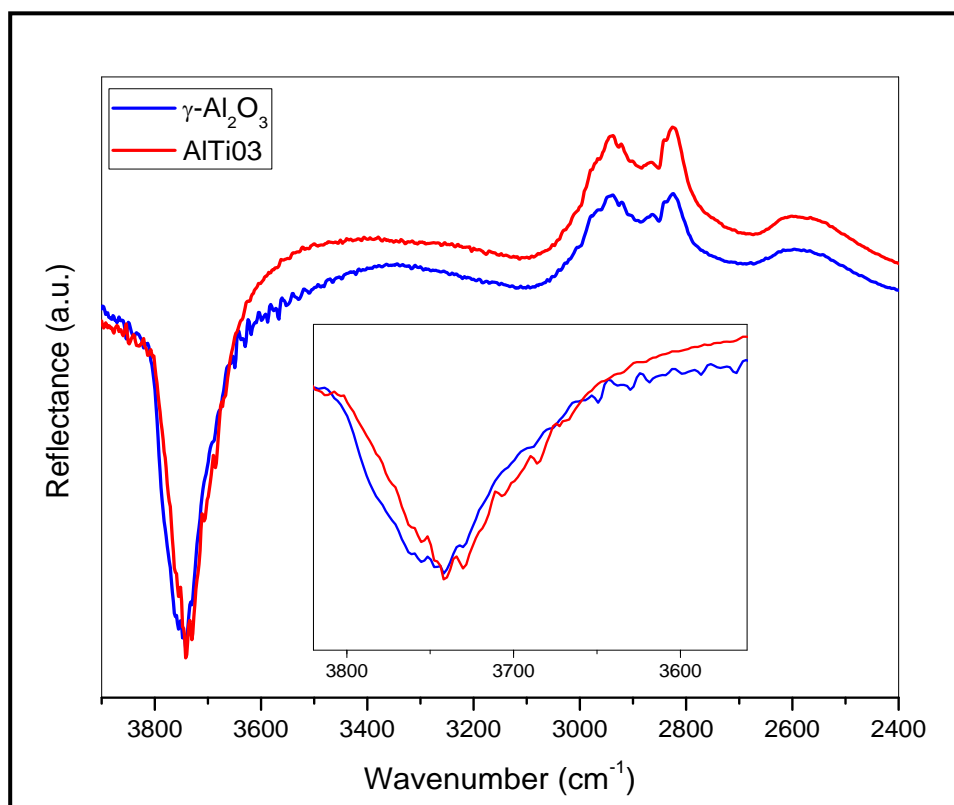


Figure 2.11: DRIFT spectra of adsorbed species over AlTiO₃ compared to γ-Al₂O₃ after adsorption at 50°C

Chapter 3: Catalytic Activity Study

3.1 Overview

In this chapter, the catalytic activity study is described. The catalytic performance of the prepared materials was studied in the dehydration of methanol to dimethyl ether (DME) reaction using a homemade fixed bed continuous flow reactor. The different prepared materials were tested, and their catalytic activity were compared in terms of methanol conversion and selectivity to DME.

3.2 Background

As was described in Chapter 1, DME could be produced from methane by two different routes, direct, where methane is converted to DME in one step, and indirect where methane is converted first to methanol, which is then converted to DME. Our project involved the conversion of methanol to DME step through vapor phase dehydration reaction over different solid acid catalysts based on γ -Al₂O₃ or zeolites.

As we have discussed earlier in Chapter 2, the dehydration reaction of methanol is affected by the textural and structural characteristics of the catalysts, which can be controlled by manipulating different preparative conditions and variables. Besides, the DME production process is influenced by the type of the reactor and its configurations. In general, there are several standards for an ideal reactor system for DME synthesis process, including: (I) simple construction, (II) uniform temperature distribution inside the reactor for high exothermic reaction, (III) easy catalyst addition, and (IV) good control of the reactor temperature to avoid catalyst sintering. In the following section, different reactor systems are discussed.

3.2.1 Types of reactors for DME synthesis

Several types of reactor designs have been employed for the direct and the indirect DME synthesis such as fixed bed reactors, internal recycle type reactors, fluidized bed reactors, batch mixed slurry reactors, and double-membrane heat exchange reactors [105, 106]. In the present research, a fixed bed reactor was employed for the dehydration reaction of methanol to DME. Fixed bed reactors are known in the industrial field for their low operation cost, simplicity, ease of operation and maintenance. In these reactors, the reaction takes place in the form of a heterogeneously catalyzed gas reaction on the surface of catalysts where the catalysts particles are packed as a fixed bed [108]. This type of reactors has some drawbacks, including the formation of hot spots inside the reactor, which affects its performance and deactivate the catalysts as it may cause catalyst sintering [107].

3.2.2 Dehydration reaction variables

During the dehydration reaction in the fixed bed reactor, temperature, pressure, and feed flow rate are the most crucial variables that need to be controlled, as they will affect the reaction rate and the catalytic activity. Various studies in the literature have assessed the role of different parameters and their effect on the selectivity, reaction rate and methanol conversion trends [7, 28, 32, 108]. They revealed that the temperature and the flow rate are the most significant controlling factors that govern the efficiency of the catalytic process. For instance, the reaction rate could be enhanced by increasing the temperature. However, theoretically, methanol dehydration is favored at relatively low temperatures range, because it is an exothermic reaction, which means that the formation of by-products such as ethylene, carbon monoxide, hydrogen and coke becomes more favorable at higher

temperatures [7, 109]. Owing to this fact, this reaction is performed within an optimum range below 300°C.

Likewise the temperature, the pressure affects the reaction process but at a smaller scale [111]. In terms of the effect of the reactant concentration, Osman [109], reported that as the methanol concentration increases the conversion decreases because of the atmosphere over the acid sites will be crowded and saturated with alcohol molecules which will hinder the dehydration [109]. In relation to the effect of the flow rate, it was found that a lower flow rate leads to a higher rate of conversion, owing to the longer residence time of the reactants on the catalyst surface and in the reactor. However, the higher flow rate was found to give better DME selectivity as higher flow rate means shorter contact time with the catalysts, resulting in a lower chance for the further decomposition of DME to carbon dioxide and methane [28, 105, 111].

Generally, studying these parameters is not easy, as each one of them could affect the other. However, overall, the studies described above highlight the main trends and parameters that should be managed appropriately to obtain sufficient DME selectivity as well as catalytic activity.

3.3 Experimental methods

The catalytic activity of all prepared materials were studied at 200°C under one atmospheric pressure using a continuous-flow fixed-bed reactor connected in-line with a gas chromatograph (GC) for products' separation, identification and quantitation, as shown schematically in Figure 3.1.

The catalyst used in all catalytic tests was in the form of sieved powder, which were sieved using 120-180 mesh stainless steel sieves. In each experiment,

120 mg of the catalyst powder was packed between a stainless-steel frit and a glass wool plug in a U-shape stainless steel tube reactor (6 mm inside diameter). The reactor was fixed inside a tube furnace equipped with a temperature controller and a K-type thermocouple, positioned in the proximity of the catalyst bed. Before each experiment, the catalyst sample was degassed for 1 hour at 400°C in a flow of Helium (90 ml/min) in order to remove any adsorbed molecules on the catalyst surface such as water. The reactor was then cooled down to the desired reaction temperature (200°C). Once the reaction temperature was stabilized, the reaction was started by allowing methanol vapor diluted in He to flow through the catalyst bed. Methanol was introduced by allowing He flow, as a carrier gas, at a flow rate of 1.5 mL/min to bubble through a methanol saturator which was kept at a temperature around 23°C. The Methanol/He stream was diluted by another He stream at a flow rate of 88.5 mL/min. The reactor line between the methanol saturator and the GC was electrically heated to around 120°C using heating tapes in order to prevent condensation of methanol. The products were sampled by injecting 1 mL samples into the GC for qualitative and quantitative evaluation of the products every 30 min during a total of 5 hours on-stream.

To investigate the effect of reaction temperature, a set of experiments were conducted at different temperatures in the range of 150°C-400°C. After analysis of the products at each, the temperature was increased stepwise by 50°C. At each reaction temperature, the system was allowed 30 min for stabilization before the first sampling at each temperature, where sampling was done at least twice during a period of one 1 hour at that temperature

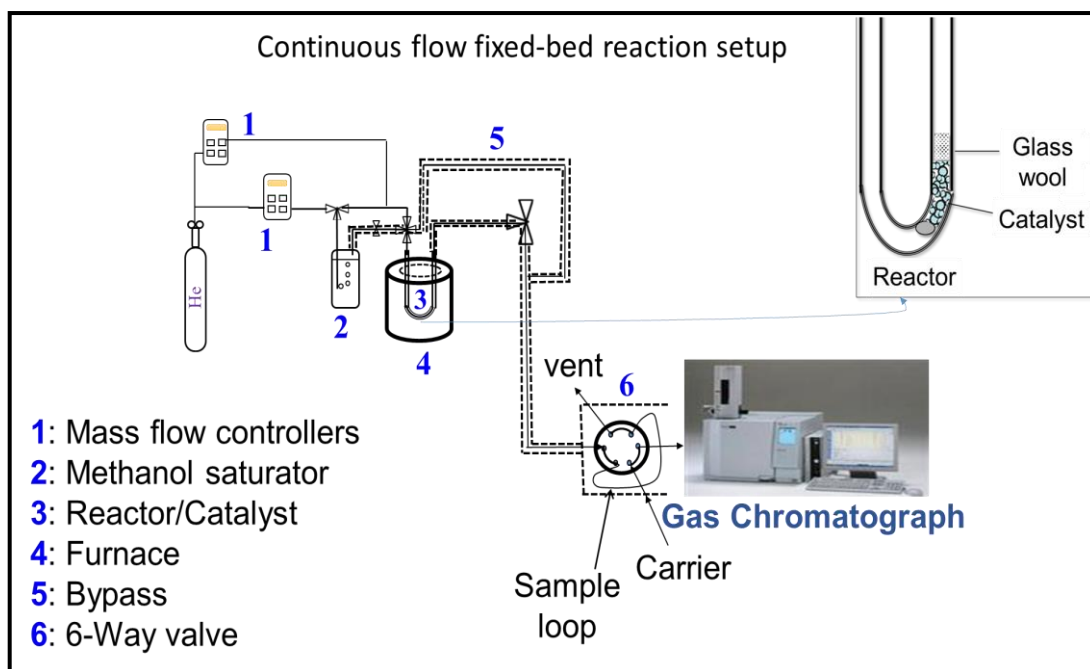


Figure 3.1: Continuous flow fixed-bed reaction setup

3.4 Data collection and product analysis

The analysis of the reaction products was carried out by an in-line GC, Shimadzu GC-2010, equipped with a capillary column Rt-Q-BOND of 30 m length and 0.32 mm ID, and a dielectric-barrier discharge ionization detector (BID). Reactor effluents were fed continuously through a 6-way valve equipped with a 1 mL sampling loop as shown in Figure 3.2. The products sample loop was injected into the GC column using the GC carrier gas, helium. The principle of BID detector is based on the generation of He plasma in a quartz tube using high voltage. The energy of the He plasma ionizes compounds that elute from the column. The BID detector is a universal detector as it generates a 17.7 eV helium plasma that ionizes almost all compounds and elements except Neon. The following temperature program was used on the GC for products' separation: a 2 min hold at 35°C, a ramp to 180°C at a rate of 20°C/min and 6 min hold. The gas chromatograph was calibrated for the expected eluents using high purity methanol and the DME.

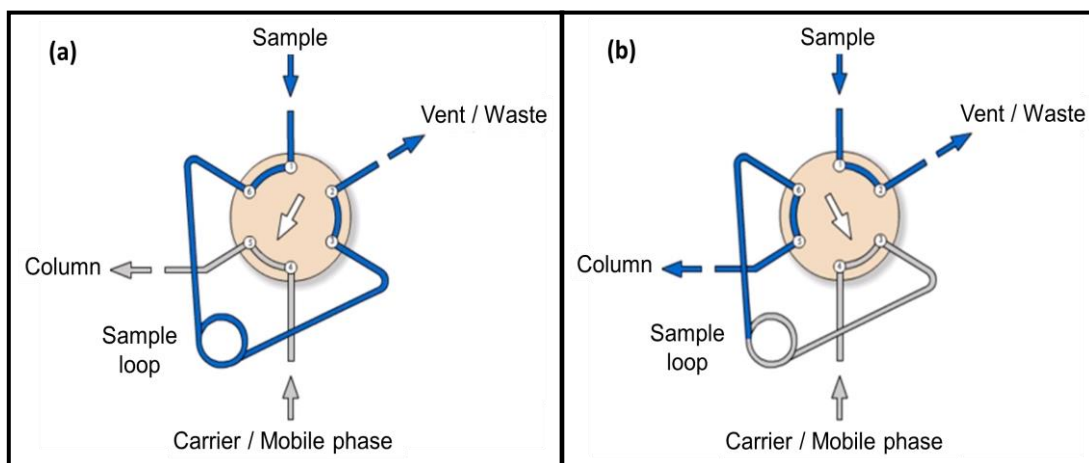


Figure 3.2: 6-way valve scheme (a) loading position (b) injection position [113]

The catalyst that were tested include pure alumina, alumina doped with Ti(IV), Ni(II), V(III), and two selected zeolites, with emphasis on Ti- and Ni-doped alumina. In addition, some Si and Zn-containing alumina were tested for quick comparison only, without detailed studies. The catalytic activity was expressed in terms of methanol conversion (Equation 3.1), and products selectivity were calculated according to the equations shown below (Equation 3.2) and (Equation 3.3). The reported results are based on the averages of three experiments with reproducibility around 99% in all measurements.

$$\text{Conversion of methanol (\%)} = \frac{[\text{MeOH}]_{\text{in}} - [\text{MeOH}]_{\text{out}}}{[\text{MeOH}]_{\text{in}}} \times 100 \quad (3.1)$$

$$\text{DME selectivity (\%)} = \frac{2[\text{DME}]}{\text{converted MeOH}} \times 100 \quad (3.2)$$

$$\text{CO}_2 \text{ selectivity (\%)} = \frac{[\text{CO}_2]}{\text{converted MeOH}} \times 100 \quad (3.3)$$

3.5 Results and discussion

3.5.1 Catalytic activity

The catalytic methanol dehydration to DME reaction was studied over different prepared and commercial materials including prepared as well as commercial γ -Al₂O₃, Ti-doped γ -Al₂O₃, Ni-doped γ -Al₂O₃ and ZSM5 zeolites. The prepared γ -Al₂O₃ showed catalytic activity comparable with and even slightly higher than that exhibited by nanoscale commercial γ -Al₂O₃ (CM-Alumina) as shown in Figure 3.3. Since, Ti-doped γ -Al₂O₃ was studied, the catalytic test was also conducted over commercial nanoscale TiO₂, which showed no catalytic activity in the methanol dehydration to DME reaction. A possible explanation is that the tested TiO₂ has a rutile structure where all Ti ions have a coordination number of 6, and the coordinatively unsaturated surface ions are either covered with strongly bound OH groups, due to the high oxidation state and the empty *d*-orbitals, or they strongly adsorb methanol molecules and intermediates, which is supported by the spectroscopic study of methanol adsorption as will be discussed in Chapter 4.

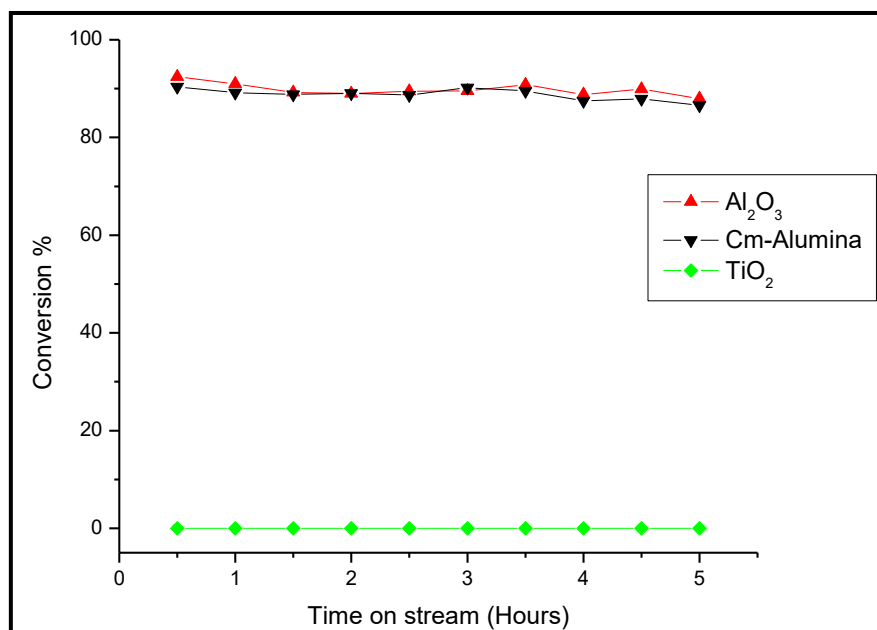


Figure 3.3: Methanol conversion at 200°C over prepared γ -Al₂O₃ compared with its commercial counterpart and TiO₂

Selected dopants, Ti and Ni, in particular, were investigated at different concentrations ranging from 2% to 15 % as shown in Figures 3.4 and 3.5. It was found that high concentrations of the dopant had a negative impact on the catalytic activity where the conversion decreased as the concentration increased. These results may indicate that high dopant concentrations lead to the substitution of a considerable number of the Al acidic sites and may also lead to the formation of small amounts of amorphous and dispersed segregated Ti and Ni oxides that are not detected by XRD.

Prepared NiAl₂O₄ was also tested for comparison. Compared with γ -Al₂O₃ that has a corundum structure, this compound has a spinel structure and was more crystalline. It showed considerably lower catalytic activity, which can be referred to the structure in which all Aluminum ions reside in octahedral holes with a coordination number of 6 and hence, lower acidic character than Aluminum ions in

γ -Al₂O₃ which has a defect spinel structure where some Aluminum ions reside in tetrahedral holes of coordination 4 enhancing their acidic character.

Interestingly, concentrations of $\leq 5\%$ Ti and $\leq 3\%$ Ni resulted in a noticeable enhancement to the methanol conversion compared with undoped γ -Al₂O₃, as shown in Figures 3.4 and 3.5. The effect of Ti⁴⁺ ions with these concentrations can be referred to different factors, including first, its higher oxidation state that may enhance methanol adsorption as the first step of the reaction. Second, its higher oxidation state and the presence of valence empty *d* orbitals increase the Brønsted acidity strength of the bridging hydroxyl groups, Al-OH-Ti. Third, its larger ionic radius (61 pm) compared to that of Al³⁺ ions (53 pm) may favor residing in octahedral interstitial holes, enhancing the occupation of Al ions in tetrahedral holes where their acidity is enhanced compared with ions in octahedral coordination. The effect of the Ni²⁺ ions can also be referred, in part, to its larger ionic radius, 69 pm. Also, Ni²⁺ has a *d*⁸ electronic configuration which favors octahedral coordination due to the significant crystal field stabilization energy associated with such configuration.

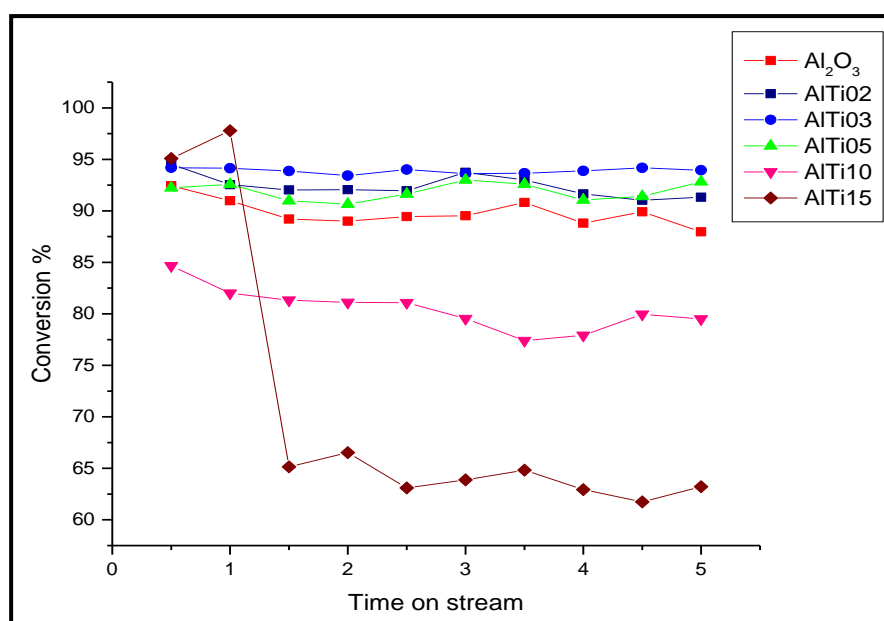


Figure 3.4: Methanol conversion at 200°C of AlTi with different concentrations compared with pure γ -Al₂O₃

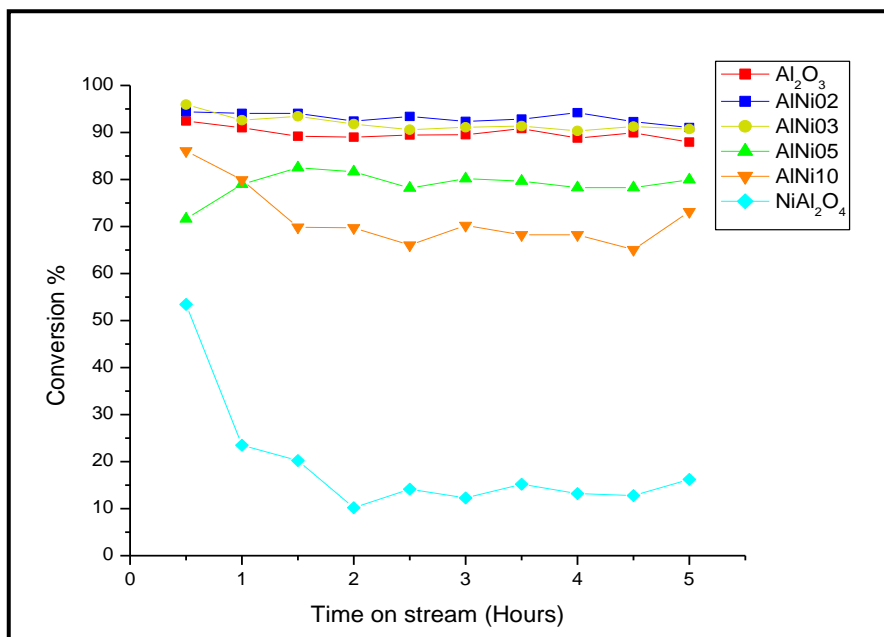


Figure 3.5: Methanol conversion at 200°C of AlNi with different concentrations compared with pure γ -Al₂O₃

Another Al-Ti oxide catalyst was prepared by impregnating the surface of already-prepared γ -Al₂O₃ by the Ti⁴⁺ precursor, 3% Ti, followed by calcination to form a Ti-rich surface for comparison with the bulk-doped catalyst. The structural characteristics of this composite were not investigated in the study, and only a catalytic activity test was performed for comparison with the bulk-doped catalyst, as shown in Figure 3.6. Although this composite showed conversion comparable with that of AlTi03 catalyst, the reaction over its surface resulted in a considerable amount of CO₂ on account of selectivity to DME as will be discussed below.

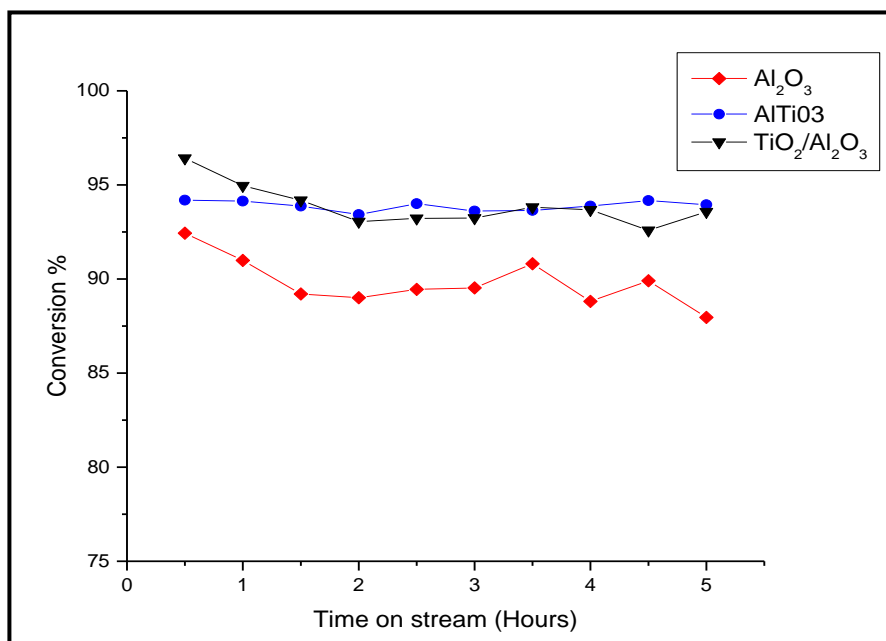


Figure 3.6: Methanol conversion at 200°C over TiO₂/Al₂O₃ compared to AlTi03% and γ -Al₂O₃

The catalytic activity was also tested on γ -Al₂O₃ doped with 3% V(III), which showed considerably lower conversion, as shown in Figure 3.7. The lower catalytic activity of AlV03 correlates with its acidity measurement and lower surface area. These results indicate that the catalytic activity of metal-doped γ -Al₂O₃ depends significantly on the type of dopant. However, more work is needed for a better understanding of the influence of different dopants.

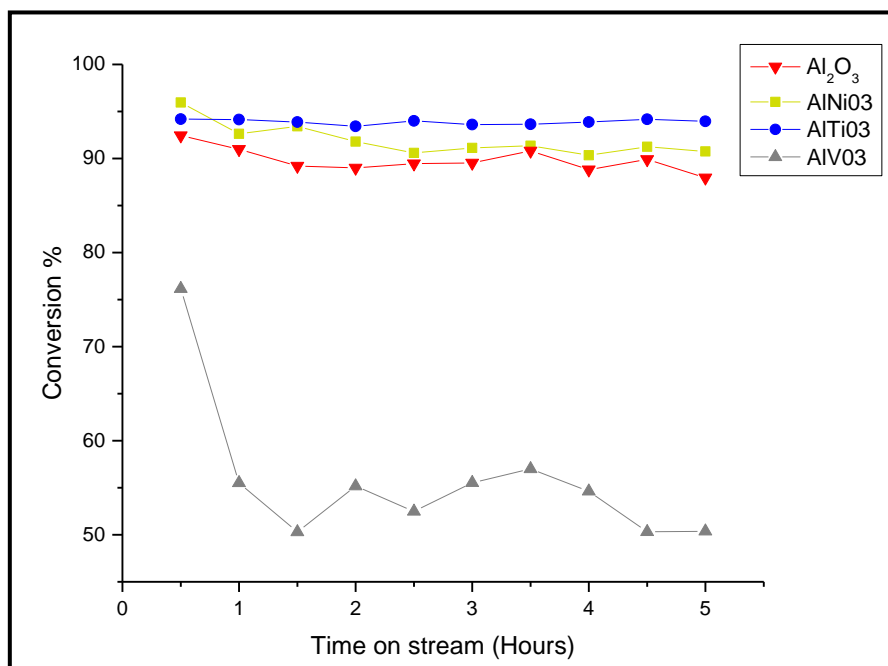


Figure 3.7: Methanol conversion at 200°C of AlM03% compared to Alumina

The catalytic activity was also studied over γ -Al₂O₃ doped with different other elements, as shown in Figure 3.8, which presents the methanol conversion over these catalysts containing different dopant ions with 10% mole concentration. The results indicate that all dopants with this concentration resulted in a decrease in the conversion except Si, which gave conversion comparable with that of pure γ -Al₂O₃. The dehydration of methanol was studied for quick comparison over these composites, which were not studied further.

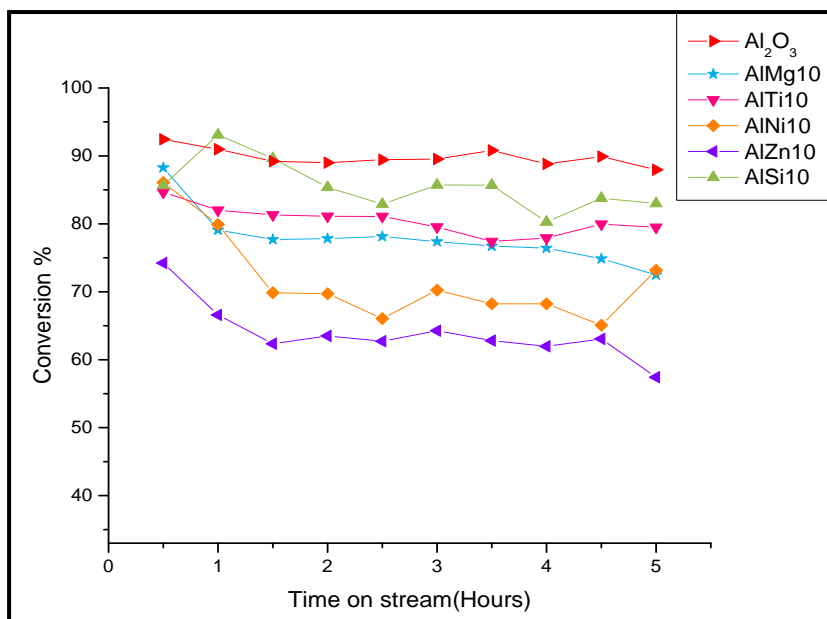


Figure 3.8: Methanol conversion at 200°C over AlM10 catalysts compared with pure γ -Al₂O₃

Figure 3.9 shows methanol conversion over a series of ZSM5 zeolites with different Si/Al ratios ranging from 25 to 360. The results presented in Figure 3.9 shows that as the Al content decreases, the conversion decreases. These results can be correlated with the fact that the decrease in the Al concentration results in a decrease in the total acid sites.

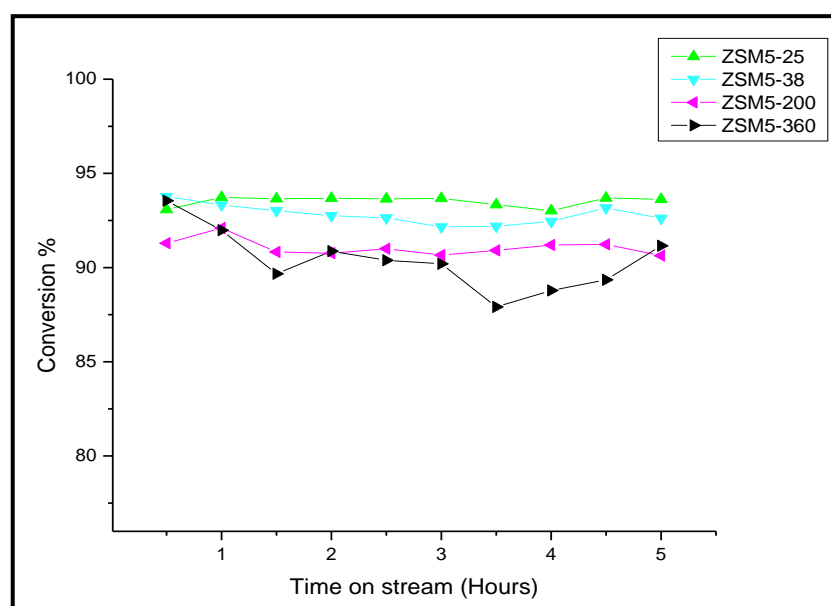


Figure 3.9: Methanol conversion at 200°C over different ZSM5 zeolites

Interestingly, the prepared AlTiO₃ catalyst gave conversions very similar, and even slightly higher than, those obtained over the well-known acidic zeolite, ZSM5-25, as shown in Figure 3.10. This finding holds a great promise toward the development of new acid catalysts based on Ti-doped alumina, with a Ti concentration around 3% which may offer advantages over zeolites in applications that require solid acid catalysts. The advantages of the AlTi composite include easier preparation and better molecular diffusion due to their higher surface area and larger mesopores compared with the micropores of zeolites.

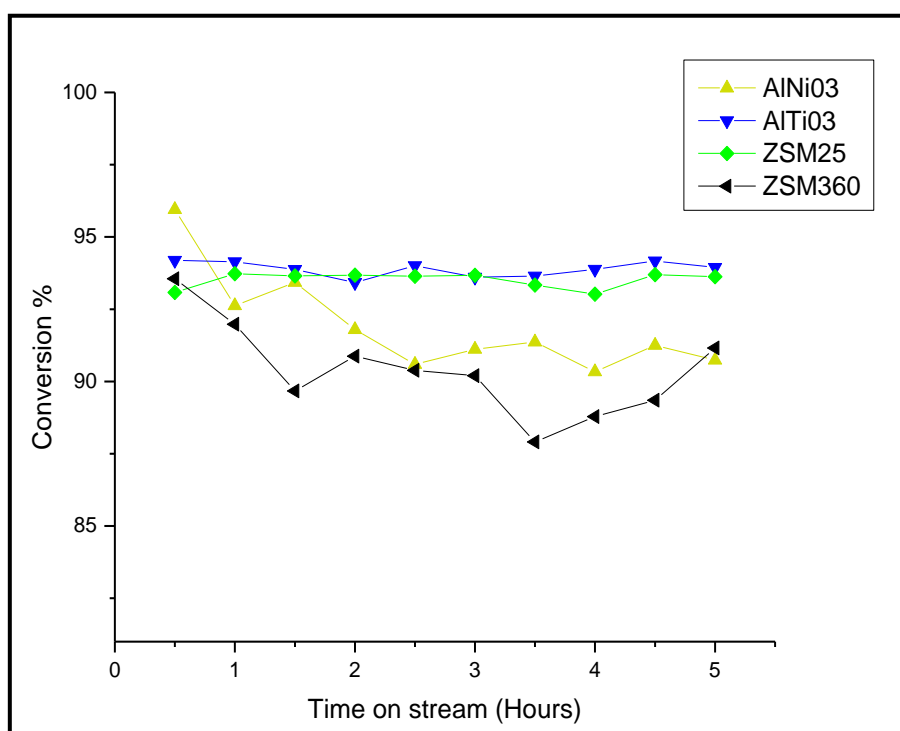


Figure 3.10: Methanol conversion at 200°C over AlM03% vs. selected Zeolites

3.5.2 Products' selectivity

The DME selectivity in reactions over AlM03% and selected zeolites catalysts is presented in Figure 3.11. AlTi03 and AlNi03 showed DME selectivity very similar to that obtained over γ -Al₂O₃, which was around 95%. However, AlV03 showed noticeably lower selectivity, which was around 90%. The higher DME selectivity usually indicates higher total acidic character of the surface indicating that γ -Al₂O₃ retained its surface acidity in the presence of Ti or Ni in its matrix. However, the presence of V ions seems to have a negative impact. It is noteworthy that in the presence of the transition metal dopants, especially V, the DME selectivity was noticeably lower at the beginning of the reaction. The lower selectivity can be referred to possible redox behavior of the transition metal ion sites, especially over the fresh surface at the beginning of reactions where surface OH groups are expected to be present and contribute to the redox process. This behavior was confirmed by the observed higher CO₂ selectivity over the V-doped catalyst as shown in Figure 3.12.

The selectivity over zeolites shows an inverse relation with Si/Al ratio where the DME selectivity increased as the ratio decreased, where the total acidity is higher. The selectivity trend was as follows: ZSM5-25 > ZSM5-38 > ZSM5-200 > ZSM5-360, as shown in Figure 3.11 which presents the selectivity of the ZSM5-25 and ZSM5-360 compared to commercial alumina, Ni-doped alumina and Ti-doped alumina.

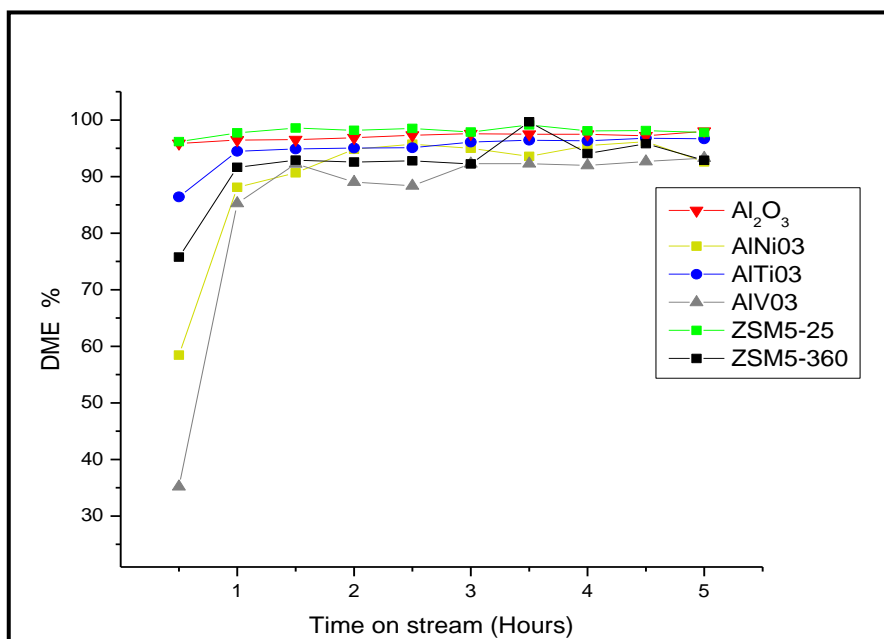


Figure 3.11: DME selectivity in reactions at 200°C over AlM03% (Ni,Ti) vs Alumina and Zeolites

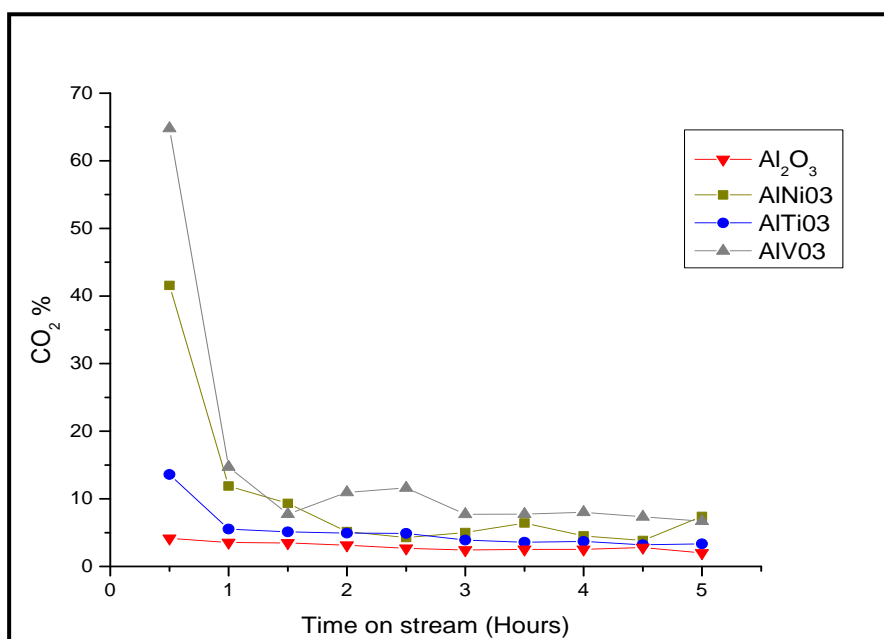


Figure 3.12: CO₂ selectivity from reactions at 200°C over AlM03% vs Alumina catalysts

Comparison between surface-doped alumina (TiO₂/γ-Al₂O₃) with its bulk-doped counterpart (AlTiO₃) shows that the surface-doped catalyst promoted oxidation of methanol more favorably, especially at the beginning resulting in a very low DME selectivity and high CO₂ selectivity as shown in Figure 3.13. It is very

likely that surface OH groups are involved in the oxidation process, which gets consumed in the redox reaction with time.

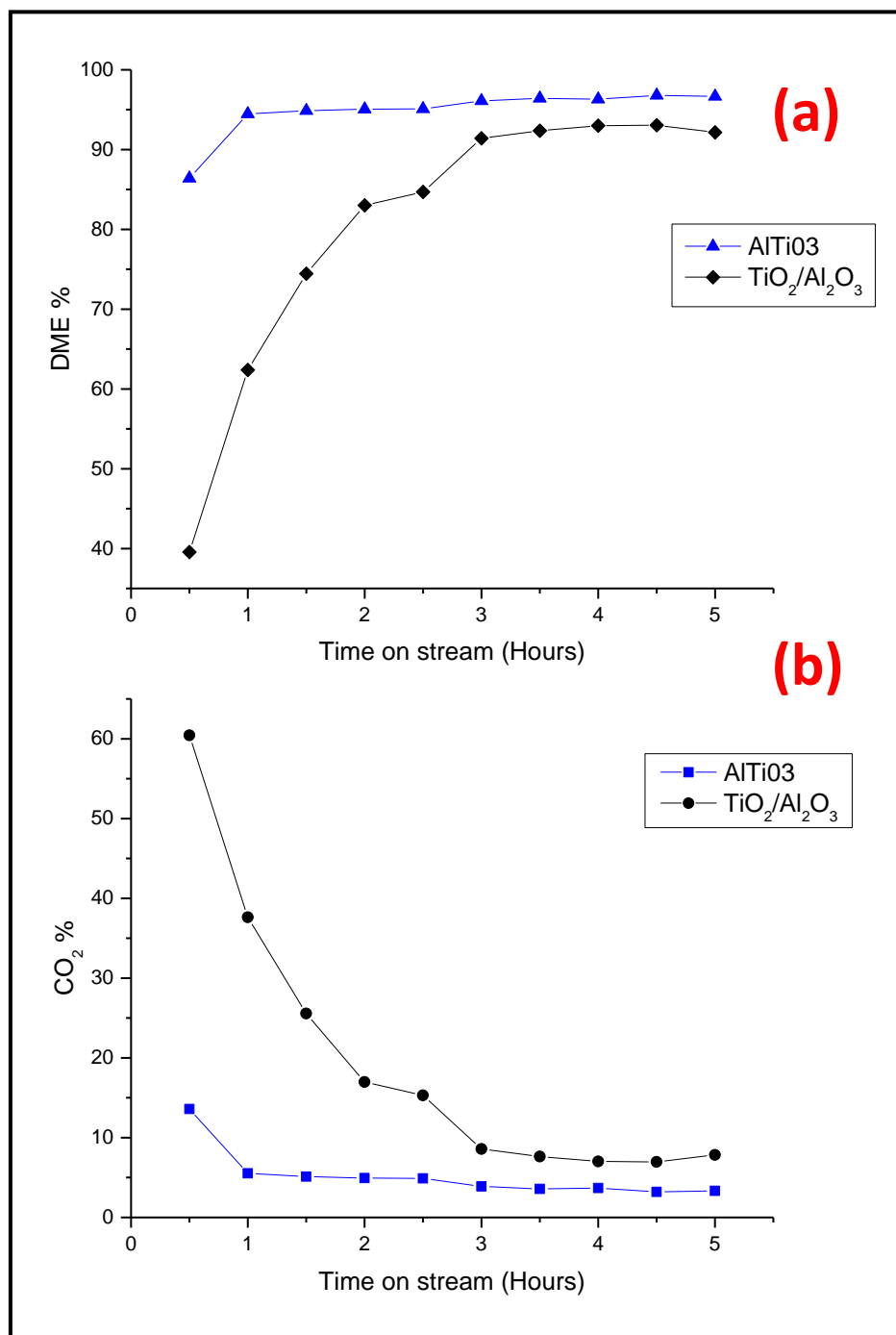


Figure 3.13: DME (a) and CO₂ (b) selectivity in the reaction at 200°C over TiO₂/Al₂O₃ vs AlTiO₃

The effect of the reaction temperature on methanol conversion and DME selectivity was evaluated on γ -Al₂O₃, AlNi03% and AlTi03% in the temperature range of 150°C to 400°C, as shown in Figure 3.14. It is clear that the methanol conversion increased with increasing the reaction temperature, as expected since the conversions drop at lower temperatures because fewer molecules have enough energy to overcome the activation energy needed to for the reaction.

While the tested catalysts showed very similar conversions at temperatures $\geq 200^\circ\text{C}$, a noticeable difference was observed at lower temperatures. The doped catalysts, AlNi3% and AlTi3%, gave noticeably higher conversions than pure alumina at 150°C. However, they showed lower DME selectivity and higher CO₂ selectivity at this temperature, as shown in Figure 3.14 (b). The results show that the DME selectivity was maximum at temperatures between 200°C and 300°C which would be the range of optimum reaction to produce DME efficiently. At higher reaction temperatures, 350-400°C, CO₂ and CH₄ were dominant products on account of DME which considerably decreased as shown in Figures 3.14 (b) and 3.14 (c). Methanol dehydration is favored at lower temperatures because it is an exothermic reaction and other possible reactions leading to the formation of by-products become favored at higher temperatures.

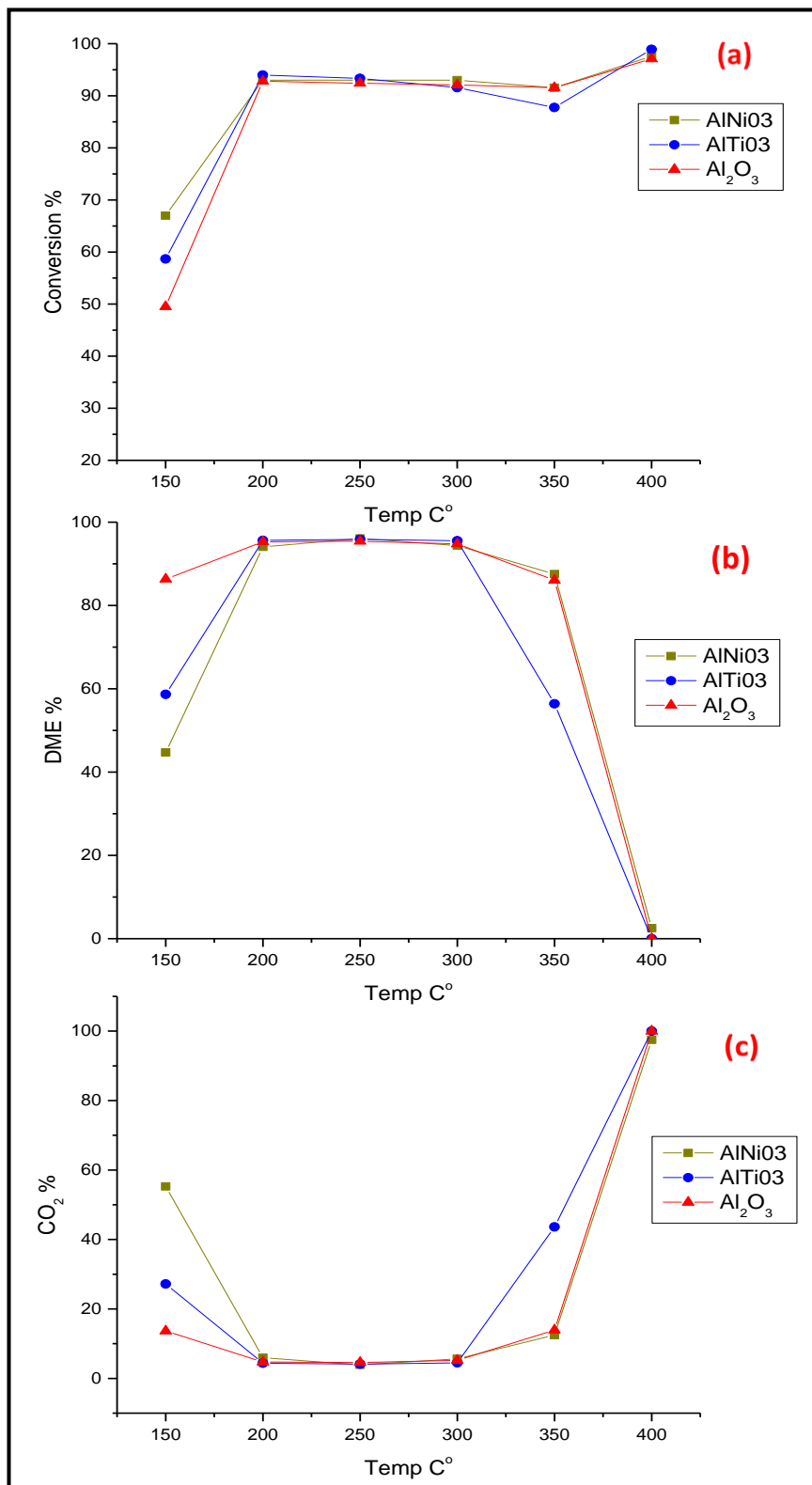


Figure 3.14: (a) Methanol conversion, (b) DME selectivity, and (c) CO₂ selectivity over AlNiO₃ compared to alumina in the temperature range from 150°C to 400°C

Chapter 4: Mechanistic Study by Methanol Chemisorption

4.1 Introduction and overview

Understanding the mechanism of methanol adsorption and dehydration is an essential study for optimization of the catalyst composition towards better performance and longer lifetime. Studying the adsorption also helps in formulating an appropriate kinetic model for this process. The reaction mechanism of the methanol dehydration reaction on both alumina and zeolites is still under debate. However, the majority of the literature reports agree that the mechanism follows either Rideal-Eley or Langmuir–Hinshelwood kinetic models [105-107]. The first route, which is known as Rideal-Eley mechanism involves only one methanol molecule adsorption which involves protonation of the methanol hydroxyl group to form a surface methoxy group and water. The methoxy group on the surface is subject to nucleophilic attack of a methanol molecule from the gas phase forming a dimethyl ether (DME) molecule. The second route, which is known as Langmuir-Hinshelwood mechanism or Bercic model [117], considers the adsorption of two methanol molecules on adjacent acid/base pairs [68, 109, 110]. The two adsorbed molecules react forming DME. There is a third proposed route which is very similar to Langmuir-Hinshelwood mechanism, except that both methanol molecules are suggested to be adsorbed on the same active site, but with different adsorption enthalpies [120]. Some studies have also proposed a different route where two methanol molecules adsorb dissociatively forming two surface methoxy groups on Lewis acid sites and two new OH groups. The two surface methoxy groups then interact to form dimethyl ether molecules [112, 113].

Based on the proposed mechanisms, the literature suggests two main pathways for the production of DME from methanol, either associative where co-adsorption of two methanol molecules occurs at Brønsted site without the formation of methoxy, or dissociative where one methanol molecule reacts with the acid site forming a surface methoxy group and a water molecule [119].

While these routes have been proposed for reactions over different zeolites and other solid acid catalysts, there is still no distinction between mechanisms over different types of catalysts, and no correlation between the proposed mechanisms and the possible active sites on the surface [107, 109]. In this work, the adsorption of methanol on γ -Al₂O₃, Ti-doped γ -Al₂O₃, Ni-doped γ -Al₂O₃ and ZSM5 was studied using in-situ Diffuse Reflectance Infrared Fourier Transform Spectroscopy (DRIFTS) aiming at first, studying the effect of doping on the adsorption and second, comparing the routes of methanol interaction over these solids.

4.2 Experimental method: Methanol adsorption and intermediates study

Adsorbed methanol and adsorption intermediates on the surface of the catalysts at different temperatures were studied using DRIFTS which is known for its simplicity and easier sample preparation compared to the conventional transmission FTIR. The employed DRIFTS accessory was equipped with a cell that enables in-situ studies at elevated temperatures, as high as 900°C.

Before each experiment, the catalyst sample, ~200 mg powder, was pretreated at 400°C under N₂ for 1 hour at a flow rate of 10 mL/min. The sample was then cooled down to 100°C and a background spectrum was recorded. The sample was then cooled down to 50°C and methanol was introduced by passing the N₂ flow through a methanol saturator at room temperature as shown schematically in Figure

4.1. After 20 min, a spectrum was recorded before the cell was purged with N₂ gas for 30 min to remove gas phase and physically adsorbed methanol molecules. After purging, a spectrum of the catalyst was recorded at the same temperature, 50°C. The catalyst was then heated to higher temperatures, up to 500°C. It was soaked at each analysis temperature for 20 min, followed by cooling to 100°C before a spectrum was collected after treatment at each temperature.

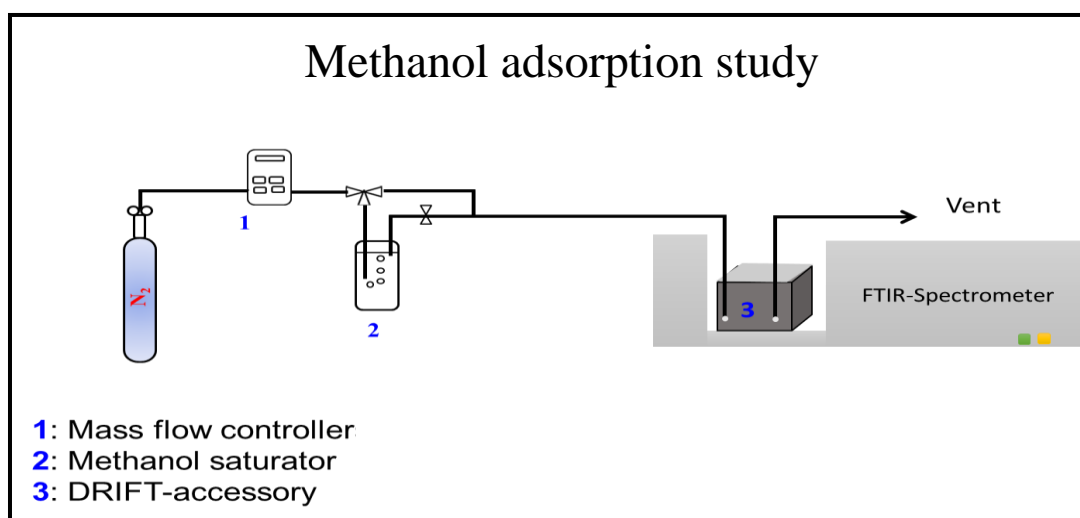


Figure 4.1: Methanol adsorption study setup

4.3 Results and discussion

Adsorption of methanol was studied over selected doped alumina catalysts, AlTiO₃ and AlNiO₃ were compared with γ -Al₂O₃ and TiO₂ as shown in Figure 4.2, which shows the spectral regions of peaks due to ν_{OH} and ν_{CH} in the spectra of the surface species after adsorption at 50°C. The surface of γ -Al₂O₃ usually possesses different OH groups that have been well studied by FTIR spectroscopy [121]. Various studies have reported seven distinguished bands due to isolated OH groups including four low-frequency bands, in the region of 3660-3740 cm⁻¹, assigned to OH groups bridging Al atoms of different coordination, and 3 high-frequency bands,

in the range of 3745-3790 cm^{-1} , assigned to terminal OH groups bound to one Al atom with different coordination numbers [112, 113]. The bands at lower frequencies are expected to involve weaker O-H bonds and, hence, are more acidic. Therefore, they usually behave as Brønsted acid sites. On the other hand, the higher frequency groups are less acidic and may even behave as basic sites.

The spectra after adsorption and before purging at 50°C, of $\gamma\text{-Al}_2\text{O}_3$, TiO_2 , AlTiO_3 and AlNiO_3 are presented in Figure 4.2. The spectra showed several overlapping negative peaks in the region of 3670-3790 cm^{-1} that are referred to ν_{OH} of bridging as well as terminal isolated OH groups [121]. According to literature, the peak at 3765 cm^{-1} refers to medium-strong Brønsted acid sites, while the peak at 3730 cm^{-1} refers to medium-weak sites and that at 3675 cm^{-1} is assigned to weak sites.

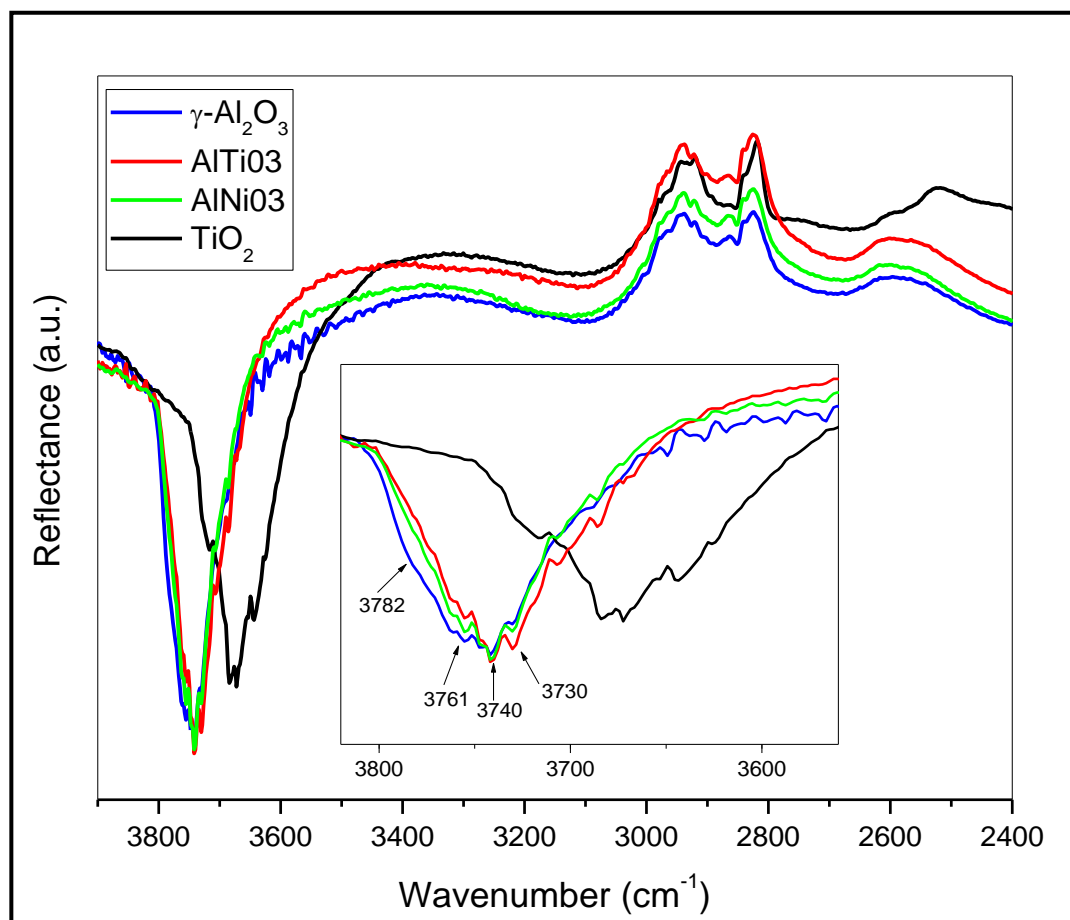


Figure 4.2: DRIFT spectra of adsorbed species over AlTiO_3 , AlNiO_3 , $\gamma\text{-Al}_2\text{O}_3$, and TiO_2 after adsorption of methanol at 50°C

The fact that the OH peaks are negative indicates that these groups existed on the surface before adsorption and were perturbed upon adsorption of methanol. The negative peaks were accompanied by broad positive peaks in the range of 3200-3400 cm^{-1} which can be assigned to hydrogen-bonded OH groups, indicating that the perturbation of the isolated OH groups is due to their engagement into hydrogen bonding with the adsorbed molecules. This observation provides an evidence for the dominance of undissociative adsorption of methanol in the first step of methanol dehydration [68]. This behavior is supported by the spectra of the same samples after purging at 150°C as shown in Figure 4.3, where the negative peaks decreased in

intensity indicating partial regeneration of those OH groups due to removal of adsorbed methanol and methoxy species [68, 114, 115].

Since changes involved the peaks in the whole ν_{OH} spectral region, it can be concluded that both types of OH groups, bridging and terminal, were involved in the interaction with adsorbed methanol molecules. The peaks in the region of 2800-3000 cm^{-1} are due to ν_{CH} ($\nu_{\text{s(CH}_3)}$) at 2920 and $\delta_{\text{s(CH}_3)}$ at 2825 cm^{-1}) which indicates the formation of adsorbed methoxy group intermediates [112, 116, 117], indicating that dissociative adsorption of methanol also takes place.

Compared to undoped $\gamma\text{-Al}_2\text{O}_3$, AlTiO₃ showed some shift of the perturbed OH peaks to lower frequencies, indicating the presence and the involvement of slightly more acidic groups in the adsorption process. This observation is also supported by the NH_3 -TPD results discussed above, where larger overall and stronger acidity was observed for AlTiO₃. On the other hand, although AlNiO₃ showed the same shift but it possesses weaker intermediate binding indicated by the less resistance to desorption at 150°C which is also supported by the TPD results where it shows desorption at a lower temperature with a smaller amount of the total acid sites.

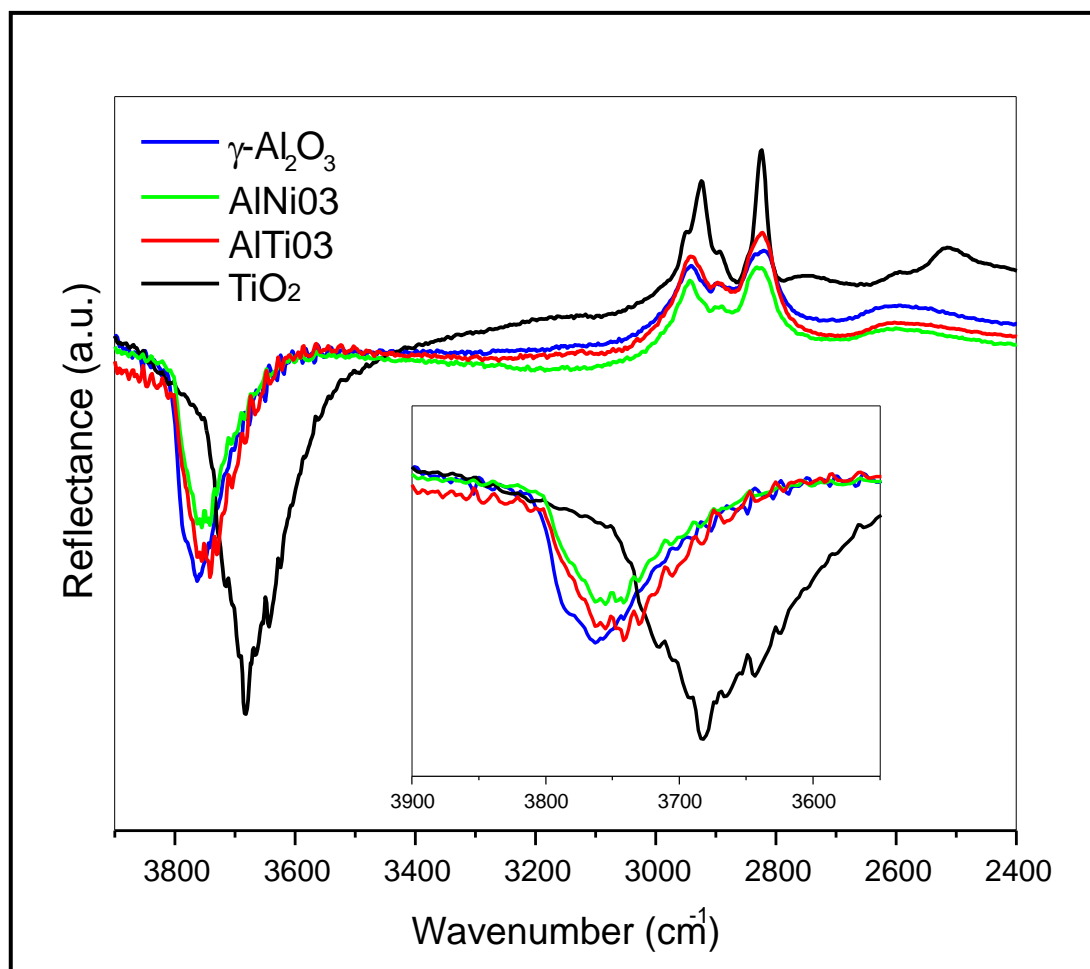


Figure 4.3: DRIFT spectra of adsorbed species over AlTiO₃, AlNiO₃, γ -Al₂O₃, and TiO₂ after desorption of methanol at 150°C

On the other hand, the peaks of the perturbed OH groups in the spectrum of TiO₂ appeared at noticeably lower frequencies, compared with γ -Al₂O₃, indicating the dominance and the involvement of more acidic OH groups on the surface of Titania, which is also confirmed by the TPD results where it shows desorption at higher temperatures indicating strong and medium acid sites. In addition, the adsorbed intermediates seem to bind more strongly to the surface of TiO₂ as indicated by their stronger resistance to desorption at 150°C retaining the perturbed OH groups to a larger extent, as shown in Figure 4.3. This could be the reason behind the significantly lower activity of TiO₂ in this reaction compared to alumina-based

solids where DME is evolved from weakly adsorbed species, whereas the more strongly bound species decompose further forming surface formates and, eventually CH₄ and CO in the gas phase. These suggestions are further supported by the literature, as discussed below [68].

The stronger binding of the OH groups to the TiO₂ surface species, as indicated by the appearance of the ν_{OH} at noticeably lower frequencies, could be referred to the presence of empty *d*-orbitals in the valence of the Ti ions and their higher oxidation state compared to the Al ions, leading to a stronger surface-O bond and hence weaker O-H bond. Adsorption on such OH groups, very likely, results in water molecules and strongly bound methoxy groups, on the account of DME formation. These observations indicate that the terminal OH groups of low-medium acid strength play a more important key role in the dehydration reaction.

Desorption at elevated temperatures resulted in gradual removal of the surface species as shown in Figure 4.4, where the negative ν_{OH} peaks gradually decreased in intensity until almost disappeared after purging at 400°C indicating regeneration of the original surface hydroxyl groups as a result of desorption of the adsorbed species. However, unlike negative ν_{OH} peaks that almost disappeared, the peaks of methoxy groups decreased at a lower rate and were retained to some extent at 400°C, indicating the remaining of some strongly bound isolated methoxy groups. It is also noteworthy that new C-H peaks developed between 2908 and 2927 cm⁻¹ at elevated temperatures, which are comparable to what was assigned to ν_{CH} of formate (-OOCH) species in another study [68, 106]. It is evident that the possible formation of such formate groups is related to the presence of Ti ions in alumina since those peaks were absent or of considerably lower intensity in the corresponding spectrum of γ -Al₂O₃ as shown in Figure 4.5 for spectra after purging at 400°C.

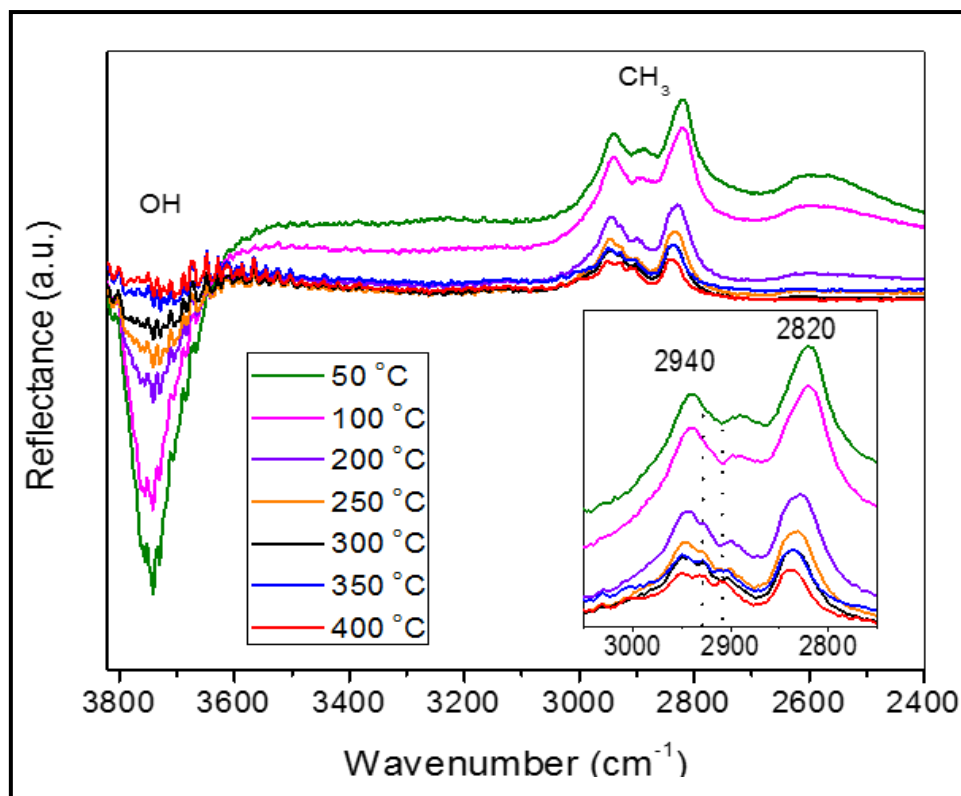


Figure 4.4: DRIFT spectra of adsorbed species after adsorption at 50 °C and subsequent desorption at different temperatures over AlTiO_3

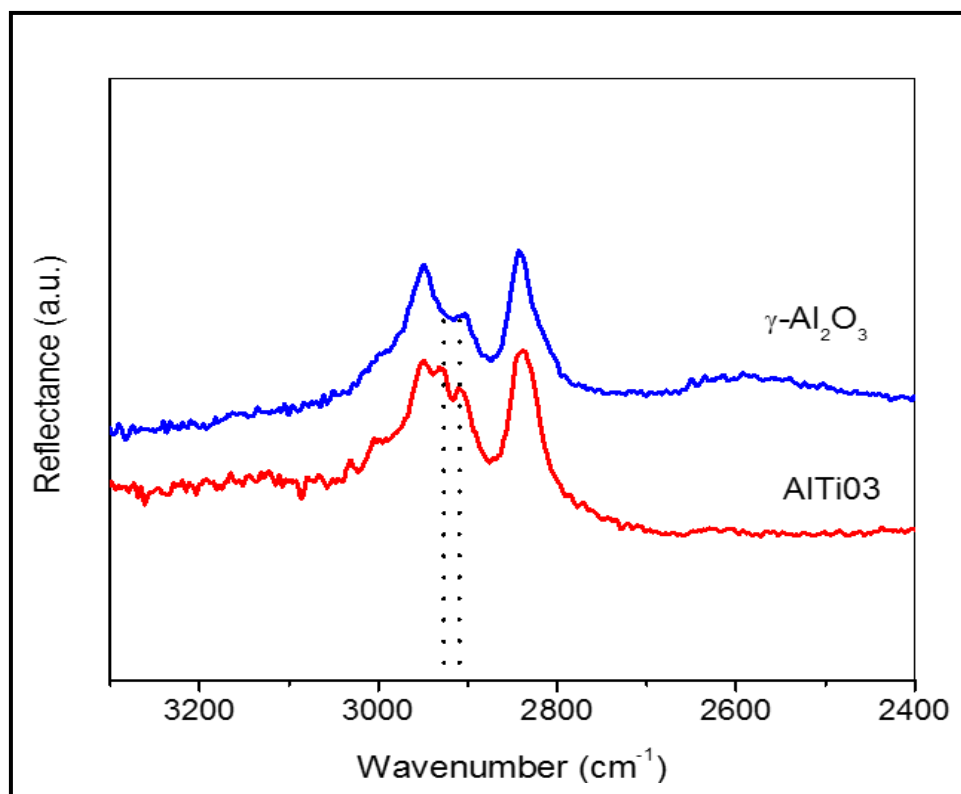


Figure 4.5: DRIFT spectra of adsorbed species over AlTiO_3 and $\gamma\text{-Al}_2\text{O}_3$ after purging at 400 °C

Adsorption of methanol over alumina-based catalysts was compared with that on the selected ZSM5 zeolites. Testing zeolites with low and high density of acid sites, depending on Si/Al ratio, allows for correlating the adsorption and conversion of methanol with surface acid site density. Figure 4.6 shows the DRIFT spectra after adsorption over ZSM5-25 and ZSM5-360 compared with γ -Al₂O₃ and AlTiO₃. The spectra show that, compared with γ -Al₂O₃ and AlTiO₃, zeolites have a higher affinity towards methanol adsorption as evident from the stronger ν_{CH} peaks in the range of 2800-3000 cm⁻¹ and the ν_{CO} peak at 1030 cm⁻¹, which refers to molecularly adsorbed methanol that disappeared completely upon purging as shown in Figure 4.6 (b). The noticeable amount of physisorbed molecules on zeolites could be referred to their ability to retain a significant amount of molecules stored in their micropores before their subsequent interaction with the surface. It is noticed that the negative OH peaks in the spectra of zeolites are at wavenumbers <3740 cm⁻¹ indicating the involvement of, mainly, the acidic bridging OH groups in the interaction with methanol molecules. Also, a significantly higher concentration of hydrogen-bonded OH groups formed on zeolites as indicated by their stronger broad bands in the range of 3200-3600 cm⁻¹. These observations may indicate that adsorption over zeolites was initially dominated by molecular adsorption in their micropores followed by interaction with Brønsted acid sites, which dominate on zeolites' surfaces, resulting in a network of hydrogen-bonded adsorbed species. This type of interaction usually results in associative adsorption and hence, weakly adsorbed intermediates, rather than dissociative adsorption as is the case when adsorption takes place on Lewis acid sites, which dominate on γ -Al₂O₃ surface [68, 106].

It is noteworthy that after purging at 150°C, Figure 4.6 (b) the zeolite with higher Al content, ZSM5-25, which has a larger concentration of Al-OH-Si sites, showed higher resistance to desorption compared with ZSM5-360. This behavior is inferred from the retained peaks of perturbed OH groups in the spectrum of ZSM5-25, especially in the lower frequency region of 3600-3700 cm^{-1} indicating stronger binding with increased Al content. The weaker adsorption on ZSM5-360 correlates with its lower activity towards methanol dehydration to dimethyl ether as was observed from the catalytic activity test in Chapter 3.

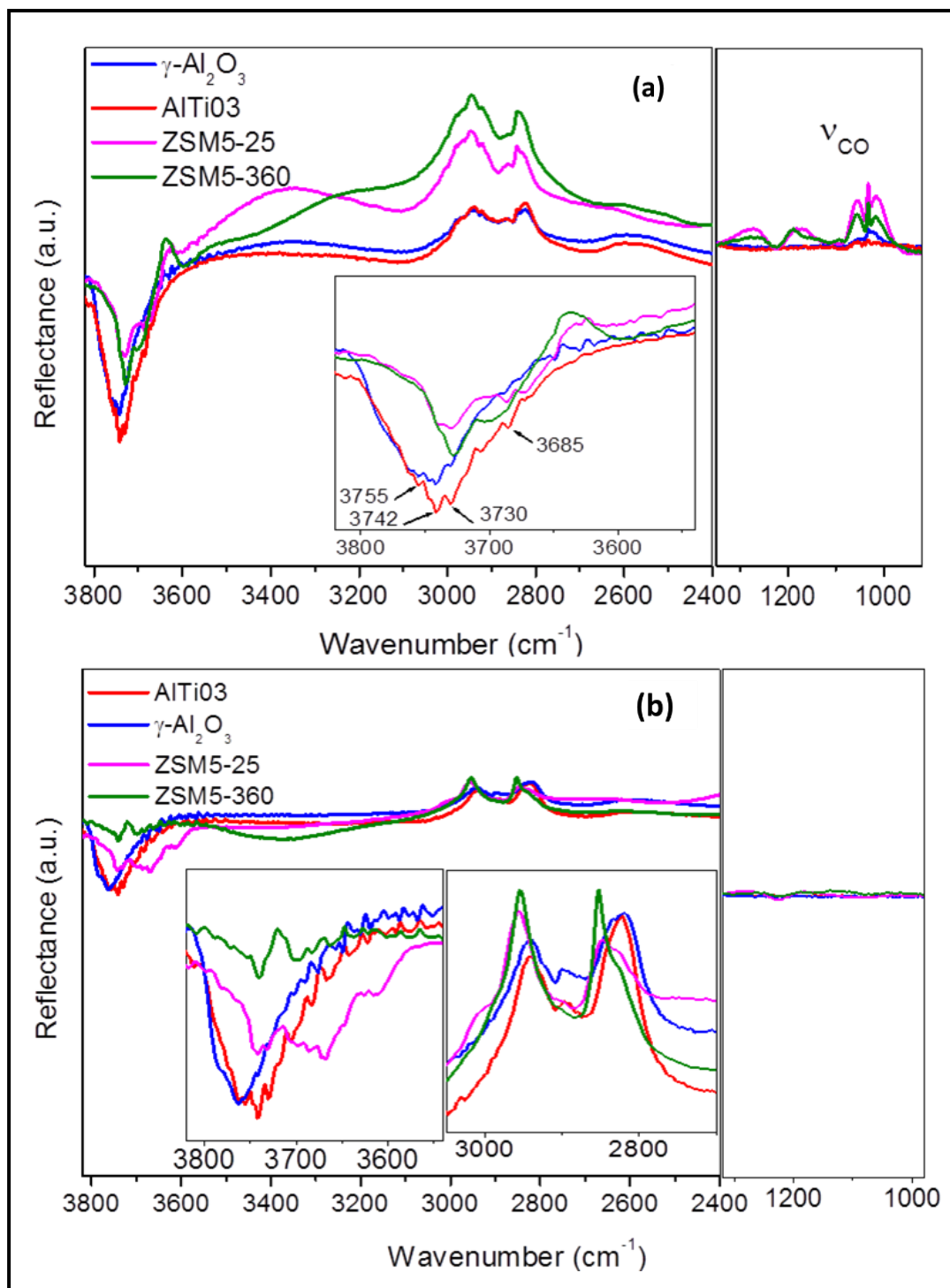


Figure 4.6: DRIFT spectra of surface species over zeolites compared with $\gamma\text{-Al}_2\text{O}_3$ and AlTiO3 after (a) adsorption of methanol at 50°C and (b) desorption at 150°C

The adsorption of methanol molecules on zeolites through, mainly, hydrogen bonding with Brønsted acid sites indicates that its interactions during the dehydration reaction to dimethyl ether take place on the surface of zeolites through an associative pathway as shown in Figure 4.7, route A, which is supported by the observed perturbation of the ν_{OH} peaks. The high concentration of acidic hydroxyl groups on the zeolites surfaces is expected to lead to a high concentration of hydrogen-bound intermediates (A1) with which gas-phase molecules, in the presence of methanol vapor, can interact (A2) to produce DME and water. It has been also proposed [115] that an adsorbed molecule dehydrates first, as shown in route B, producing a surface methoxy group, B1, which can react with a gas phase molecule in the presence of methanol vapor to produce a DME molecule. However, theoretical calculations showed that this route is less favorable [127], which allows proposing that route A dominates on Brønsted acid-rich surfaces such as zeolites. This suggested route may explain the observed enhanced resistance to desorption on the more acidic zeolite, ZSM5-25, Figure 4.6 (b), which can be referred to the high concentration of bridging OH groups, Si-OH-Al, which may result in a larger number of hydrogen bonds.

The broader ν_{OH} as well as the weaker ν_{CH} peaks on ZSM5-25 compared to ZSM-360 further supports this explanation. These observations allow proposing Al-rich ZSM5 zeolites as better catalysts for the dehydration reaction of methanol to DME since more rapid desorption over low-Al-content zeolites would enhance removal of methanol molecules from the surface before undergoing the dehydration reaction. This explanation correlates with the fact that zeolites yield more coke at higher reaction temperatures compared to alumina because of this stronger binding that leads to decomposition at higher temperatures.

Compared with zeolites, adsorption over the alumina-based surfaces, which are usually dominated by Lewis acid sites, resulted in more pronounced perturbation of the terminal OH groups as indicated by more intense negative ν_{OH} peaks, especially for groups at frequencies $>3750 \text{ cm}^{-1}$. Those OH groups are less acidic than the low-frequency groups and can act as basic sites. The presence of such basic OH group in the vicinity of a Lewis acid-base pair site may promote dissociative adsorption of a methanol molecule, as shown in route C of Figure 4.7, leading to the formation of an isolated methoxy group bound to a Lewis acid site and a new OH group on a neighboring oxide basic site, intermediate C1. The basic nature of the terminal OH group promotes dehydration with the newly created OH group creating a new reactive Lewis acid site (C2) that promote dissociative adsorption of a second methanol molecule which condenses with the already existing methoxy group (C3) resulting in a DME molecule and regenerated surface. This suggested role of the basic OH groups is supported by the significant perturbation of these groups on the alumina-based solids as indicated by the strong negative peaks in their spectra. On fully dehydrated alumina surface, there will be a chance for two molecules to co-adsorb dissociatively on two Lewis acid-base pairs producing two methoxy and two hydroxyl groups. However, the proposed mechanism (route C) is more likely on the alumina-based solids in the present study due to the presence of a significant concentration of terminal OH groups on their surfaces as evident from their DRIFT spectra. In summary, the dehydration reaction seems to take place via an associative route over zeolites with a key role of Bronsted acid sites, while a dissociative route dominates over the surfaces of alumina-based solids where Lewis acid-base pair sites and basic OH groups play key roles.

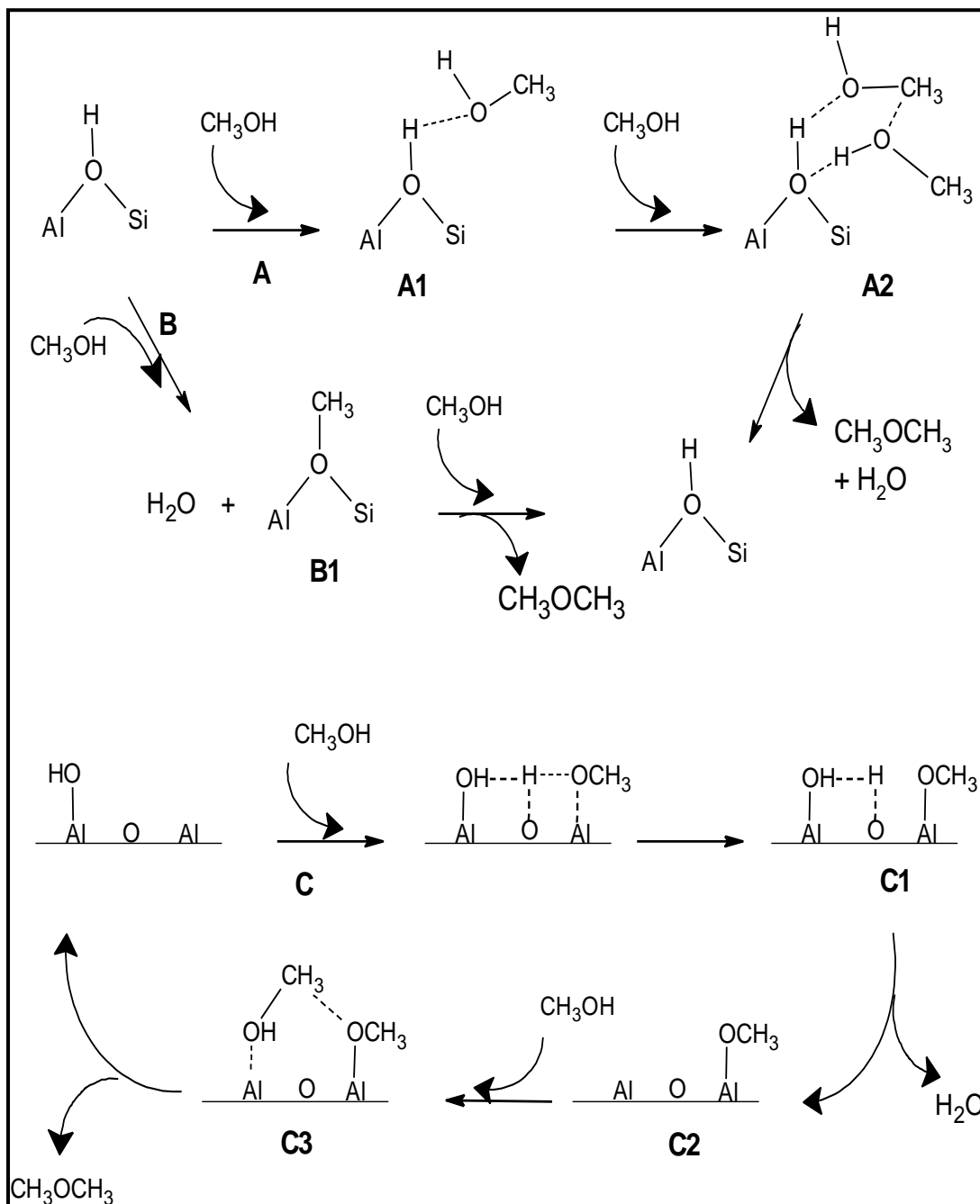


Figure 4.7: Suggested mechanistic steps for the adsorption of methanol on γ - Al_2O_3 -based solids compared with ZSM5 zeolites

Chapter 5: Conclusion and Future Work

In this work, γ -Al₂O₃ and metal-doped γ -Al₂O₃ catalytic materials were prepared using the sol-gel method and were characterized by various physical and chemical techniques. The prepared catalysts were tested in the methanol dehydration to dimethyl ether reaction at temperatures in the range of 150-400°C. The surface acid-base properties and the catalytic activity of the prepared γ -Al₂O₃-based catalysts were compared with those of selected commercial zeolites.

The prepared modified catalytic materials were based on γ -Al₂O₃ doped with different metal ions, including Ti(IV), Ni(II), and V(III). The employed preparation conditions resulted in well-dispersion of the dopant ions with concentrations between 3-10% in the amorphous γ -Al₂O₃ structure, where no segregated phases of the dopant oxides were observed. The study showed that doping of γ -Al₂O₃ resulted in significant textural modifications including higher surface areas, larger total pore volumes, and more homogeneous mesopores compared with their undoped counterpart. These textural modifications, especially the significant mesoporosity, in the prepared catalysts offer a great advantage to these materials over the studied zeolites, which contain only micropores that limit reactants and products diffusion during reactions, especially when the reactions are associated with coke formation that blocks such pores.

The catalytic activity study showed that the incorporation of certain concentrations of Ti(IV) and Ni(II) ions in the γ -Al₂O₃ matrix resulted in enhanced catalytic activity, especially at the lower reaction temperature, < 200°C. The study also showed that the optimum reaction temperature is in the range of 200-250°C, and at higher temperatures, CO₂ and methane were the main products.

The catalytic activity and the role of the dopants were correlated with the surface acid characteristics of the studied catalysts. The surface acid-base properties of the prepared materials and the commercial zeolites were characterized by chemisorption of ammonia as a probe molecule. The study showed that doping with Ti(IV) ions resulted in an enhanced overall acidity compared to γ -Al₂O₃. The role of the dopants was also correlated with their electronic structures, especially the effect of the oxidation state and the *d*-configuration of the dopant ions on the Al ion coordination and the tendency for methanol adsorption and activation.

The in-situ methanol adsorption study revealed that Ti ions dispersed in γ -Al₂O₃ showed a noticeable effect on the characteristics of its surface hydroxyl groups, which was associated with enhanced chemisorption of methanol. The study also showed that the differences in the nature of the surface hydroxyl groups on the surface of γ -Al₂O₃ and ZSM5 zeolites lead to different routes of methanol adsorption and dehydration over the surfaces of both types of materials. It was evident that associative adsorption dominates over zeolites with a key role of Brønsted acid sites in the formation of DME. In contrast, dissociative adsorption dominates over the surfaces of alumina-based catalysts where Lewis acid-base pair sites and basic OH groups play key roles.

Future recommended work includes studying the effect of the pretreatment conditions of the γ -Al₂O₃-based catalysts as the surface characteristics depend on the pretreatment temperature. Chemisorption of pyridine as a probe molecule is another important study that helps in distinguishing between the types of the acid sites on the surface. Furthermore, investigating other different reaction parameters such as the flow rate and the concentration of methanol in the feed stream would be significant studies to establish the kinetics of the reaction.

References

- [1] U. Mondal and G. D. Yadav, "Perspective of dimethyl ether as fuel: Part I. Catalysis," *Journal of CO₂ Utilization*, vol. 32, pp. 299–320, Jul. 2019, doi: 10.1016/j.jcou.2019.02.003.
- [2] T. H. Fleisch, A. Basu, and R. A. Sills, "Introduction and advancement of a new clean global fuel: The status of DME developments in China and beyond," *Journal of Natural Gas Science and Engineering*, vol. 9, pp. 94–107, Nov. 2012, doi: 10.1016/j.jngse.2012.05.012.
- [3] G. Thomas, B. Feng, A. Veeraragavan, M. J. Cleary, and N. Drinnan, "Emissions from DME combustion in diesel engines and their implications on meeting future emission norms: A review," *Fuel Processing Technology*, vol. 119, pp. 286–304, Mar. 2014, doi: 10.1016/j.fuproc.2013.10.018.
- [4] S. S. A. Hosseinijad, "Catalytic and kinetic study of methanol dehydration to dimethyl ether," M.S., University of Alberta, Canada, 2010.
- [5] "Dimethyl Ether Market," *MarketsAndMarkets*. <https://secure.livechatinc.com/> (Accessed Mar. 07, 2020).
- [6] Y. Zhu, S. Wang, X. Ge, Q. Liu, Z. Luo, and K. Cen, "Experimental study of improved two step synthesis for DME production," *Fuel Processing Technology*, vol. 91, no. 4, pp. 424–429, Apr. 2010, doi: 10.1016/j.fuproc.2009.05.001.
- [7] Z. Azizi, M. Rezaeimanesh, T. Tohidian, and M. R. Rahimpour, "Dimethyl ether: A review of technologies and production challenges," *Chemical Engineering and Processing: Process Intensification*, vol. 82, pp. 150–172, Aug. 2014, doi: 10.1016/j.cep.2014.06.007.
- [8] Y. Wang *et al.*, "One-step synthesis of dimethyl ether from syngas on ordered mesoporous copper incorporated alumina," *Journal of Energy Chemistry*, vol. 25, no. 5, pp. 775–781, Sep. 2016, doi: 10.1016/j.jechem.2016.04.014.
- [9] I. A. Kurzina, S. I. Reshetnikov, N. I. Karakchieva, and L. N. Kurina, "Direct synthesis of dimethyl ether from synthesis gas: Experimental study and mathematical modeling," *Chemical Engineering Journal*, vol. 329, pp. 135–141, Dec. 2017, doi: 10.1016/j.cej.2017.04.132.
- [10] D. Mao, J. Xia, Q. Chen, and G. Lu, "Highly effective conversion of syngas to dimethyl ether over the hybrid catalysts containing high-silica HMCM-22 zeolites," *Catalysis Communications*, vol. 10, no. 5, pp. 620–624, Jan. 2009, doi: 10.1016/j.catcom.2008.11.003.

- [11] Z. Chen, H. Zhang, W. Ying, and D. Fang, "Global Kinetics of Direct Dimethyl Ether Synthesis Process from Syngas in Slurry Reactor over a Novel Cu-Zn-Al-Zr Slurry Catalyst," vol. 4, no. 8, p. 7, 2010, doi: 10.5281/zenodo.1085064
- [12] M. De Falco, M. Capocelli, and A. Basile, "Selective membrane application for the industrial one-step DME production process fed by CO₂ rich streams: Modeling and simulation," *International Journal of Hydrogen Energy*, vol. 42, no. 10, pp. 6771–6786, Mar. 2017, doi: 10.1016/j.ijhydene.2017.02.047.
- [13] C. Mevawala, Y. Jiang, and D. Bhattacharyya, "Plant-wide modeling and analysis of the shale gas to dimethyl ether (DME) process via direct and indirect synthesis routes," *Applied Energy*, vol. 204, pp. 163–180, Oct. 2017, doi: 10.1016/j.apenergy.2017.06.085.
- [14] "Solid Acid Catalysis: From Fundamentals to Applications," *Focus on Catalysts*, vol. 2015, no. 8, p. 7, Aug. 2015, doi: 10.1016/j.focat.2015.07.088.
- [15] "Catalyst | chemistry," *Encyclopedia Britannica*, Dec. 14, 2017. <https://www.britannica.com/science/catalyst> (Accessed Sep. 22, 2018).
- [16] A. I. Osman, J. K. Abu-Dahrieh, D. W. Rooney, S. A. Halawy, M. A. Mohamed, and A. Abdelkader, "Effect of precursor on the performance of alumina for the dehydration of methanol to dimethyl ether," *Applied Catalysis B: Environmental*, vol. 127, pp. 307–315, Oct. 2012, doi: 10.1016/j.apcatb.2012.08.033.
- [17] F. Yaripour, Z. Shariatinia, S. Sahebdehfar, and A. Irandoukht, "The effects of synthesis operation conditions on the properties of modified γ -alumina nanocatalysts in methanol dehydration to dimethyl ether using factorial experimental design," *Fuel*, vol. 139, pp. 40–50, Jan. 2015, doi: 10.1016/j.fuel.2014.08.029.
- [18] F. Yaripour, F. Baghaei, I. Schmidt, and J. Perregaard, "Catalytic dehydration of methanol to dimethyl ether (DME) over solid-acid catalysts," *Catalysis Communications*, vol. 6, no. 2, pp. 147–152, Feb. 2005, doi: 10.1016/j.catcom.2004.11.012.
- [19] J. Ereña, R. Garoña, J. M. Arandes, A. T. Aguayo, and J. Bilbao, "Direct Synthesis of Dimethyl Ether From (H₂+CO) and (H₂+CO₂) Feeds. Effect of Feed Composition," *International Journal of Chemical Reactor Engineering*, vol. 3, no. 1, Oct. 2005, doi: 10.2202/1542-6580.1295.
- [20] F. S. Ramos *et al.*, "Role of dehydration catalyst acid properties on one-step DME synthesis over physical mixtures," *Catalysis Today*, vol. 101, no. 1, pp. 39–44, Mar. 2005, doi: 10.1016/j.cattod.2004.12.007.

- [21] K. S. Yoo, J.H. Kim, M.-J. Park, S.J. Kim, O.S. Joo, and K.D. Jung, "Influence of solid acid catalyst on DME production directly from synthesis gas over the admixed catalyst of Cu/ZnO/Al₂O₃ and various SAPO catalysts," *Applied Catalysis A: General*, vol. 330, pp. 57–62, Oct. 2007, doi: 10.1016/j.apcata.2007.07.007.
- [22] J. H. Flores, D. P. B. Peixoto, L. G. Appel, R. R. de Avillez, and M. I. P. da Silva, "The influence of different methanol synthesis catalysts on direct synthesis of DME from syngas," *Catalysis Today*, vol. 172, no. 1, pp. 218–225, Aug. 2011, doi: 10.1016/j.cattod.2011.02.063.
- [23] S.M. Kim, Y.J. Lee, J. W. Bae, H. S. Potdar, and K.W. Jun, "Synthesis and characterization of a highly active alumina catalyst for methanol dehydration to dimethyl ether," *Applied Catalysis A: General*, vol. 348, no. 1, pp. 113–120, Sep. 2008, doi: 10.1016/j.apcata.2008.06.032.
- [24] E. Taveras, "Innovative Catalyst Development for Synthesis of Dimethyl Ether (DME): A Renewable Diesel Substitute," M.S., State University of New York at Stony Brook, USA, 2017.
- [25] D. M. Sung, Y. H. Kim, E. D. Park, and J. E. Yie, "Correlation between acidity and catalytic activity for the methanol dehydration over various aluminum oxides," *Res Chem Intermed*, vol. 36, no. 6, pp. 653–660, Nov. 2010, doi: 10.1007/s11164-010-0201-y.
- [26] M. Sobhani, H. Tavakoli, M. D. Chermahini, and M. Kazazi, "Preparation of macro-mesoporous γ -alumina via biology gelatin assisted aqueous sol-gel process," *Ceramics International*, vol. 45, no. 1, pp. 1385–1391, Jan. 2019, doi: 10.1016/j.ceramint.2018.09.056.
- [27] M. Farahmandjou and S. Motaghi, "Sol-gel synthesis of Ce-doped α -Al₂O₃: Study of crystal and optoelectronic properties," *Optics Communications*, vol. 441, pp. 1–7, Jun. 2019, doi: 10.1016/j.optcom.2019.02.029.
- [28] M. Nazari, R. M. Behbahani, A. Goshtasbi, and M. Ghavipour, "Optimizing the Operating Parameters for DME Production," *Energy Sources, Part A: Recovery, Utilization, and Environmental Effects*, vol. 37, no. 7, pp. 766–774, Apr. 2015, doi: 10.1080/15567036.2011.590858.
- [29] A. I. Osman, J. K. Abu-Dahrieh, D. W. Rooney, J. Thompson, S. A. Halawy, and M. A. Mohamed, "Surface hydrophobicity and acidity effect on alumina catalyst in catalytic methanol dehydration reaction," *Journal of Chemical Technology & Biotechnology*, vol. 92, no. 12, pp. 2952–2962, Dec. 2017, doi: 10.1002/jctb.5371.

- [30] D. M. Sung, Y. H. Kim, E. D. Park, and J. E. Yie, "Role of surface hydrophilicity of alumina in methanol dehydration," *Catalysis Communications*, vol. 20, pp. 63–67, Apr. 2012, doi: 10.1016/j.catcom.2012.01.005.
- [31] A. J. Jones, "Acid Strength and Solvation in Catalysis by Solid Acids," PhD, University of California, Berkeley, USA, 2014.
- [32] Hamed Bateni and Chad Able, "Development of Heterogeneous Catalysts for Dehydration of Methanol to Dimethyl Ether: A Review," *Catal. Ind.*, vol. 11, no. 1, pp. 7–33, Jan. 2019, doi: 10.1134/S2070050419010045.
- [33] E. Catizzone *et al.*, "Catalytic application of ferrierite nanocrystals in vapour-phase dehydration of methanol to dimethyl ether," *Applied Catalysis B: Environmental*, vol. 243, pp. 273–282, Apr. 2019, doi: 10.1016/j.apcatb.2018.10.060.
- [34] D. Masih, S. Rohani, J. N. Kondo, and T. Tatsumi, "Low-temperature methanol dehydration to dimethyl ether over various small-pore zeolites," *Applied Catalysis B: Environmental*, vol. 217, pp. 247–255, Nov. 2017, doi: 10.1016/j.apcatb.2017.05.089.
- [35] E. P. Schreiner, "Manipulation of zeolite active site acidity and atomic structure to control hydrocarbon conversion and selectivity," Thesis, University of Delaware, USA, 2017.
- [36] E. Catizzone, M. Migliori, A. Purita, and G. Giordano, "Ferrierite vs. γ -Al₂O₃: The superiority of zeolites in terms of water-resistance in vapour-phase dehydration of methanol to dimethyl ether," *Journal of Energy Chemistry*, vol. 30, pp. 162–169, May 2018, doi: 10.1016/j.jechem.2018.05.004.
- [37] M. Migliori, A. Aloise, and G. Giordano, "Methanol to dimethylether on H-MFI catalyst: The influence of the Si/Al ratio on kinetic parameters," *Catalysis Today*, vol. 227, pp. 138–143, May 2014, doi: 10.1016/j.cattod.2013.09.033.
- [38] A. E.A. A. Said, M. M. Abd El-Wahab, and M. A. El-Aal, "The catalytic performance of sulfated zirconia in the dehydration of methanol to dimethyl ether," *Journal of Molecular Catalysis A: Chemical*, vol. 394, pp. 40–47, Nov. 2014, doi: 10.1016/j.molcata.2014.06.041.
- [39] V. Vishwanathan, H.S. Roh, J.W. Kim, and K.W. Jun, "Surface Properties and Catalytic Activity of TiO₂–ZrO₂ Mixed Oxides in Dehydration of Methanol to Dimethyl Ether," *Catalysis Letters*, vol. 96, no. 1, pp. 23–28, Jul. 2004, doi: 10.1023/B:CATL.0000029524.94392.9f.
- [40] F. Yaripour, F. Baghaei, I. Schmidt, and J. Perregaard, "Synthesis of dimethyl ether from methanol over aluminium phosphate and silica–titania catalysts,"

Catalysis Communications, vol. 6, no. 8, pp. 542–549, Aug. 2005, doi: 10.1016/j.catcom.2005.05.003.

- [41] M. A. Armenta, V. M. Maytorena, R. G. Alamilla, R. Valdez, and A. Olivas, “Thermodynamic and catalytic properties of Cu- and Pd- oxides over mixed γ - χ - Al_2O_3 for methanol dehydration toward dimethyl ether,” *International Journal of Hydrogen Energy*, vol. 44, no. 14, pp. 7276–7287, Mar. 2019, doi: 10.1016/j.ijhydene.2019.01.243.
- [42] Y. Wang, F. Ren, D. Pan, and J. Ma, “A Hierarchically Micro-Meso-Macroporous Zeolite CaA for Methanol Conversion to Dimethyl Ether,” *Crystals*, vol. 6, no. 11, Art. no. 11, Nov. 2016, doi: 10.3390/cryst6110155.
- [43] J. Palomo, J. Rodríguez-Mirasol, and T. Cordero, “Methanol Dehydration to Dimethyl Ether on Zr-Loaded P-Containing Mesoporous Activated Carbon Catalysts,” *Materials (Basel)*, vol. 12, no. 13, Jul. 2019, doi: 10.3390/ma12132204.
- [44] J. Palomo, M. Á. Rodríguez-Cano, J. M. Rosas, J. Rodríguez-Mirasol, and T. Cordero, “Kinetic study of methanol dehydration over ZrO_2 supported-activated carbons,” Jul. 2018, Accessed: Apr. 16, 2020. [Online]. Available: <https://riuma.uma.es/xmlui/handle/10630/16207>.
- [45] A. Abdelkader, A. I. Osman, S. A. Halawy, and M. A. Mohamed, “Preparation and characterization of mesoporous γ - Al_2O_3 recovered from aluminum cans waste and its use in the dehydration of methanol to dimethyl ether,” *J Mater Cycles Waste Manag*, vol. 20, no. 3, pp. 1428–1436, Jul. 2018, doi: 10.1007/s10163-018-0702-0.
- [46] A. E.A. A. Said and M. A. El-Aal, “Effect of different metal sulfate precursors on structural and catalytic performance of zirconia in dehydration of methanol to dimethyl ether,” *Journal of Fuel Chemistry and Technology*, vol. 46, no. 1, pp. 67–74, Jan. 2018, doi: 10.1016/S1872-5813(18)30004-5.
- [47] A. Bordoloi *et al.*, “Process for the preparation of phosphorous containing mesoporous alumina catalyst for selective dehydration of methanol to dimethyl ether,” United States Patent US9468914B2, Oct. 18, 2016.
- [48] Y. Wei, P. E. de Jongh, M. L. M. Bonati, D. J. Law, G. J. Sunley, and K. P. de Jong, “Enhanced catalytic performance of zeolite ZSM5 for conversion of methanol to dimethyl ether by combining alkaline treatment and partial activation,” *Applied Catalysis A: General*, vol. 504, pp. 211–219, Sep. 2015, doi: 10.1016/j.apcata.2014.12.027.

- [49] S. Liu and L. Zhang, "Effects of Reaction Conditions on Methanol Produced to Dimethyl Ether," *Energy Sources, Part A: Recovery, Utilization, and Environmental Effects*, vol. 37, no. 18, pp. 1937–1942, Sep. 2015, doi: 10.1080/15567036.2012.654901.
- [50] J. Xiang *et al.*, "(Al_{1-x}Cr_x)₄B₆O₁₅ (0.08 ≤ x ≤ 0.14): Metal borates catalyze the dehydration of methanol into dimethyl ether," *Materials Research Bulletin*, vol. 65, pp. 279–286, May 2015, doi: 10.1016/j.materresbull.2015.02.010.
- [51] E. Kianfar, "Synthesis and Characterization of AlPO₄/ZSM5 Catalyst for Methanol Conversion to Dimethyl Ether," *Russ J Appl Chem*, vol. 91, no. 10, pp. 1711–1720, Oct. 2018, doi: 10.1134/S1070427218100208.
- [52] A. E.A. A. Said, M. M. M. Abd El-Wahab, and M. Abd El-Aal, "Effect of ZrO₂ on the catalytic performance of nano γ -Al₂O₃ in dehydration of methanol to dimethyl ether at relatively low temperature," *Res Chem Intermed*, vol. 42, no. 2, pp. 1537–1556, Feb. 2016, doi: 10.1007/s11164-015-2101-7.
- [53] M. A. Armenta, R. Valdez, J. M. Quintana, R. Silva-Rodrigo, L. Cota, and A. Olivas, "Highly selective CuO/ γ -Al₂O₃ catalyst promoted with hematite for efficient methanol dehydration to dimethyl ether," *International Journal of Hydrogen Energy*, vol. 43, no. 13, pp. 6551–6560, Mar. 2018, doi: 10.1016/j.ijhydene.2018.02.051.
- [54] M. J. Valero-Romero, E. M. Calvo-Muñoz, R. Ruiz-Rosas, J. Rodríguez-Mirasol, and T. Cordero, "Phosphorus-Containing Mesoporous Carbon Acid Catalyst for Methanol Dehydration to Dimethyl Ether," *Ind. Eng. Chem. Res.*, vol. 58, no. 10, pp. 4042–4053, Mar. 2019, doi: 10.1021/acs.iecr.8b05897.
- [55] S. Y. Hosseini and M. R. Khosravi-Nikou, "Synthesis and characterization of nano-sized γ -Al₂O₃ for investigation the effect of temperature on catalytic dehydration of methanol to dimethyl ether," *Energy Sources, Part A: Recovery, Utilization, and Environmental Effects*, vol. 38, no. 7, pp. 914–920, Apr. 2016, doi: 10.1080/15567036.2011.652757.
- [56] S. M. K. Aboul Fotouh, "Production of dimethylether (DME) as a clean fuel using sonochemically prepared CuO and/or ZnO-modified γ -alumina catalysts," *Journal of Fuel Chemistry and Technology*, vol. 42, no. 3, pp. 350–356, Mar. 2014, doi: 10.1016/S1872-5813(14)60020-7.
- [57] C.L. Chiang and K.S. Lin, "Preparation and characterization of CuOAl₂O₃ catalyst for dimethyl ether production via methanol dehydration," *International Journal of Hydrogen Energy*, vol. 42, no. 37, pp. 23526–23538, Sep. 2017, doi: 10.1016/j.ijhydene.2017.01.063.

- [58] Z. Chen *et al.*, “Fabrication of nano-sized SAPO-11 crystals with enhanced dehydration of methanol to dimethyl ether,” *Catalysis Communications*, vol. 103, pp. 1–4, Jan. 2018, doi: 10.1016/j.catcom.2017.09.002.
- [59] W. Dai, W. Kong, G. Wu, N. Li, L. Li, and N. Guan, “Catalytic dehydration of methanol to dimethyl ether over aluminophosphate and silico-aluminophosphate molecular sieves,” *Catalysis Communications*, vol. 12, no. 6, pp. 535–538, Feb. 2011, doi: 10.1016/j.catcom.2010.11.019.
- [60] E. Catizzone, A. Aloise, M. Migliori, and G. Giordano, “The effect of FER zeolite acid sites in methanol-to-dimethyl-ether catalytic dehydration,” *Journal of Energy Chemistry*, vol. 26, no. 3, pp. 406–415, May 2017, doi: 10.1016/j.jechem.2016.12.005.
- [61] D. Macina, Z. Piwowarska, K. Tarach, K. Góra-Marek, J. Ryczkowski, and L. Chmielarz, “Mesoporous silica materials modified with alumina polycations as catalysts for the synthesis of dimethyl ether from methanol,” *Materials Research Bulletin*, vol. 74, pp. 425–435, Feb. 2016, doi:10.1016/j.materresbull.2015.11.018.
- [62] M. Migliori *et al.*, “New insights about coke deposition in methanol to DME reaction over MOR, MFI and FER-type zeolites,” *Journal of Industrial and Engineering Chemistry*, vol. 68, pp. 196–208, Dec. 2018, doi: 10.1016/j.jiec.2018.07.046.
- [63] Z. Hosseini, M. Taghizadeh, and F. Yaripour, “Synthesis of nanocrystalline γ - Al_2O_3 by sol-gel and precipitation methods for methanol dehydration to dimethyl ether,” *Journal of Natural Gas Chemistry*, vol. 20, no. 2, pp. 128–134, Mar. 2011, doi: 10.1016/S1003-9953(10)60172-7.
- [64] K. C. Tokay, T. Dogu, and G. Dogu, “Dimethyl ether synthesis over alumina based catalysts,” *Chemical Engineering Journal*, vol. 184, pp. 278–285, Mar. 2012, doi: 10.1016/j.cej.2011.12.034.
- [65] D. Liu, C. Yao, J. Zhang, D. Fang, and D. Chen, “Catalytic dehydration of methanol to dimethyl ether over modified γ - Al_2O_3 catalyst,” *Fuel*, vol. 90, no. 5, pp. 1738–1742, May 2011, doi: 10.1016/j.fuel.2011.01.038.
- [66] V. V. Volkov, E. G. Novitskii, G. A. Dibrov, P. V. Samokhin, M. A. Kipnis, and A. B. Yaroslavtsev, “Catalytic conversion of methanol to dimethyl ether on polymer/ceramic composite membranes,” *Catalysis Today*, vol. 193, no. 1, pp. 31–36, Oct. 2012, doi: 10.1016/j.cattod.2012.05.017.
- [67] R. M. Ladera, J. L. G. Fierro, M. Ojeda, and S. Rojas, “ TiO_2 -supported heteropoly acids for low-temperature synthesis of dimethyl ether from

- methanol,” *Journal of Catalysis*, vol. 312, pp. 195–203, Apr. 2014, doi: 10.1016/j.jcat.2014.01.016.
- [68] S. S. Akarmazyan, P. Panagiotopoulou, A. Kambolis, C. Papadopoulou, and D. I. Kondarides, “Methanol dehydration to dimethylether over Al_2O_3 catalysts,” *Applied Catalysis B: Environmental*, vol. 145, no. Supplement C, pp. 136–148, Feb. 2014, doi: 10.1016/j.apcatb.2012.11.043.
- [69] R. Ladera, E. Finocchio, S. Rojas, G. Busca, J. L. G. Fierro, and M. Ojeda, “Supported WOX-based catalysts for methanol dehydration to dimethyl ether,” *Fuel*, vol. 113, pp. 1–9, Nov. 2013, doi: 10.1016/j.fuel.2013.05.083.
- [70] B. M. Abu-Zied, “Controlled synthesis of praseodymium oxide nanoparticles obtained by combustion route: Effect of calcination temperature and fuel to oxidizer ratio,” *Applied Surface Science*, vol. 471, pp. 246–255, Mar. 2019, doi: 10.1016/j.apsusc.2018.12.007.
- [71] N. K. Renuka, A. V. Shijina, and A. K. Praveen, “Mesoporous γ -alumina nanoparticles: Synthesis, characterization and dye removal efficiency,” *Materials Letters*, vol. 82, pp. 42–44, Sep. 2012, doi: 10.1016/j.matlet.2012.05.043.
- [72] J. Yi, Y. Sun, J. Gao, and C. Xu, “Synthesis of crystalline γ - Al_2O_3 with high purity,” *Transactions of Nonferrous Metals Society of China*, vol. 19, no. 5, pp. 1237–1242, Oct. 2009, doi: 10.1016/S1003-6326(08)60435-5.
- [73] S. Said, S. Mikhail, and M. Riad, “Recent progress in preparations and applications of meso-porous alumina,” *Materials Science for Energy Technologies*, vol. 2, no. 2, pp. 288–297, Aug. 2019, doi: 10.1016/j.mset.2019.02.005.
- [74] T. K. Tseng, Y. S. Lin, Y. J. Chen, and H. Chu, “A Review of Photocatalysts Prepared by Sol-Gel Method for VOCs Removal,” *Int J Mol Sci*, vol. 11, no. 6, pp. 2336–2361, May 2010, doi: 10.3390/ijms11062336.
- [75] G. V. Aguilar, “Introductory Chapter: A Brief Semblance of the Sol-Gel Method in Research,” *Sol-Gel Method Design and Synthesis of New Materials with Interesting Physical, Chemical and Biological Properties*, Dec. 2018, doi: 10.5772/intechopen.82487.
- [76] A. Khaleel, M. Nawaz, and B. Hindawi, “Sol-gel derived Cr(III) and Cu(II)/ γ - Al_2O_3 doped solids: Effect of the dopant precursor nature on the structural, textural and morphological properties,” *Materials Research Bulletin*, vol. 48, no. 4, pp. 1709–1715, Apr. 2013, doi: 10.1016/j.materresbull.2013.01.027.

- [77] A. Durán, Y. Castro, A. Conde, and J. J. de Damborenea, “Sol–Gel Protective Coatings for Metals,” *Handbook of Sol-Gel Science and Technology*, pp. 1–65, 2016, doi: 10.1007/978-3-319-19454-7_70-1.
- [78] S. Park, C.H. Kim, W.J. Lee, S. Sung, and M.H. Yoon, “Sol-gel metal oxide dielectrics for all-solution-processed electronics,” *Materials Science and Engineering: R: Reports*, vol. 114, pp. 1–22, Apr. 2017, doi: 10.1016/j.mser.2017.01.003.
- [79] M. Yao *et al.*, “Dielectric properties under high electric field for silicon doped alumina thin film with glass-like structure derived from sol-gel process,” *Journal of Alloys and Compounds*, vol. 690, pp. 249–255, Jan. 2017, doi: 10.1016/j.jallcom.2016.07.125.
- [80] A. Vázquez, T. López, R. Gómez, Bokhimi, A. Morales, and O. Novaro, “X-Ray Diffraction, FTIR, and NMR Characterization of Sol–Gel Alumina Doped with Lanthanum and Cerium,” *Journal of Solid State Chemistry*, vol. 128, no. 2, pp. 161–168, Feb. 1997, doi: 10.1006/jssc.1996.7135.
- [81] H. Cui, M. Zayat, and D. Levy, “A sol–gel route using propylene oxide as a gelation agent to synthesize spherical NiAl_2O_4 nanoparticles,” *Journal of Non-Crystalline Solids*, vol. 351, no. 24, pp. 2102–2106, Aug. 2005, doi: 10.1016/j.jnoncrysol.2005.04.060.
- [82] A. Khaleel, S. Al-Zuhair, S. Al-Mamary, M. Parvin, and A. H. Khan, “Structural, Textural, and Catalytic Properties of Ti(IV)-Fe(III) Mixed Oxides Prepared by a Modified Sol-Gel Route,” *ChemistrySelect*, vol. 2, pp. 791–799, Jan. 2017, doi: 10.1002/slct.201601742.
- [83] A. Khaleel, M. Parvin, M. AlTabaji, and A. Al-zamly, “Ti(IV)-doped $\gamma\text{-Fe}_2\text{O}_3$ nanoparticles possessing unique textural and chemical properties: Enhanced suppression of phase transformation and promising catalytic activity,” *Journal of Solid State Chemistry*, vol. 259, pp. 91–97, Mar. 2018, doi: 10.1016/j.jssc.2018.01.008.
- [84] N. H. Amin, L. I. Ali, S. A. El-Molla, A. A. Ebrahim, and H. R. Mahmoud, “Effect of Fe_2O_3 precursors on physicochemical and catalytic properties of $\text{CuO}/\text{Fe}_2\text{O}_3$ system,” *Arabian Journal of Chemistry*, vol. 9, pp. S678–S684, Sep. 2016, doi: 10.1016/j.arabjc.2011.07.026.
- [85] S. El-Nahas, A. Abdelkader, S. A. Halawy, and M. A. Mohamed, “Nanocrystalline MgO samples (11.5 and 12.6 nm) derived from two different precursors: characterization and catalytic activity,” *J Therm Anal Calorim*, vol. 129, no. 3, pp. 1313–1322, Sep. 2017, doi: 10.1007/s10973-017-6277-5.

- [86] B. Huang, C. H. Bartholomew, and B. F. Woodfield, "Facile structure-controlled synthesis of mesoporous γ -alumina: Effects of alcohols in precursor formation and calcination," *Microporous and Mesoporous Materials*, vol. 177, pp. 37–46, Sep. 2013, doi: 10.1016/j.micromeso.2013.04.013.
- [87] M. May, J. Navarrete, M. Asomoza, and R. Gomez, "Tailored mesoporous alumina prepared from different aluminum alkoxide precursors," *J Porous Mater*, vol. 14, no. 2, pp. 159–164, Jun. 2007, doi: 10.1007/s10934-006-9020-3.
- [88] B. Kaur and S. N. Bhattacharya, "7 - Automotive dyes and pigments," in *Handbook of Textile and Industrial Dyeing*, vol. 2, M. Clark, Ed. Woodhead Publishing, 2011, pp. 231–251.
- [89] M. Y. Byun, J. S. Kim, D.-W. Park, and M. S. Lee, "Influence of calcination temperature on the structure and properties of Al_2O_3 as support for Pd catalyst," *Korean J. Chem. Eng.*, vol. 35, no. 5, pp. 1083–1088, May 2018, doi: 10.1007/s11814-018-0015-y.
- [90] Z.X. Sun, T.T. Zheng, Q.B. Bo, M. Du, and W. Forsling, "Effects of calcination temperature on the pore size and wall crystalline structure of mesoporous alumina," *Journal of Colloid and Interface Science*, vol. 319, no. 1, pp. 247–251, Mar. 2008, doi: 10.1016/j.jcis.2007.11.023.
- [91] M. T. Ravanchi, M. R. Fard, S. Fadaeeraeyeni, and F. Yaripour, "Effect of Calcination Conditions on Crystalline Structure and Pore Size Distribution for a Mesoporous Alumina," *Chemical Engineering Communications*, vol. 202, no. 4, pp. 493–499, Apr. 2015, doi: 10.1080/00986445.2013.850577.
- [92] S. D. Ros, E. Barbosa-Coutinho, M. Schwaab, V. Calsavara, and N. R. C. Fernandes-Machado, "Modeling the effects of calcination conditions on the physical and chemical properties of transition alumina catalysts," *Materials Characterization*, vol. 80, pp. 50–61, Jun. 2013, doi: 10.1016/j.matchar.2013.03.005.
- [93] S. Mourdikoudis, R. M. Pallares, and N. T. K. Thanh, "Characterization techniques for nanoparticles: comparison and complementarity upon studying nanoparticle properties," *Nanoscale*, vol. 10, no. 27, pp. 12871–12934, 2018, doi: 10.1039/C8NR02278J.
- [94] S. Erdem, B. Erdem, R. M. Öksüzoğlu, and A. Çıtak, "Effect of calcination temperature on the structural and magnetic properties of Ni/SBA-15 nanocomposite," *J Porous Mater*, vol. 22, no. 3, pp. 689–698, Jun. 2015, doi: 10.1007/s10934-015-9941-9.

- [95] L. Smoláková, M. Kout, E. Koudelková, and L. Čapek, “Effect of Calcination Temperature on the Structure and Catalytic Performance of the Ni/Al₂O₃ and Ni–Ce/Al₂O₃ Catalysts in Oxidative Dehydrogenation of Ethane,” *Ind. Eng. Chem. Res.*, vol. 54, no. 51, pp. 12730–12740, Dec. 2015, doi: 10.1021/acs.iecr.5b03425.
- [96] S. Komeili, M. Takht Ravanchi, and A. Taeb, “Influence of calcination parameters on the properties of alumina as a catalyst support,” *Scientia Iranica*, vol. 23, no. 3, pp. 1128–1135, Jun. 2016, doi: 10.24200/sci.2016.3883.
- [97] J. Wang, X. Dong, Y. Wang, and Y. Li, “Effect of the calcination temperature on the performance of a CeMoOx catalyst in the selective catalytic reduction of NOx with ammonia,” *Catalysis Today*, vol. 245, pp. 10–15, May 2015, doi: 10.1016/j.cattod.2014.07.035.
- [98] F. Sima, C. Ristoscu, L. Duta, O. Gallet, K. Anselme, and I. N. Mihailescu, “3 - Laser thin films deposition and characterization for biomedical applications,” in *Laser Surface Modification of Biomaterials*, R. Vilar, Ed. Woodhead Publishing, 2016, pp. 77–125.
- [99] S. T. Misture and R. L. Snyder, “X-ray Diffraction,” in *Encyclopedia of Materials: Science and Technology*, K. H. J. Buschow, R. W. Cahn, M. C. Flemings, B. Ilshner, E. J. Kramer, S. Mahajan, and P. Veysseyre, Eds. Oxford: Elsevier, 2001, pp. 9799–9808.
- [100] T. Ishii and T. Kyotani, “Chapter 14 - Temperature Programmed Desorption,” in *Materials Science and Engineering of Carbon*, M. Inagaki and F. Kang, Eds. Butterworth-Heinemann, 2016, pp. 287–305.
- [101] J. R. A. Sietsma, A. Jos van Dillen, P. E. de Jongh, and K. P. de Jong, “Application of ordered mesoporous materials as model supports to study catalyst preparation by impregnation and drying,” in *Studies in Surface Science and Catalysis*, vol. 162, E. M. Gaigneaux, M. Devillers, D. E. De Vos, S. Hermans, P. A. Jacobs, J. A. Martens, and P. Ruiz, Eds. Elsevier, 2006, pp. 95–102.
- [102] J. Boon, J. van Kampen, R. Hoogendoorn, S. Tanase, F. P. F. van Berkel, and M. van Sint Annaland, “Reversible deactivation of γ -alumina by steam in the gas-phase dehydration of methanol to dimethyl ether,” *Catalysis Communications*, vol. 119, pp. 22–27, Jan. 2019, doi: 10.1016/j.catcom.2018.10.008.
- [103] O. Tursunov, L. Kustov, and Z. Tilyabaev, “Catalytic activity of H-ZSM5 and Cu-HZSM5 zeolites of medium SiO₂/Al₂O₃ ratio in conversion of n-hexane to aromatics,” *Journal of Petroleum Science and Engineering*, vol. 180, pp. 773–778, Sep. 2019, doi: 10.1016/j.petrol.2019.06.013.

- [104] L. Shirazi, E. Jamshidi, and M. R. Ghasemi, "The effect of Si/Al ratio of ZSM5 zeolite on its morphology, acidity and crystal size," *Crystal Research and Technology*, vol. 43, no. 12, pp. 1300–1306, 2008, doi: 10.1002/crat.200800149.
- [105] E. G. Derouane *et al.*, "The Acidity of Zeolites: Concepts, Measurements and Relation to Catalysis: A Review on Experimental and Theoretical Methods for the Study of Zeolite Acidity," *Catalysis Reviews*, vol. 55, no. 4, pp. 454–515, Oct. 2013, doi: 10.1080/01614940.2013.822266.
- [106] A. Bakhtyari, M. Parhoudeh, and M. R. Rahimpour, "Optimal conditions in converting methanol to dimethyl ether, methyl formate, and hydrogen utilizing a double membrane heat exchanger reactor," *Journal of Natural Gas Science and Engineering*, vol. 28, pp. 31–45, Jan. 2016, doi: 10.1016/j.jngse.2015.11.028.
- [107] U. Mondal and G. D. Yadav, "Perspective of dimethyl ether as fuel: Part II- analysis of reactor systems and industrial processes," *Journal of CO₂ Utilization*, vol. 32, pp. 321–338, Jul. 2019, doi: 10.1016/j.jcou.2019.02.006.
- [108] G. Eigenberger, "Fixed bed reactors," vol. B4, pp. 199–238, 1992, doi: <http://dx.doi.org/10.18419/opus-1831>.
- [109] A. I. Osman and J. K. Abu-Dahrieh, "Kinetic Investigation of η -Al₂O₃ Catalyst for Dimethyl Ether Production," *Catal Lett*, vol. 148, no. 4, pp. 1236–1245, Apr. 2018, doi: 10.1007/s10562-018-2319-2.
- [110] C. Ortega, M. Rezaei, V. Hessel, and G. Kolb, "Methanol to dimethyl ether conversion over a ZSM5 catalyst: Intrinsic kinetic study on an external recycle reactor," *Chemical Engineering Journal*, vol. 347, pp. 741–753, Sep. 2018, doi: 10.1016/j.cej.2018.04.160.
- [111] S. Kim, Y. T. Kim, C. Zhang, G. Kwak, and K.-W. Jun, "Effect of Reaction Conditions on the Catalytic Dehydration of Methanol to Dimethyl Ether Over a K-modified HZSM5 Catalyst," *Catal Lett*, vol. 147, no. 3, pp. 792–801, Mar. 2017, doi: 10.1007/s10562-017-1981-0.
- [112] L. Zhang, H. Zhang, W. Ying, and D. Fang, "Dehydration of methanol to dimethyl ether over γ -Al₂O₃ catalyst: Intrinsic kinetics and effectiveness factor," *The Canadian Journal of Chemical Engineering*, vol. 91, no. 9, pp. 1538–1546, 2013, doi: 10.1002/cjce.21760.
- [113] "VICI - Valco Instruments Company Incorporated." <https://www.vici.com/index.php> (Accessed Dec. 31, 2019).
- [114] A. J. Jones and E. Iglesia, "Kinetic, Spectroscopic, and Theoretical Assessment of Associative and Dissociative Methanol Dehydration Routes in Zeolites,"

Angewandte Chemie International Edition, vol. 53, no. 45, pp. 12177–12181, 2014, doi: 10.1002/anie.201406823.

- [115] Z. Zuo, W. Huang, P. Han, Z. Gao, and Z. Li, “Theoretical studies on the reaction mechanisms of AlOOH- and γ -Al₂O₃-catalysed methanol dehydration in the gas and liquid phases,” *Applied Catalysis A: General*, vol. 408, no. 1, pp. 130–136, Nov. 2011, doi: 10.1016/j.apcata.2011.09.011.
- [116] L. Kubelková, J. Nováková, and K. Nedomová, “Reactivity of surface species on zeolites in methanol conversion,” *Journal of Catalysis*, vol. 124, no. 2, pp. 441–450, Aug. 1990, doi: 10.1016/0021-9517(90)90191-L.
- [117] G. Bercic and J. Levec, “Intrinsic and global reaction rate of methanol dehydration over γ -alumina pellets,” *Ind. Eng. Chem. Res.*, vol. 31, no. 4, pp. 1035–1040, Apr. 1992, doi: 10.1021/ie00004a010.
- [118] J. J. SPIVEY, “Review: Dehydration Catalysts for the Methanol/Dimethyl Ether Reaction,” *Chemical Engineering Communications*, vol. 110, no. 1, pp. 123–142, Dec. 1991, doi: 10.1080/00986449108939946.
- [119] A. Sierraalta, R. Añez, D. S. Coll, and P. Alejos, “Conversion of methanol to dimethyl ether over silicoaluminophosphates: Isolated acid sites and the influence of silicon islands. A DFT-ONIOM study,” *Microporous and Mesoporous Materials*, vol. 292, p. 109732, Jan. 2020, doi: 10.1016/j.micromeso.2019.109732.
- [120] J. Palomo, M. A. Rodríguez-Cano, J. Rodríguez-Mirasol, and T. Cordero, “On the kinetics of methanol dehydration to dimethyl ether on Zr-loaded P-containing mesoporous activated carbon catalyst,” *Chemical Engineering Journal*, vol. 378, p. 122198, Dec. 2019, doi: 10.1016/j.cej.2019.122198.
- [121] J. Ryzkowski, “IR spectroscopy in catalysis,” *Catalysis Today*, vol. 68, no. 4, pp. 263–381, Jul. 2001, doi: 10.1016/S0920-5861(01)00334-0.
- [122] K. Faungnawakij, T. Fukunaga, R. Kikuchi, and K. Eguchi, “Deactivation and regeneration behaviors of copper spinel–alumina composite catalysts in steam reforming of dimethyl ether,” *Journal of Catalysis*, vol. 256, no. 1, pp. 37–44, May 2008, doi: 10.1016/j.jcat.2008.02.022.
- [123] A. R. McInroy *et al.*, “An infrared and inelastic neutron scattering spectroscopic investigation on the interaction of η -alumina and methanol,” *Phys. Chem. Chem. Phys.*, vol. 7, no. 16, pp. 3093–3101, Aug. 2005, doi: 10.1039/B505974G.

- [124] A. R. McInroy, D. T. Lundie, J. M. Winfield, C. C. Dudman, P. Jones, and D. Lennon, "The Application of Diffuse Reflectance Infrared Spectroscopy and Temperature-Programmed Desorption To Investigate the Interaction of Methanol on η -Alumina," *Langmuir*, vol. 21, no. 24, pp. 11092–11098, Nov. 2005, doi: 10.1021/la051429c.
- [125] S. -J. Huang, A. B. Walters, and M. A. Vannice, "NO reduction by CH₄ over La₂O₃: temperature-programmed reaction and in situ DRIFTS studies," *Catalysis Letters*, vol. 64, no. 2, pp. 77–83, Feb. 2000, doi: 10.1023/A:1019024128469.
- [126] S. Srinivasan, C. R. Narayanan, and A. K. Datye, "The role of sodium and structure on the catalytic behavior of alumina: II. IR spectroscopy," *Applied Catalysis A: General*, vol. 132, no. 2, pp. 289–308, Nov. 1995, doi: 10.1016/0926-860X(95)00162-X.
- [127] S. R. Blazkowski and R. A. van Santen, "The Mechanism of Dimethyl Ether Formation from Methanol Catalyzed by Zeolitic Protons," *J. Am. Chem. Soc.*, vol. 118, no. 21, pp. 5152–5153, Jan. 1996, doi: 10.1021/ja954323k.

List of Publications

A. Khaleel, M. Ahmed, and S. B. Sowaid, “Ti-doped γ -Al₂O₃ versus ZSM5 zeolites for methanol to dimethyl ether conversion: In-situ DRIFTS investigation of surface interactions and reaction mechanism,” *Colloids and Surfaces A: Physicochemical and Engineering Aspects*, vol. 571, pp. 174–181, Jun. 2019, doi: 10.1016/j.colsurfa.2019.03.052.